GEOCHEMISTRY OF ROCK WEATHERING IN THE UPPER PART OF MAHANADI RIVER BASIN

A Thesis Submitted
In Partial Fulfilment of the Requirements
for the Degree of
DOCTOR OF PHILOSOPHY

by

BIJAYA KUMAR PANIGRAHY

to the

DEPARTMENT OF CIVIL ENGINEERING
INDIAN INSTITUTE OF TECHNOLOGY KANPUR
December, 1991

C E R T I F I C A T E

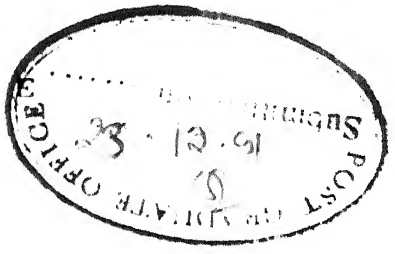

It is certified that the work contained in the thesis entitled **GEOCHEMISTRY OF ROCK WEATHERING IN THE UPPER PART OF MAHANADI RIVER BASIN** by Bijaya Kumar Panigrahy, has been carried out under my supervision and that this work has not been submitted elsewhere for a degree.

(Bikash C. Raymahashay)
Professor
Department of Civil Engineering
Indian Institute of Technology
Kanpur - 208 016, INDIA

December, 1991

SYNOPSIS

The Mahanadi is one of the major rivers in Peninsular India draining into the Bay of Bengal. It has a catchment area of 148,589 km^2 and is occupied by a variety of rocks, alluvial deposits and soils. As one of the main objectives of this thesis was to study the details of weathering of bed rocks, field work was confined to the upper part of the river basin which is relatively free of recent deposits and human interference.

The source area of the Mahanadi is occupied by granites and granite gneisses of Archaean age. The river then flows for a considerable length through the well known Chhattisgarh Basin containing Proterozoic dolomitic limestones and calcareous shales. The granitic and limestone terrains together cover 46,700 km^2 (31.4% of the entire drainage basin) and form the study area for this work. A mineralogical study of rocks and soils collected from this area was combined with a 5-year water and sediment database obtained from the Central Water Commission (CWC), Government of India and was supplemented by spot checks. The CWC sampling stations are spread over 13 locations throughout the Mahanadi Basin.

Geomorphological data for longitudinal profile and hypsometric analysis indicate that the river is actively eroding granitic rocks in the source area. Satellite imageries at the same time show typical karst features in the limestone terrain. Presence of unweathered felspar and occasional calcite in suspended sediments point to a transport dominated (weathering limited) denudation regime. The overall ratio of physical to chemical erosion rate works out to be around 7:1.

Ca^{2+}, Mg^{2+}, Na^{+}, K^{+} are the major cations and HCO_3^-, Cl^-, SO_4^{2-} are the major anions in river water. The concentration of major ions at the confluence of tributaries matches fairly well with the calculated values obtained by weighting the concentration in individual tributaries according to their drainage areas. This indicates a major contribution from weathering of rocks in the drainage area.

River and ground water containing dissolved CO_2 are the principal weathering agents. The apparent partial pressure of CO_2, calculated from pH and HCO_3 in river water, averages around $10^{-2.46}$ atmosphere. The total HCO_3 can be distributed between two sources namely, carbonate weathering and silicate weathering. A rough calculation using global averages for this fractionation shows that the ratio of carbonate derived HCO_3 to silicate derived HCO_3 reaches a value of 2.0 in the limestone terrain and is more

than 1.0 all along the river course. This suggests that the influence of weathering of carbonate minerals is dominant over weathering of silicate minerals even in the downstream segments outside the limestone terrain. The same conclusion is supported by a balance between $(Ca + Mg)_{total}$ and $(HCO_3)_{total}$ and a cluster of river water analyses near the HCO_3 apex in a ternary plot of HCO_3, SiO_2 and SO_4 on an equivalent basis. An R-mode Factor Analysis of water composition also indicated that a Na-Ca-Mg-HCO_3 factor can explain 70% of the total variance among the ions.

Mineral water equilibria were further verified through thermodynamic data on (1) carbonate and (2) silicate systems. The river is generally undersaturated with respect to calcite and dolomite which explains its aggressive weathering of dolomitic limestone. In the standard silicate mineral stability diagrams for K, Na and Mg systems, river water analyses at different sampling stations plot within the kaolinite field. On the other hand, the analyses plot near the kaolinite-Ca montmorillonite boundary in the stability diagram for the Ca-system suggesting that these two clay minerals can co-exist in the river water environment. This conclusion is consistent with the presence of kaolinite and a glycol expansive 14Å clay mineral in suspended sediments and soils.

A limited number of analysis of heavy metals in soils and sediments showed a general distribution pattern of Pb < Cu < Mn < Zn in the granitic terrain and Pb < Zn < Cu < Mn in the carbonate terrain.

A detailed study of soil profiles in a pilot area within the Chhattisgarh Basin confirmed the dual weathering scheme of carbonate and silicate minerals. While a congruent weathering of calcite and dolomite has produced typical solution features, weathering of glauconite present in stromatolitic limestones has led to the formation of a lateritic soil cover. Relative mobility of elements during weathering has been in the order Ca > Mg > Na ≥ K > Si > Al > Fe.

ACKNOWLEDGEMENT

I wish to express my deep sense of gratitude to Prof. S.C. Raymahashay for suggesting me this topic and for his valuable guidance and encouragement at every stage of this work.

I am thankful to Prof. M.R. Madhav, Prof. K.V.G.K. Gokhale, Prof. Yudhbir and Dr. R.P. Singh for their encouragement and timely assistance. Thanks are also due to Prof. A.S. Dave, Dr. G.S. Pande, Dr. A. Mukherjee and Dr. H.S. Diwan of Ravi Shankar University, Raipur for providing all necessary help in the field and laboratory work. I thank Mr. B.M. Bansal, Executive Engineer, Dhamtari for providing me transport facility in that area. Dr. S. K. Acharyya and Dr. S.B. Ray of G.S.I., Bhubaneswar and Mr. V.P. Mishra, Senior Geologist, Raipur provided useful suggestions and advice during the development of this work. Discussions with Dr. C.D. Murthy were highly useful for better understanding of the geology of my study area.

I am also thankful to Mr. Y.D. Pendse, Member (WP); Mr. Parambrahman, Director (BPMO) and several assistant directors (BPMO) of Central Water Commission, New Delhi who were kind enough to provide me necessary data and information on the Mahanadi river

My sincere acknowledgements are also due to Prof. V. Subramaniam Iyer, I.I.T. Bombay for providing me the landsat imagery. Useful suggestions regarding aluminium speciation from Dr. Colin Neal, Institute of Hydrology, U.K. are gratefully appreciated. Thanks are also due to Prof. V. Subramanian, J.N.U., Delhi for permitting the use of his laboratory facility at the initial stage of this work. Help in heavy metal analysis from Mr. Dilip Patnaik and Mr. G.J. Chakrapani is gratefully acknowledged. I owe a great deal to my friends Pranab, Devanand, Yaqoob, Trinath, Sukhram ,Venugopal and Nilanchal for their whole-hearted cooperation at various stages of my work. Special thanks are due to Dr. Pratima Mishra and Dr. Anil Agrawal who were helpful throughout my research period.

And finally, special recognition is due to my wife Shanto who provided 4 years of patient understanding and encouragement.

(B.K. Panigrahy)

dedicated

to

my daughter

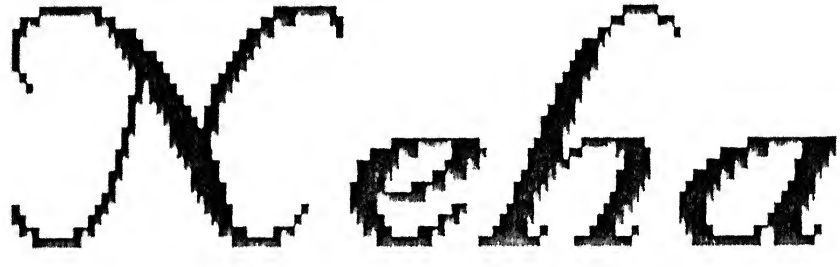

C O N T E N T S

LIST OF FIGURES

LIST OF TABLES

CHAPTER 1

INTRODUCTION AND OBJECTIVE

Rock weathering is a fundamental step within the fluvial erosion cycle. River water can cause physical breakdown of rocks in the drainage basin as well as chemical decomposition of the constituent minerals. As a result, the river acquires its sediment load and its dissolved chemical content. Therefore, a study of weathering processes in a river basin is important in any water quality assessment programme.

1.1 Weathering in River Basins

A large river basin contains enough variation in lithology and geomorphology so that a comparative study of physical and chemical processes is usually possible. The compilation of data on erosion rates from individual basins leads to a global estimate of river input to the ocean systems. Many fundamental geochemical concepts dealing with atmosphere-hydrosphere-lithosphere interactions are based on such studies (e.g. Garrels and Mackenzie, 1971; Holland, 1978).

A detailed investigation of a river basin may incorporate the following components.

1) Material transport

   a) Bed rock geology

   b) Geomorphology and soil characteristics

   c) Mineralogy and grain size of sediments

d) Sediment delivery

e) Erosion rates

) Hydrological parameters

a) Precipitation and infiltration

b) Ground water recharge rate

c) Discharge, elevation, catchment area inter-relationships

) Geochemical models

a) Mass balance of weathering reactions

b) Thermodynamic stability of minerals

c) Statistical evaluation

d) Kinetics of weathering reaction

e) Isotope studies.

On a continental scale, the rate of physical (mechanical) erosion shows a wide variation. Some workers like Garrels and Mackenzie (1971) and Holland (1978) have observed an exponential relationship between this rate and the relief of drainage area. Similar trends are noticed among individual river basins for example, in Himalayan and Peninsular Indian rivers as discussed later.

The rate of chemical erosion, on the other hand, varies within narrow limits. This rate is mainly controlled by rock types in the drainage basin which are subjected to chemical weathering under a more or less uniform CO_2-pressure in the earth's atmosphere.

1.2 Controls on River Water Composition

Many attempts have been made to infer the source of dissolved components in river water. A common approach is to estimate the composition of primary and secondary minerals in a selected weathering scheme that will be consistent with the observed water chemistry. A simplified mass balance equation that depicts the input and output concepts in a river basin can be written as

Precipitation + Weathering = Run-off + Storage + Biomass.

Good examples of this line of investigation are available from Cleaves et al. (1970), Holland (1978), Stallard and Edmond (1983), Meybeck (1987), Berner and Berner (1987) and Drever (1988).

In a study to identify the environmental factors that influence river water chemistry, Gibbs (1970) suggested the following classification of rivers. (1) Low TDS, high Na/(Na+Ca) waters controlled by rainfall, (2) Intermediate TDS, low Na/(Na+Ca) waters controlled by rock weathering and (3) High TDS, high Na/(Na+Ca) waters controlled by evaporation. Subsequent revision by Stallard and Edmond (1983) as discussed by Berner and Berner (1987) showed that these three groups are in fact representative of three types of rock weathering. For example, the first group is controlled by unreactive drainage basins containing cation-poor siliceous sediments and soils which have already undergone intense weathering. The second group includes most of the major rivers of the world and represents weathering of sedimentary rocks dominated by a $CaCO_3$ component. In these

rivers, Ca^{2+} and HCO_3^- would be the main dissolved ions. The third group, in contrast, represents weathering of evaporite beds. The TDS of these rivers is typically more than 250 mg/l with relatively high concentrations of Na^+ and Cl^-. In addition to the importance of rock types in controlling river water composition, Berner and Berner (1987) as well as Drever (1988) list some other natural environmental factors. These are 1) amount and nature of rainfall and evaporation, 2) temperature, 3) relief, 4) vegetation and 5) time. It is also obvious that in populated areas, these natural factors are superimposed by anthropogenic contributions like agricultural, domestic and industrial effluents. Meade (1969) has discussed the various sources of suspended and dissolved constituents due to human activity.

1.3 Geochemical Studies on Weathering in Indian River Basins

It is well known that the sub-continent of India is drained by some of the largest rivers of the world. Among these, the Ganges and the Brahmaputra jointly deliver possibly the largest sediment load to the world ocean (Milliman and Meade, 1983). One of the early attempts to quantify erosion rates in the Himalayan region was by Raymahashay (1973). This was followed by a large volume of work on Himalayan as well as Peninsular rivers by V. Subramanian and co-workers which has been summarized by Subramanian (1979, 1987) and Subramanian et al. (1987a, 1987b). Table 1.1 shows data from Subramanian (1979) on sediment yield and the apparent control of basin relief on Himalayan versus

Table 1.1 Sediment yield and relief of Indian river basins (modified from Subramanian, 1979)

Basin	Mean elevation (m)	Sediment yield ($t/km^2/yr$)
Himalayan Rivers		
Brahmaputra	5000	865.5
Ganges	3000	591.5
Peninsular rivers		
Narmada	760	58.7
Tapti	740	41.7
Cauvery	630	8.1
Mahanadi	500	15.6
Krishna	420	42.2
Godavari	400	56.0

eninsular rivers. The clay mineralogy of bed loads has been lescribed by Naidu et al. (1985). A weathering model based on icarbonate content was suggested by Raymahashay (1986). More ecently, the major ion chemistry and the abundance of adionuclides in the Ganges-Brahmaputra system has been discussed y Sarin et al. (1989, 1990).

The Mahanadi basin specifically has been studied by Chakrapani and Subramanian (1990a, 1990b). This is one of the largest rivers in Peninsular India. The drainage basin contains a vide variety of rocks and there is some controversy about the nature and source of sediment mineralogy. Ray et al. (1984) had earlier studied the chemical flux at the estuary of the Mahanadi river.

In addition to detailed geochemical studies mentioned above, routine monitoring of all the major river basins is undertaken by various government agencies like the Central Water Commission, Central Soil and Materials Research Station, National Environmental Engineering Research Institute. However, there are large differences in the details of water quality, sediment mineralogy and basin geology. There is an obvious need for a systematic study of the nature of bed rocks, weathering and soil formation with special reference to the acquisition of dissolved and suspended load by rivers of India. It is interesting to note that the Department of Science and Technology, Government of India has recognized some of these aspects as challenging areas in Earth Sciences in the next decade (Tandon and Gupta, 1990).

1.4 Objectives of Present Work

With this background of the present status of river basin studies in India, it was decided to select a representative area of bed rock exposures in the upper reaches of the Mahanadi river and go into the details of rock-water interaction. The main objectives of this project can be summarized as follows.

1. To compile a mineralogical description of the major rock types exposed within the Proterozoic Chhattisgarh Basin and its southern fringe of Archaean basement where the source of the Mahanadi river is located.
2. To distinguish between primary and secondary minerals in weathered rock and soil profile with the ultimate aim of setting up a series of weathering reactions.
3. To establish a reliable database for the variation of water composition along the river course by a critical assessment of available literature and through spot checks.
4. To summarize the quantitative geomorphology of the Mahanadi basin through a comparative study of physical and chemical erosion processes.
5. To trace the mobility of major elements and a few environmentally significant heavy metals during weathering and soil formation.
6. To explore the relationship between rock weathering and river water composition by testing existing models which are based on Mass Balance, Thermodynamics and Statistics.

CHAPTER 2

SAMPLING AND ANALYSIS

2.1 Field Work

Field work for sample collection was confined to the upper part of the Mahanadi basin. Sampling of rock, soil and sediment was carried out from all the geologic formations exposed in the area. At least 3 representative fresh and weathered rocks were sampled from each formation. Residual soil samples were collected wherever a soil profile was available. Flood plain sediments were collected from 0-10 cm depth. Suspended sediment was collected at the site by filtering large volumes of turbid river water in the rainy season through Whatman 42 filter paper. Water samples were collected during post-monsoon period of 1989 from four selected CWC stations at Baronda, Rajim, Simga and Andhiyarkore. A sample of monsoonal rain (August 1990) was collected by a specially erected rain gauge at I.G. University of Agriculture, Raipur. To avoid aerosols, rainwater was collected ten minutes after the rain commenced. pH and bicarbonate were determined at the sampling site while conductivity was measured in a nearby chemical laboratory within six hours of collection.

2.2 Laboratory Work

Laboratory work consisted of chemical analysis of a limited number of water samples for major ions, chemical analysis of rocks for major oxides, mineralogical analysis of rock, soil and sediment, grain size analysis of suspended sediments and heavy metal analysis of sediments and soils. Prior to chemical analysis of water, it was filtered through 0.45 μm millipore paper and stored in polyethylene container in a refrigerator. Analyses were carried out within 15 days of sample collection. The procedures adopted for water analysis are summarized in Table 2.1. Bulk chemical analysis of a few representative rock samples were carried out by X-ray fluorescence (XRF) unit at Regional Research Laboratory, Bhubaneshwar. USGS rock standard G-1 was also analyzed for calibration.

2.2.1 Mineralogical Analysis

Mineralogical analysis of rock, soil and sediment was carried out by petrographic examination of thin sections, X-ray diffraction (Siefert XRD unit with CrKα radiation), differential thermal analysis (Lynseis Type 2045) and scanning electron microscopy (JEOL-840A model coupled with a KEVEX energy dispersive X-ray analytical system). X-ray studies were carried out with two sets of samples namely bulk powder and smear slide. Preheated

able 2.1 Analytical methods for water samples

pH	: pH meter in laboratory within six hours of sample collection
Bicarbonate	: Acid (HCl) titration at site
Conductivity	: Conductivity meter within six hours of sample collection
Chloride	: $AgNO_3$ titration
Sulphate	: $BaCl_2$ titration
Na and K	: Flame AAS
Ca and Mg	: EDTA titration

powder samples were also subjected to X-ray diffraction in some cases. Smear slides were glycolated wherever necessary.

2.2.2 Grain Size Analysis

Size analysis of suspended sediments was performed by a Coulter Counter. Sediment suspension was prepared in NaCl solution to produce the desired voltage pulse which was scaled and counted.

2.2.3 Heavy Metal Analysis

Heavy metal analysis of soils and flood plain deposits was carried out by digestion in HNO_3-HCl-HF mixture in a teflon bomb. The extract was analyzed in a Perkin Elmer model 2380 AAS unit. USGS rock standards MAG-1 and SGR-1 were used for calibration.

CHAPTER 3

PHYSIOGRAPHY AND GEOLOGY OF THE MAHANADI RIVER BASIN

The Mahanadi is the second major river in Peninsular India with respect to its water potential. The river basin is located in the states of Madhya Pradesh and Orissa. With a catchment area of 148589 square kilometers, the basin lies between the longitudes $80^{o}30'$ E, $84^{o}50'$ E and latitudes $19^{o}20'$ N and $23^{o}35'$ N. The Mahanadi river rises from a pool 6 kms away from Pharsiya village near Nagri town of M.P. at an elevation of 457 metres. Hydrologically, the river basin can be divided into 11 smaller sub-basins (Fig. 3.1). The principal tributaries are Pairi, Seonath, Jonk, Hasdo, Mand, Ib and Tel. Fig. 3.2 shows the course of main Mahanadi and its tributaries.

3.1 Physiographic Divisions of the Basin

The following physiographic zones can be identified in the basin area.

a) Highlands at the south-west margin.

b) Erosional plains at western and central parts.

c) Plateau areas towards north

d) Eastern ghats towards south

e) Alluvial plains towards east.

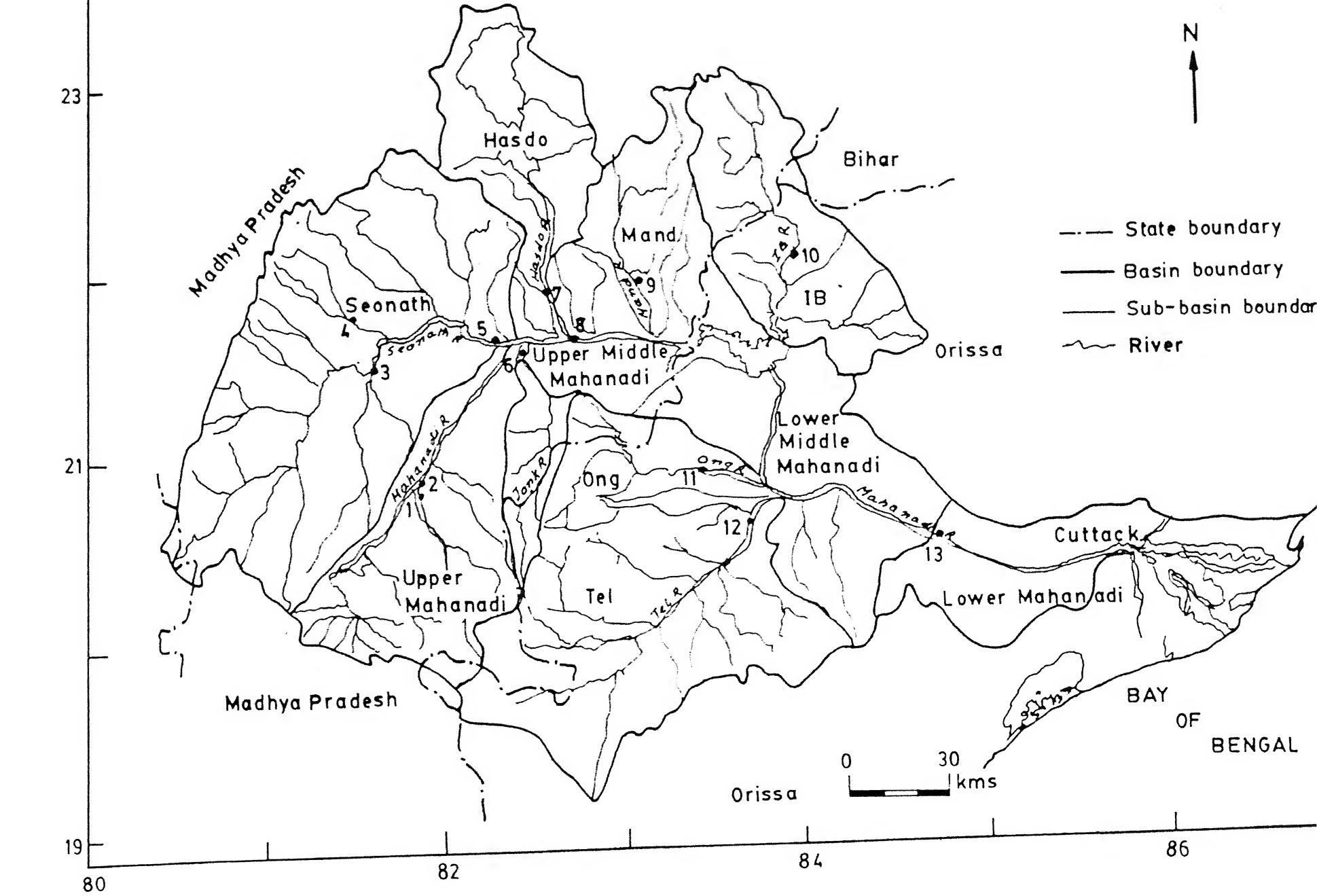
N
State boundary
Basin boundary
Sub-basin boundar
River
Hasdo
Bihar
Madhya Pradesh
Mand
Seonath
Upper Middle Mahanadi
Orissa
1B
Lower Middle Mahanadi
Ong
Upper Mahanadi
Tel
Cuttack
Lower Mahanadi
Madhya Pradesh
BAY OF BENGAL
Orissa
0 30 kms
23
21
19
80
82
84
86

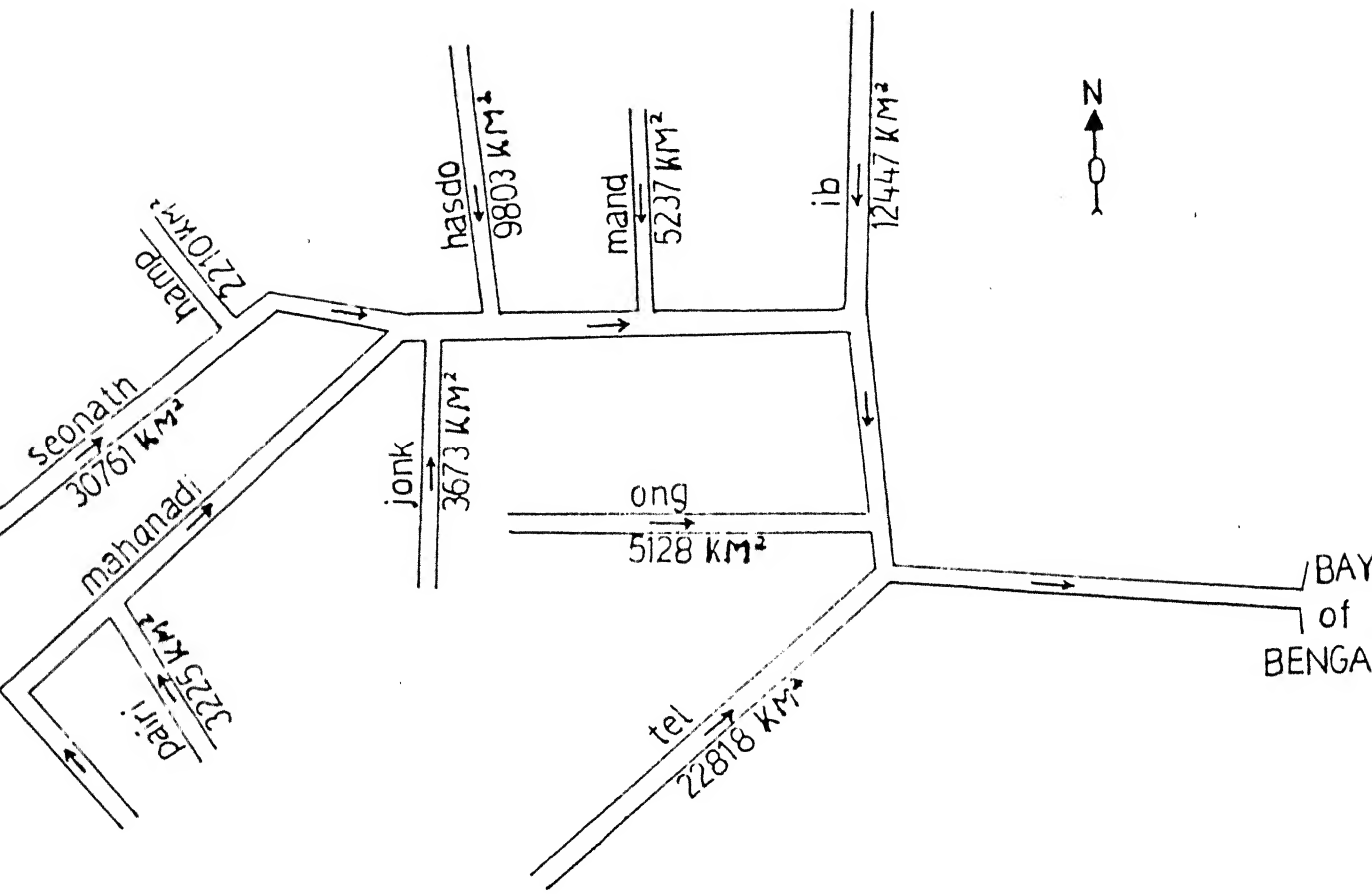

Fig. 3.2 Sketch of flow diagram of the Mahanadi and its tributaries

The highlands at the SW margin comprise parts of Durg, Raipur and Bastar districts in M.P. Erosional plains at western and central parts cover the well known Chhattisgarh region encompassing Rajnandgaon, Durg, Raipur, Bilaspur and a part of Raigarh district. Plateau areas in the northern part include Korba, Champa and Raigarh districts of M.P. The eastern ghats towards south have a gentle slope from north to south and include Mayurbhanj, Keonjhar, Bolangir, Phulbani and parts of Dhenkanal and Koraput districts in Orissa. This region is characterized by undulating country sides with hill ranges of 1000 metres and above. The coastal plains form an extensive and wide alluvial tract which cover Cuttack and parts of Puri district in Orissa. This area also contains high level laterite covered plateaus. They represent the uplifted and dissected erosional surfaces. These surfaces truncate against the eastern ghats. The mean basin elevation is around 500 metres.

3.2 Climate

3.2.1 Rainfall and Evaporation

The overall climate is tropical to subtropical. Winter season normally sets over the basin from December to February. Precipitation during this period is mostly confined to the northern half of the catchment. The summer season is relatively

long, continuing from March till June. South-west monsoon normally advances over the basin by the third week of June and the whole catchment receives moderate rainfall till the first week of October.

There are about 212 rain gauge stations maintained by IMD (Indian Meteorological Department) which are fairly distributed all over the basin. Rainfall intensity is not marked by any significant variation in the Mahanadi catchment. Bulk of rainfall (91%) occurs in the monsoon period from mid June to first week of December. Average annual rainfall is 144 cm. Monthly distribution of annual rainfall for the entire basin is given in Table 3.1.

The basin has a high rate of potential evapo-transpiration. IMD have reported that the annual potential evaporation varies from 174.5 cm in the west to 152 cm in the east. The highest relative humidity of around 80 percent is experienced in August.

3.2.2 Temperature

December is the coldest and May is the hottest month of the year. The western part of the basin records both the extremes of temperature. Diurnal range of temperature in July-August is in the order of 5^{o} to 6^{o}C and during winter season, it is as high as

Table 3.1 Monthly distribution of normal annual rainfall in the Mahanadi river basin (Source: CWC)

Month	Rainfall(mm)	% of annual total
January	14.9	1.0
February	23.4	1.8
March	17.8	1.4
April	20.1	1.4
May	28.9	2.0
June	214.9	14.9
July	404.9	28.2
August	390.0	27.3
September	227.8	15.8
October	70.6	4.9
November	16.8	1.2
December	4.3	0.3
Monsoon total	1308.1	91.0
Annual total	1438.1	100.0

4° to 16°C. The highest ever recorded temperature in the basin s 47.2°C at five stations Raigarh, Sambalpur, Titlagarh, Champa nd Raipur during different years while the lowest value is 3.9°C t Kanker.

.3 Physiographic Divisions vs. Geologic Formations

A broad correlation seems to exist between the opography and the geologic formations in the basin. However, it s difficult to evaluate any lithological control on the evolution f the sub-basins. Each of the physiographic zones described in ection 3.1 appear to correspond to a particular geologic ormation. A simplified geologic map is given in Fig. 3.3. It is een that the highlands at the SW margin belong to hard silicate ocks like Archaean granite and granite gneiss where as the erosional plains at the western and central parts of the basin correspond to Chhattisgarh Supergroup formations consisting of easily erodible sedimentaries like limestone, shale and sandstone. Plateau areas at the northern part represent outliers of Gondwana formations. Sandstone, grit, conglomerate and carbonaceous shale are the dominant rock types in this region. The eastern ghats, on the other hand, constitute of Precambrian khondalite and charnockite suite of metamorphic rocks. The coastal alluvial plains consisting of eroded materials from upstream regions are of

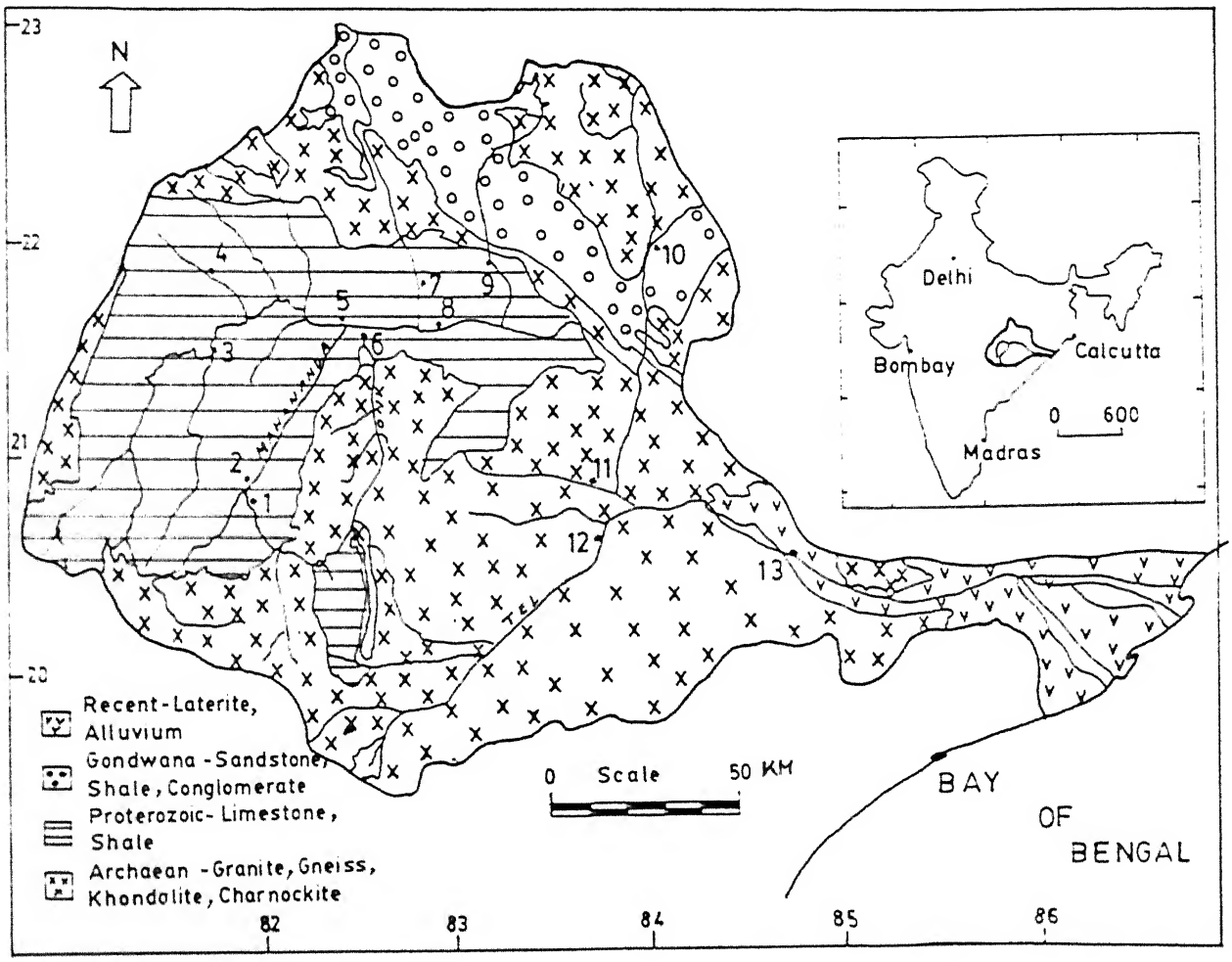

Fig. 3.3 Geological map of the Mahanadi basin (compiled from GSI maps, 1977)

ecent age. The formations in the lower reaches of the river onsist of low level laterites and highly unconsolidated sands ıith little or no clay.

1.4 Selection of Study Area

As discussed earlier, the present study aims at ınderstanding the weathering processes in the watershed that influence the chemical character of the stream water. Existing literature shows that most of the work on Indian rivers have been carried out near the river mouth. This may be due to easy accessibility in the coastal areas. On the other hand, it is obvious that any effect of rock type on water chemistry will not be clearly discernible near the mouth due to human interferences. Even the physical aspects of weathering should be more clear in the hard rock part near the drainage divides rather than in the alluvium covered lower reaches. Therefore, in this work, more attention has been focussed at the portion hydrologically considered as the upstream part of the river. It has the Seonath, the largest tributary, the Pairi, the Hamp and the Mahanadi river up to Jondhra. Together, these tributary basins cover 46, 700 km^2 which is nearly one-third of the total basin area.

The selection of the upper part of the basin was also prompted by the general nature of weathering as evident from the

Landsat imagery (M.S.S., Landsat 2, band 4, Scene No. 153-045). Fig. 3.4 shows that the limestone area has a typical karst topography giving a dark tone while the marginal part with non-carbonate rocks has a lighter tone. The area covered in the imagery includes the entire Chhattisgarh basin and the basement rocks. A detailed discussion of the geology of this area is given in the following section.

3.5 Regional Geology

The upper Mahanadi basin contains the Chhattisgarh basin. This basin is one of the seven Purana basins in India which are believed to have developed under a dominantly extensional tectonic regime and fed with eroded material from the Archaean and Early Proterozoic continental crust of the Peninsular shield. They are repositories of shallow marine sediments in an unmetamorphosed and marginally deformed state (Kale, 1991). Rocks of different formations are exposed in the basin. A geologic map of upper part of the basin is given in Fig. 3.5. The Archaean group of rocks underlie the sedimentary formations of the Chhattisgarh supergroup. There is very little information available on these basement rocks which occur in the source area of the Mahanadi river.

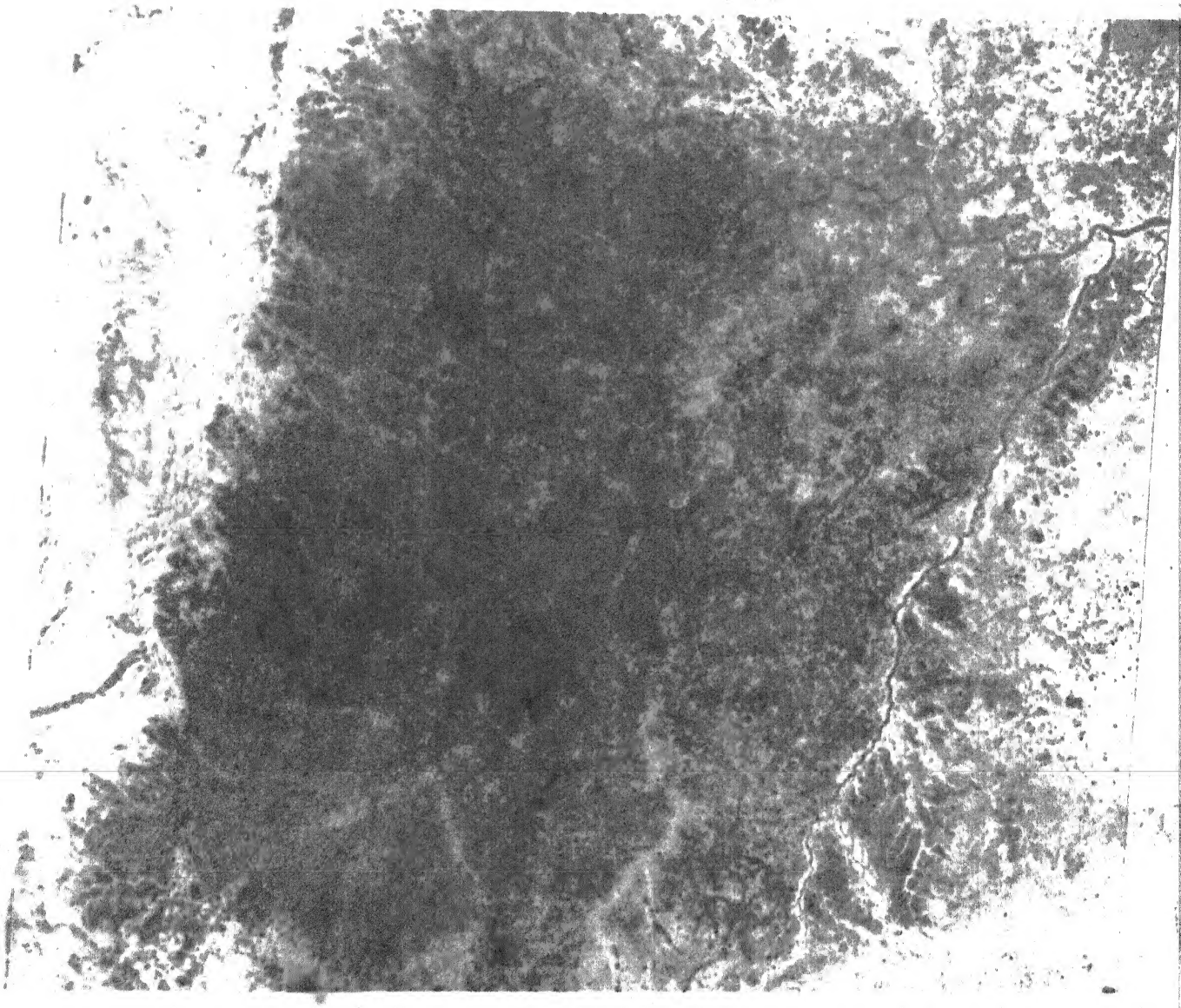

Fig. 3.4 Landsat imagery of the upper part of Mahanadi river basin

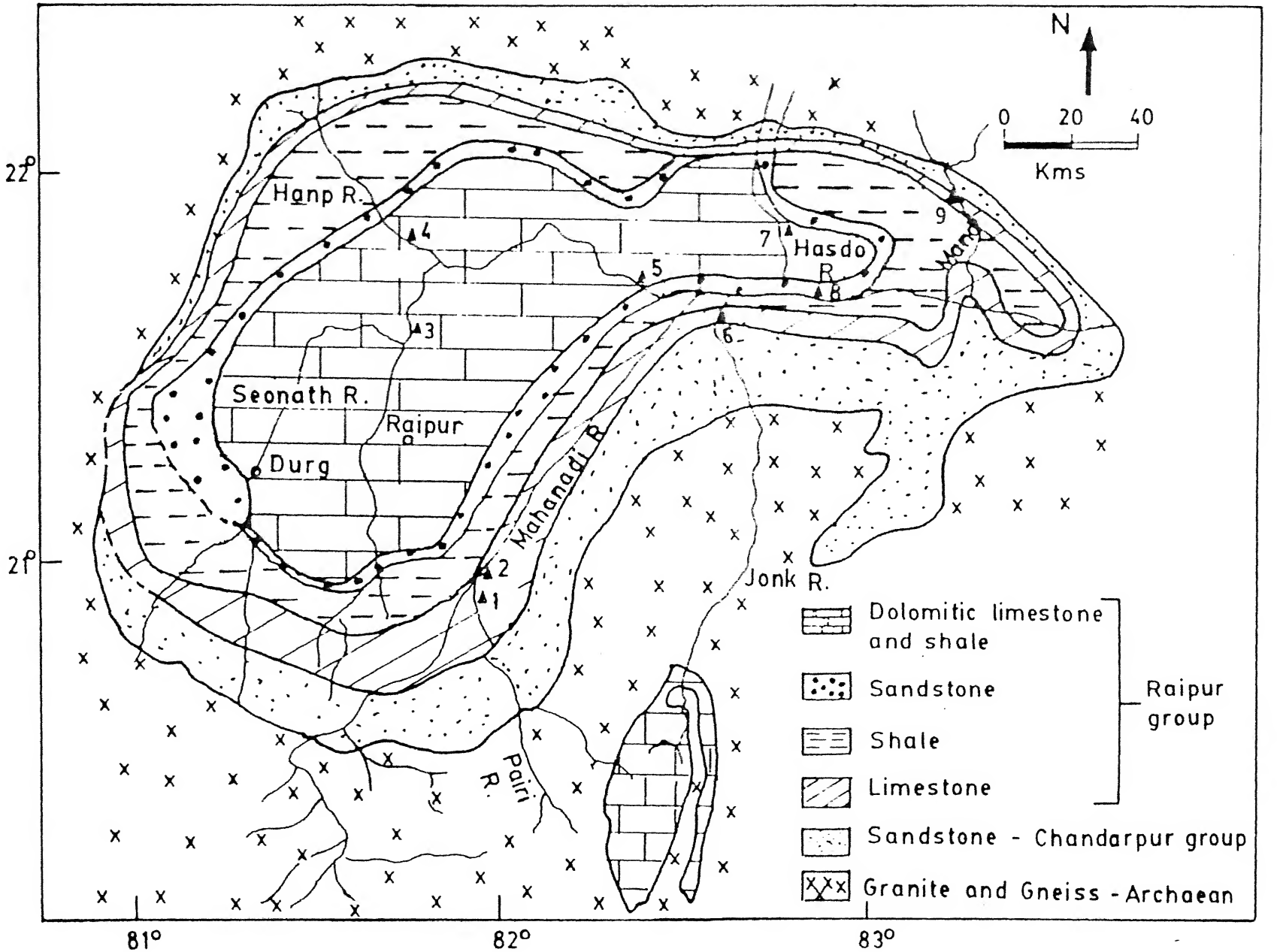

Fig. 3.5 Geological map of Chhattisgarh basin and adjoining areas

Pascoe (1950) was the first to divide the sediments in the basin into two broad categories viz. quartzo-conglomeratic Chandarpur series and overlying Raipur series of shale-limestone sequence. Dutt (1962 and 1964), on the basis of detailed field mapping in the southern part of the basin proposed the first comprehensive stratigraphic succession of the Chhattisgarh basin. He also indicated the possibility of correlating the same with the sediments of adjoining Kurnool and Bastar groups. Schnitzer (1975) reported the cyclic nature of sedimentation within the Raipur series of rocks. He identified five cycles. The formations within each cycle have been demarcated on the basis of sedimentary structures like ripple marks and stromatolites as also the Ca and Mg content of limestones. Murti (1987) established the stratigraphy of the central part of the basin. Das et al..(1989) and Mukherjee (1990) gave the stratigraphic sequence of north-western and south-western part of the basin. A comparative scheme of different parts of the Chhattisgarh basin adopted from Mukherjee (1990) is given in Table 3.2. A simplified and integrated account of lithostratigraphy as applicable to the entire Chhattisgarh supergroup is given in Table 3.3. A summary of the mineralogy of rock samples collected from each formation is given in Table 3.4.

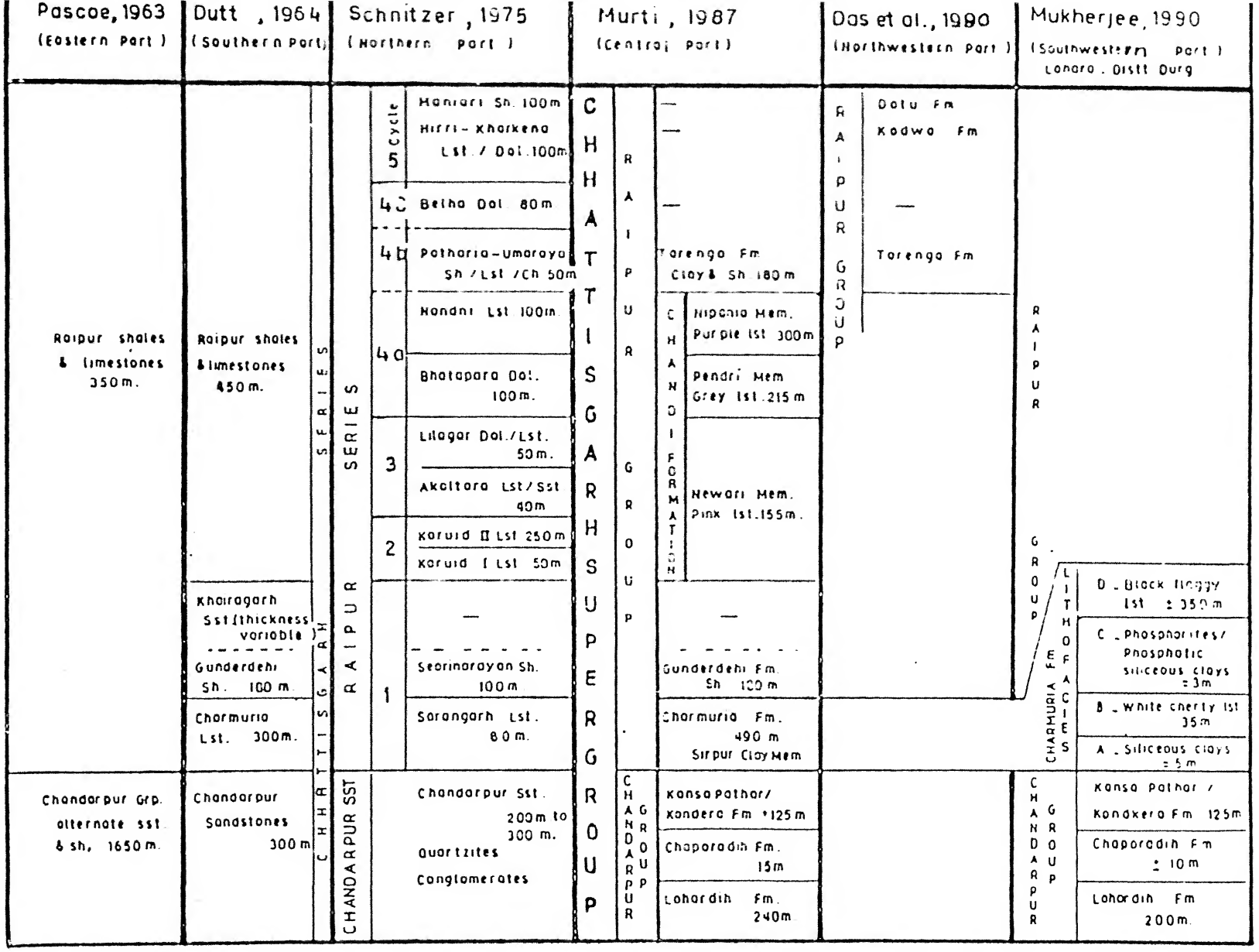

Table - 3.2 Comparative stratigraphic scheme of Chhattisgarh Supergroup.

Table 3.3 Lithostratigraphy of the Chattishgarh Basin (modified after Murti, 1987 and Das et al., 19

Age	Group	Formation	Lithology
Recent			Alluvium and laterite
Chattisgarh Super-group (Mid. to Upper Proterozoic)	Raipur group	Dotu Fm.	Red shale and gypsum
		Kodwa Fm.	Grey and purple dolomitic limestone
		Tarenga Fm.	Purple green and grey shale
		Chandi Fm.	Purple and grey stromatolitic limestone
		Khairagarh Fm.	Ferruginous sandstone
		Gunderdehi Fm.	Purple and grey shale
		Charmuria Fm.	Purple and grey limestone
		~~Unconformity~~~	
	Chandarpur group	Kansa Pathar/ Kondkera Fm.	Siliceous and ferruginous quartz-arenite
		Chapordih Fm.	Reddish brown and olive green glauconitic sandstone
		Lohardih Fm.	White and light pink sub-arkosic sandstone Basal conglomerate
		~~Unconformity~~~	
Archaean			Granite and granite gneiss

Table 3.4 Summary of mineralogy of rock samples by XRD and microscopic examination

Formation	Location	Rock type	Mineralogy
Dotu	Andhiyarkore	Reddish shale	Q + I + Chl + F + K + Hem
Kodwa	Kodwa	Grey limestone	D + Q + C + F
	Rajpura	Shaly limestpne	D + Q + I + F + K + C
Tarenga	Singarpur	Green shale	Q + F + D + C + Chl + K
	Singarpur	Black shale	Q + F + I + D
	Simra	Purple shale	Q + F + K + I + Chl + D
Chandi	Sonadih	Purple limestone	A + C + Q + F + Gl + K + Chl
	Lakchanpur Nala	-do-	D + C + Q + I + K
	Dhaneli	-do-	A + Q + I + F
	Sonbarsa	Grey limestone	D + C + Q + I + K + I/Gl + F
	Dhabadih	-do-	D + C + Q
	Nipania	-do-	D + C + Q
Khairagarh	Binayakpur	Reddish sandstone	Q + Hem + I + K
Gunderdehi	Khorsi Nala	Purple shale	Q + C + F + I + K + Chl + D
Charmuria	Rajim	Grey limestone	C + Q + I
	Durg	Purple limestone	C + Q + I + F + D
Chandarpur	Banrodh and Mudpar	Sandstone and quartz-arenite	Q + F + Gl
Archaean	Several locations	Granite and gneiss	Q + F + B + Px

Q-Quartz, F-Felspar, C-Calcite, D-Dolomite, A-Ankerite, B-Biotite, I-Illite K-Kaolinite, Hem-Hematite, Px-Pyroxene, Chl-Chlorite, Gl-Glauconite

3.5.1 Archaean Basement

Rocks of Archaean age which form the basement of the Chhattisgarh supergroup are exposed in the southernmost part of the region and covers the source area of the Mahanadi river. Grey as well as pink granites and their metamorphic equivalents constitute the predominant rock types. Grey granites are more abundant than the pink ones and show exfoliated surfaces. Grain size increases from grey to pink granites. Laxmi Narayan and Kuity (1988) have suggested a metasomatic origin for these granitic rocks.

Thin section study shows that the granites have two types of felspar, plagioclase and orthoclase in addition to quartz, biotite and pyroxene among the major minerals. Plagioclase grains have pitted surfaces and rarely exhibit lamellar twinning indicating incipient to moderate weathering to clay minerals. The plagioclase composition was estimated to be in the range An_{60}-An_{70} by measuring extinction angles on sections parallel to (001) and perpendicular to (001) and (010) crystallographic planes (after Wahlstrom, 1955). XRD pattern of the samples show characteristic peaks for an anorthite rich plagioclase. K-felspar grains on the other hand, are relatively fresh and show typical cross-hatched twinning.

Granite gneisses are characterized by crudely banded texture. They contain quartz, plagioclase felspar, pyroxene and iron oxides. This plagioclase is also anorthite rich and extensively weathered. Pyroxene grains show alteration to chlorite and clay. A sketch of typical granite gneiss in thin section is given in Fig.3.6. Bulk chemical analysis of one grey granite by XRF gave the following composition in weight percentage.

SiO_2	= 69.93	MgO	= 0.58	K_2O	= 4.87
Al_2O_3	= 14.81	CaO	= 1.66		
Fe_2O_3	= 4.56	Na_2O	= 1.66		

3.5.2 Chandarpur Group

Following the nomenclature of Murti (1987) the Chandarpur group can be sub-divided into three formations namely 1) Lohardih, 2) Chapordih and 3) Kansapathar/Kondkera. This group consists of various types of sandstone and quartz-arenite. These are well developed along the southern margin of the Chhattisgarh basin. It is found that detrital quartz constitutes more than 90% of the sandstones and quartz-arenites. Felspars are scarce to absent. Occurrence of authigenic glauconite pellets in the sandstones of Chapordih formation and detrital glauconites in

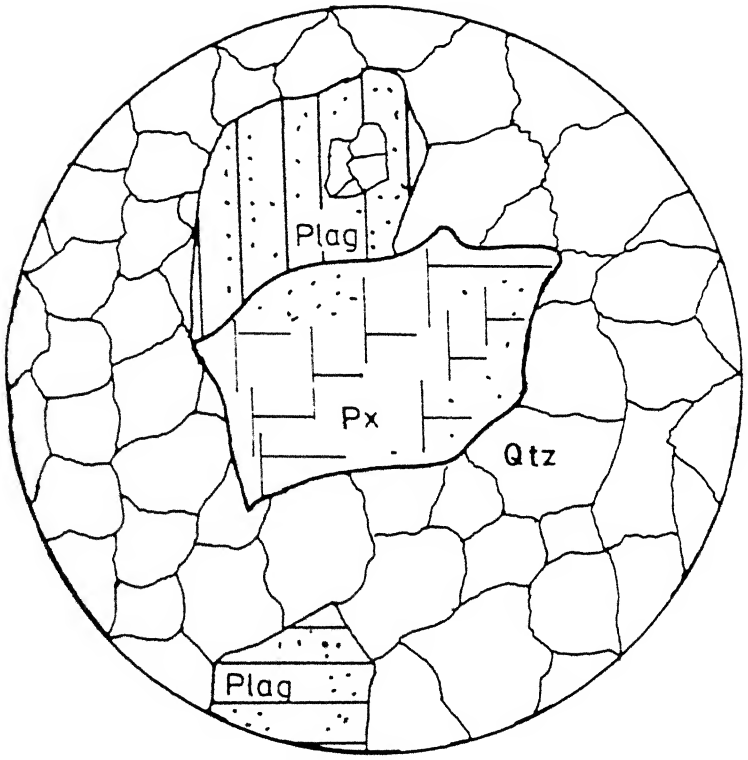

CR_{13} (75 x)

Fig. 3.6 Granite gneiss from chinnar village near Kanker

Kansapathar sandstones have been reported by Murti (1987) and Khan and Mukherjee (1990).

3.5.3 Raipur group

This group of sediments overlie the Chandarpur group of rocks with an erosional disconformity. It essentially consists of limestone-shale sequences with occasional surface and sub-surface occurrences of gypsum. The Raipur group of rocks can be divided into seven formations, viz. 1) Dotu, 2) Kodwa, 3) Tarenga, 4) Chandi, 5) Khairagarh, 6) Gunderdehi and 7) Charmuria. Some of the above formations are either absent or poorly represented in many parts of the basin.

3.5.3.1 Charmuria Formation

This formation is well developed over large areas in the southern part of the basin. It is represented by grey and purple limestones of micritic texture. Towards Rajim, grey varieties of thickly bedded limestone (Fig. 3.7) are exposed while in Durg area massive varieties of purple limestone are noticed. Mineralogically Charmuria limestones are rich in calcite (specially in the grey varieties) and dolomite followed by significant amounts of quartz, plagioclase felspar, illite and kaolinite. Mukherjee and Khan (1989) recorded the presence of quartz, occasional mica, detrital glauconite and pyrite nodules in

Fig. 3.7 Bedding planes in Charmuria limestone

thinly bedded limestones from Lohara (Durg district). Murti (1987) reported a clay horizon (Sirpur member) underlying the Charmuria limestone in the central part of the basin.

Dutt (1962) was perhaps the first to present the chemical composition of charmuria limestone (Table 3.5a) from a number of localities spread over a large area in southern part of Chhattisgarh basin (Fig. 3.8). A much recent set of analysis (Mukherjee, 1990) from Lohara, Durg is given in Table 3.5b for comparison. In both sets of analysis, high CaO in limestone corresponds with low SiO_2 value. To illustrate this, CaO, SiO_2, latitude and longitude values (Table 3.5a) were utilized to generate three dimensional trend surfaces by using a graphics package SURFER. It is seen that a trough in SiO_2 (Fig. 3.9) corresponds to a crest in CaO (Fig. 3.10).

3.5.3.2 Gunderdehi Formation

This formation is well developed in south and southeastern part of the basin. It is represented by purple shales which are medium to very fine grained, thinly laminated and very friable. XRD of samples from Khorsi Nala near Baloda Bazar, show the presence of quartz, calcite, plagioclase, illite/glauconite, kaolinite, chlorite and dolomite (Table 3.4). Authigenic glauconite in purple shale and authigenic baryte in

Table 3.5a Chemical composition of Charmuria limestone (Dutt, 1962)

Sample	SiO_2	Al_2O_3	Fe_2O_3	CaO	MgO	Lat / Long
C5	11.86	2.00		47.72	1.86	$21^0 01' / 80^0 54'$
C9	20.02	3.53	10.85	31.16	0.00	$20^0 52' / 81^0 17'$
C11	31.83	3.81	9.07	29.59	1.21	$20^0 51' / 81^0 49'$
C12	34.13	4.02	11.56	27.81	0.00	$20^0 55' / 81^0 48'$
C13	15.09	2.01	15.17	38.13	0.00	$20^0 58' / 81^0 51'$
C14	23.49	3.59	7.78	36.03	0.00	$20^0 59' / 82^0 00'$
C15	14.60	4.16		43.35	1.20	$21^0 05' / 82^0 03'$

Table 3.5b Chemical composition of Charmuria limestone, Lohara, Durg (Mukherjee, 1990)

Sample	SiO_2	Al_2O_3	Fe_2O_3	CaO	MgO	K_2O
WSC9	20.07	0.80	0.62	42.92	0.26	0.06
LC4	14.93	1.01	0.69	45.83	0.48	0.21
L1	19.23	1.35	0.85	43.15	0.44	0.25
L7	21.36	3.45	1.97	38.21	0.98	0.72
L4	13.79	1.73	1.12	45.38	0.75	0.24

All values of oxides in weight percent

Fig. 3.8 GEOLOGY OF
THE SOUTHERN PART OF CHHATTISGARH, MADHYA PRADESH.
(after Dutt, 1962)

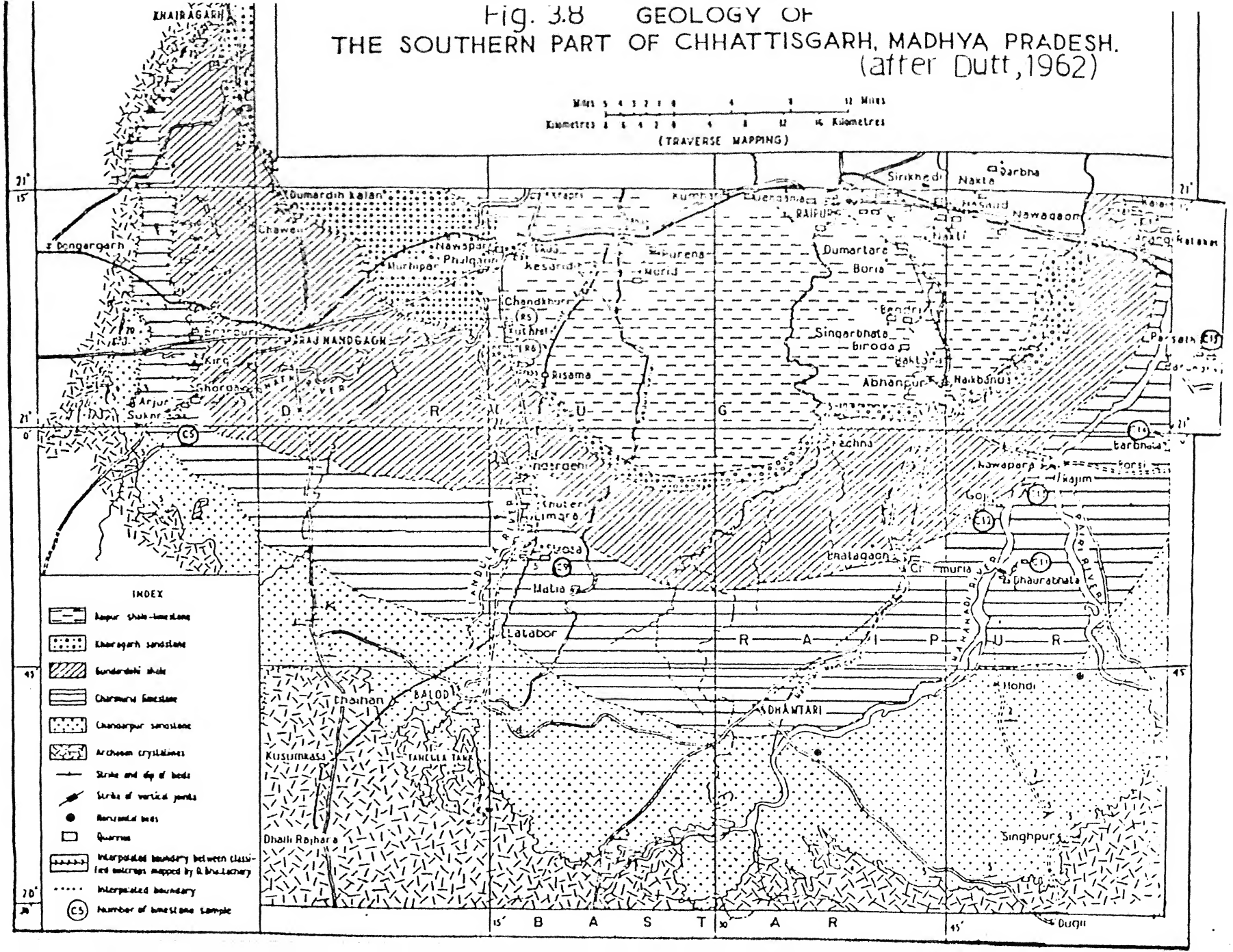

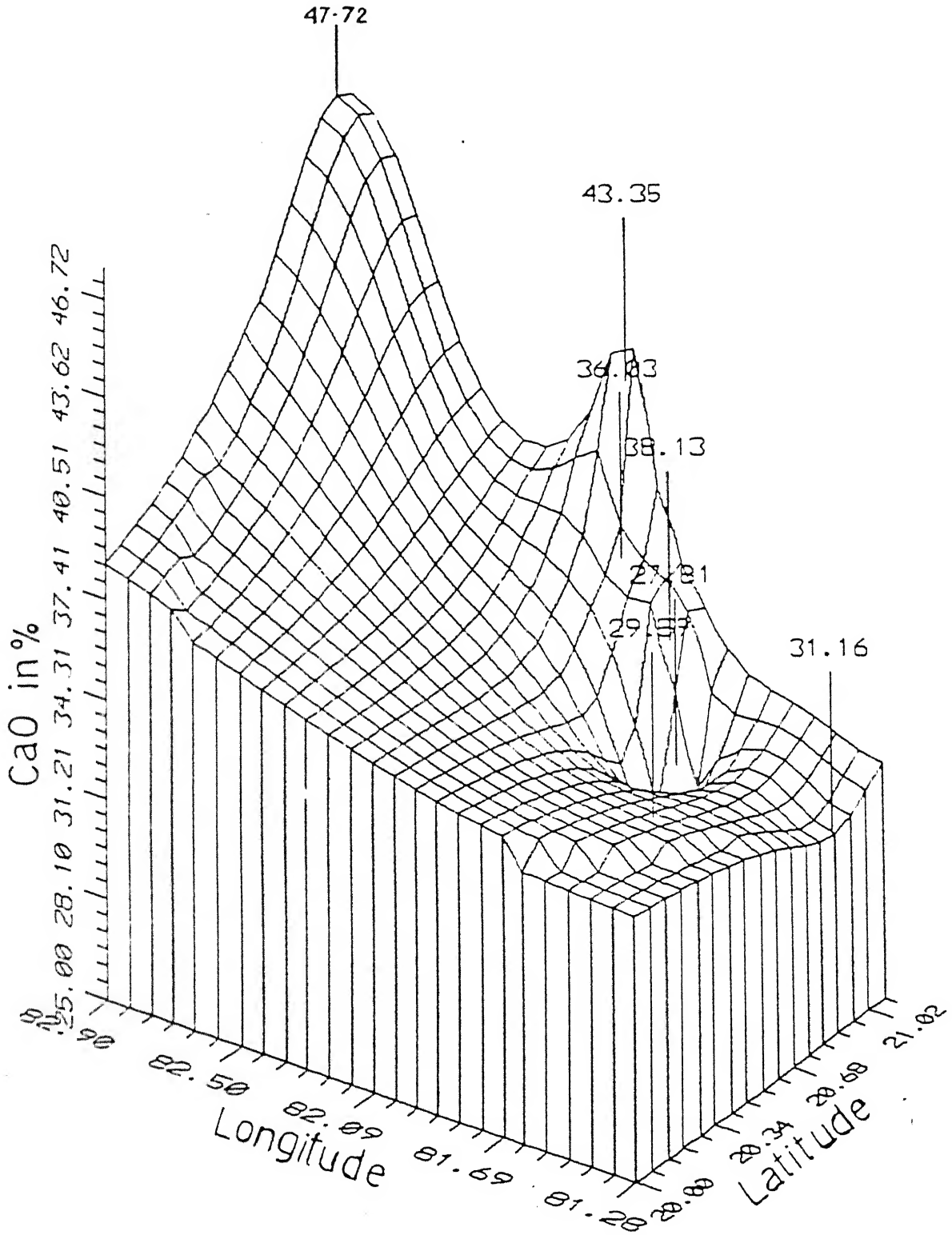

Fig. 3.9 3D trend surface showing variation of CaO in Charmuria limestone

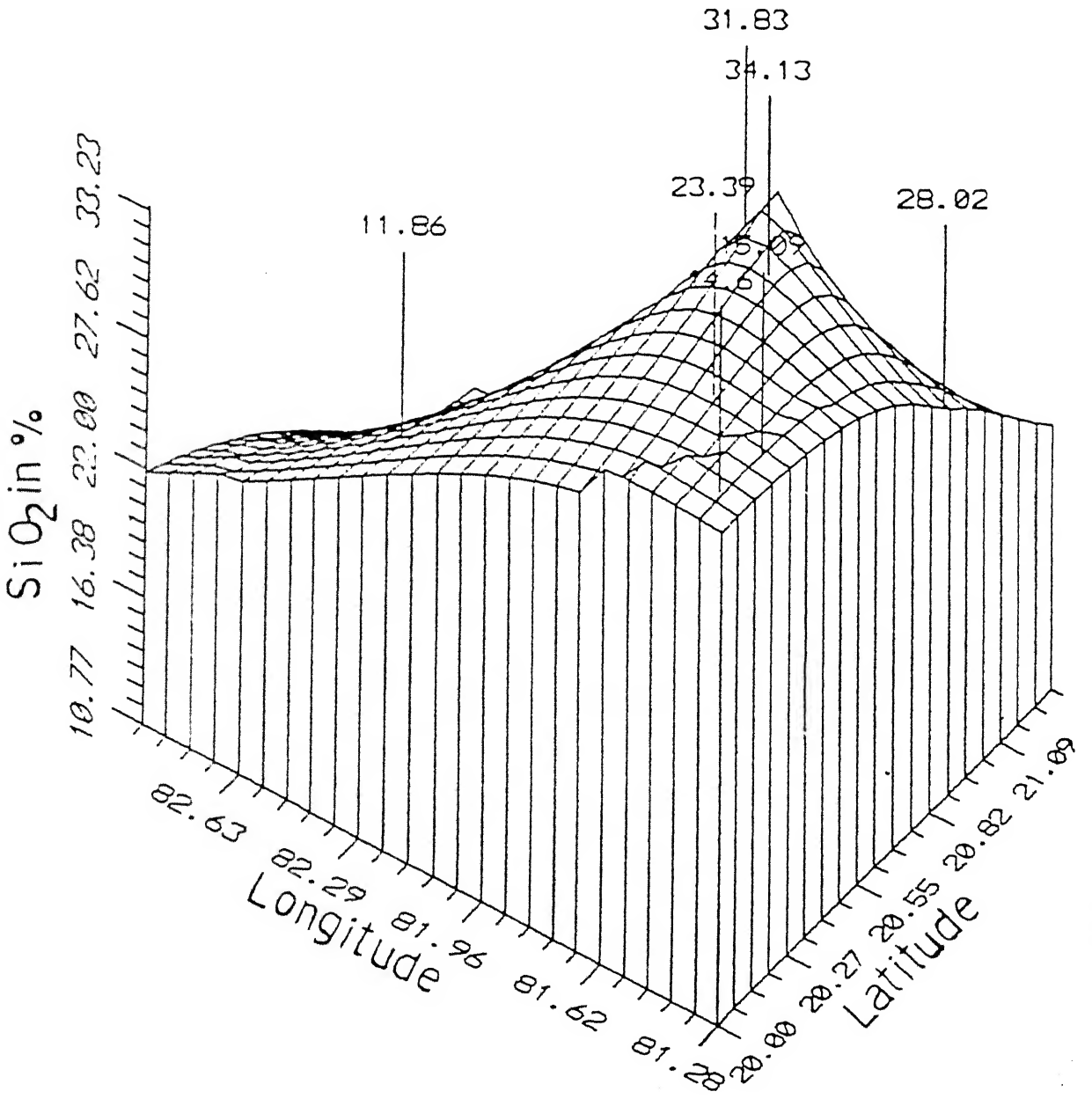

Fig. 3.10 3D trend surface showing variation of SiO_2 in Charmuria limestone

localized grey shale of Gunderdehi formation have been reported by Murti (1987). Sedimentary structures like ripple marks and mud cracks are easily noticeable.

3.5.3.3 Khairagarh Formation

Dutt (1964) suggested that this formation is younger than Gunderdehi shales. It is well developed only in the southern part of the basin and is represented by medium grained ferruginous sandstone. The sandstone is deep red in colour and contains abundant black iron mineral grains. Under the microscope, irregular black iron-oxide grains are observed to surround the oval quartz grains. Microscopic and X-ray analysis of samples from Binayakpur, 15 km south of Durg, showed the presence of quartz and hematite in equal proportions followed by the clay minerals illite and kaolinite.

3.5.3.4 Chandi Formation

This formation conformably overlies the Gunderdehi and is widely exposed in the basin. It is represented by massive limestones of grey and purple colour. Grey varieties are more fine grained than the purple varieties. One prominent feature of these limestones is the extensive growth of stromatolites. The stromatolites are either LLH (laterally linked hemispheroids) or

SH (discrete vertically stacked hemispheroids) type. Both LLH-C and LLH-S modes are common while SH-V modes are noticed in larger blocks of limestone. Stromatolite columns are separated by calcareous mud and stand out prominently on weathering.

Structural features such as bedding planes are not very common although joints, both open and closed, are observed in massive varieties. Stylolites are found at places. Dark grey limestones often carry thin veins of pure calcite in them. XRD analysis of a number of samples from Chandi formation revealed that these limestones are impure. They contain silicate minerals like quartz, albitic felspar, illite/glauconite, kaolinite and chlorite in addition to calcite, dolomite and ankerite. Detailed study of the nature of weathering of this limestone is separately treated in Chapter-7.

3.5.3.5 Tarenga Formation

This formation which overlies the Chandi limestone is well exposed in the central part of the basin. It consists of shales of different colour and composition. Calcareous ones are generally purple with interbedded chert while the more argillaceous varieties are green and dark grey. X-ray diffraction study of shale samples collected near Singarpur village, showed calcite and dolomite in varying proportions while the green and

purple shales were found to contain additional chlorite and kaolinite. Dark grey varieties were almost devoid of any clay mineral. Montmorillonite could not be confirmed in any of the samples collected during this work although Murti (1987) reported occurrence of pure montmorillonite in cherty pink shales from the above area.

3.5.3.6 Kodwa and Dotu Formations

These two formations conformably overlie Tarenga shales. Dotu formation being the youngest of the two, has been exposed in the north-western part of the basin (Das et al., 1990). Kodwa formation consists of reddish, medium to coarse grained shaly dolomitic limestone and fine grained dark grey dolomitic limestone. X-ray mineralogy of reddish limestone from Rajpura near Kodwa, shows abundance of dolomite and negligible amount of calcite. Other silicate minerals are quartz, illite, felspar, kaolinite and chlorite. Grey limestones of Kodwa, on the other hand, are composed of significant amounts of dolomite and calcite besides minor proportions of quartz and felspar.

The lithounit representing Dotu formation is essentially an argillaceous red shale horizon. Extensive exposures are observed at Bemetra and on the banks of the Hamp river at Andhiyarkore (Fig. 3.11). Andhiyarkore shale consists of quartz,

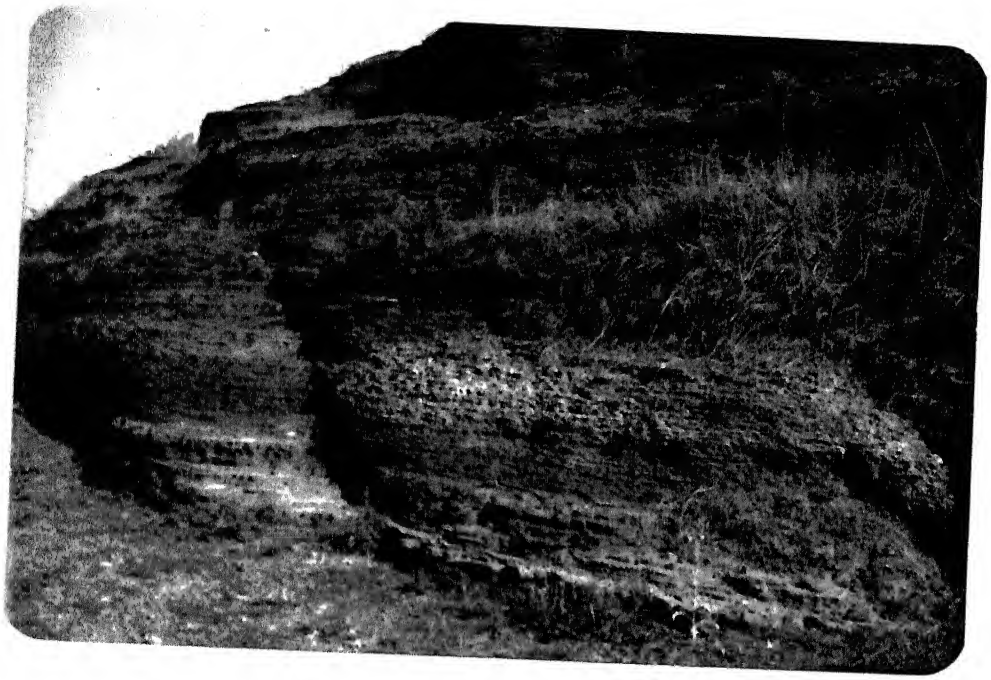

Fig. 3.11 Bedded red shale of Dotu formation exposed at Andhiyarkore

illite, expandable chlorite, felspar, kaolinite and hematite minerals as identified by X-ray diffraction analysis. These shales are found to contain calcite crystals in vugs. Das et al. (1990) reported the occurrence of gypsum beds mainly within the Dotu formation and partly in the Kodwa formation based on few surface occurrence and drill hole data.

CHAPTER-4

PHYSICAL VERSUS CHEMICAL EROSION

Study of river erosion and sedimentation processes is important because of their environmental and economic impact. The effect of river on watershed is evident through physical and chemical weathering. A large river like Mahanadi supplies suspended as well as dissolved inputs to the ocean. Neglecting human activities, the suspended load is mainly derived by the physical breakdown (disintegration) of rocks in the drainage area. The stage of erosion is reflected in river landforms like channel and valley features. In a similar way, the dissolved load of the river is controlled by chemical reaction between river water and rock-forming minerals. The details of these processes are discussed below.

4.1 Stage of River Erosion

Longitudinal profiles, hypsometric curves and sediment fluxes are some of the morphological information which help in expressing river erosion in a quantitative way. In order to assess the stage of erosion in the Upper Mahanadi basin, a fourth order tributary near the source area was selected. A longitudinal profile of this stream (Fig. 4.1) was plotted by

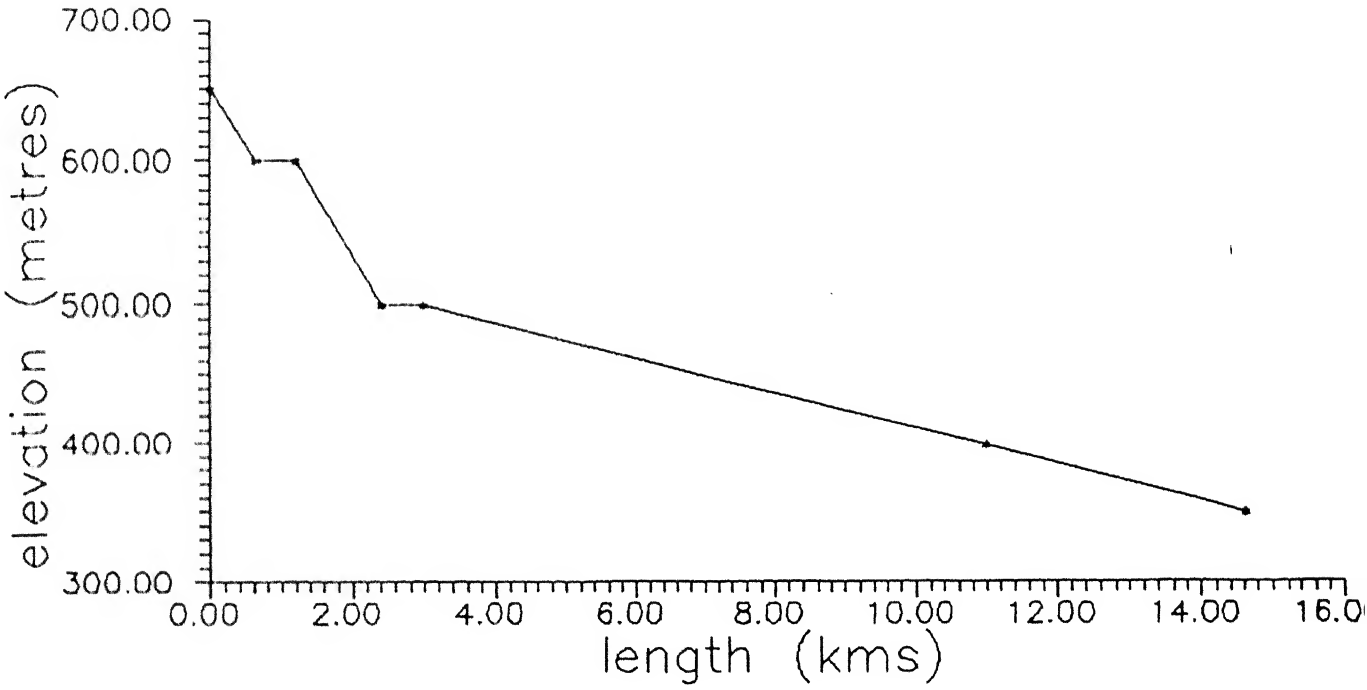

Fig. 4.1 Longitudinal profile of the Turi Nadi

using Toposheet No. 64H of scale 1:250,000. The data are listed in Table 4.1(a). This profile shows nick points and steep slopes which are indicative of an active physical erosion process in the upland area. The downstream segment has already approached an equilibrium profile.

The hypsometric curve which investigates the area-altitude relationship within a drainage basin also helps in identifying the stage of river erosion. Following the method of Strahler (1952), height ratios were obtained by first determining the total range of contours between the confluence with the main river and the summit point of the Turi Nadi. The height of each measured contour above the confluence is then determined and ratios to total basin height computed [Table 4.1(b)]. The ratios were then plotted and a smooth curve was drawn passing through the data points (Fig. 4.2). It is seen from this hypsometric analysis that 64.4% of the land mass has already been eroded and 35.6% of the land mass in the drainage basin remains to be eroded.

4.2 Denudation Regime

Topography produced by weathering, mass movement and stream run-off is complex. The concept of denudation regimes (Carson and Kirby, 1972) is explained in terms of weathering and transport in relatively flat or steep terrains. Two extremes of

Table 4.1(a) Data for longitudinal profile of Turi Nadi

Elevation (m)	Stream length (km)
650	0
600	0.63
600	1.20
500	2.42
500	3.00
400	11.00
350	14.62

Table 4.1(b) Hypsometric data for Turi Nadi

Absolute contour(m)	Relative height(m) <h>	Total height(m) <H>	Area above contour(km^2) <a>	Total basin area(km^2) <A>	h/H	a/A
800	450	450	0	141.036	1	0
700	350	450	8.876	141.036	0.77	0.063
600	250	450	33.566	141.036	0.55	0.238
500	150	450	63.786	141.036	0.33	0.452
400	50	450	132.426	141.036	0.11	0.939
350	0	450	141.036	141.036	0	1

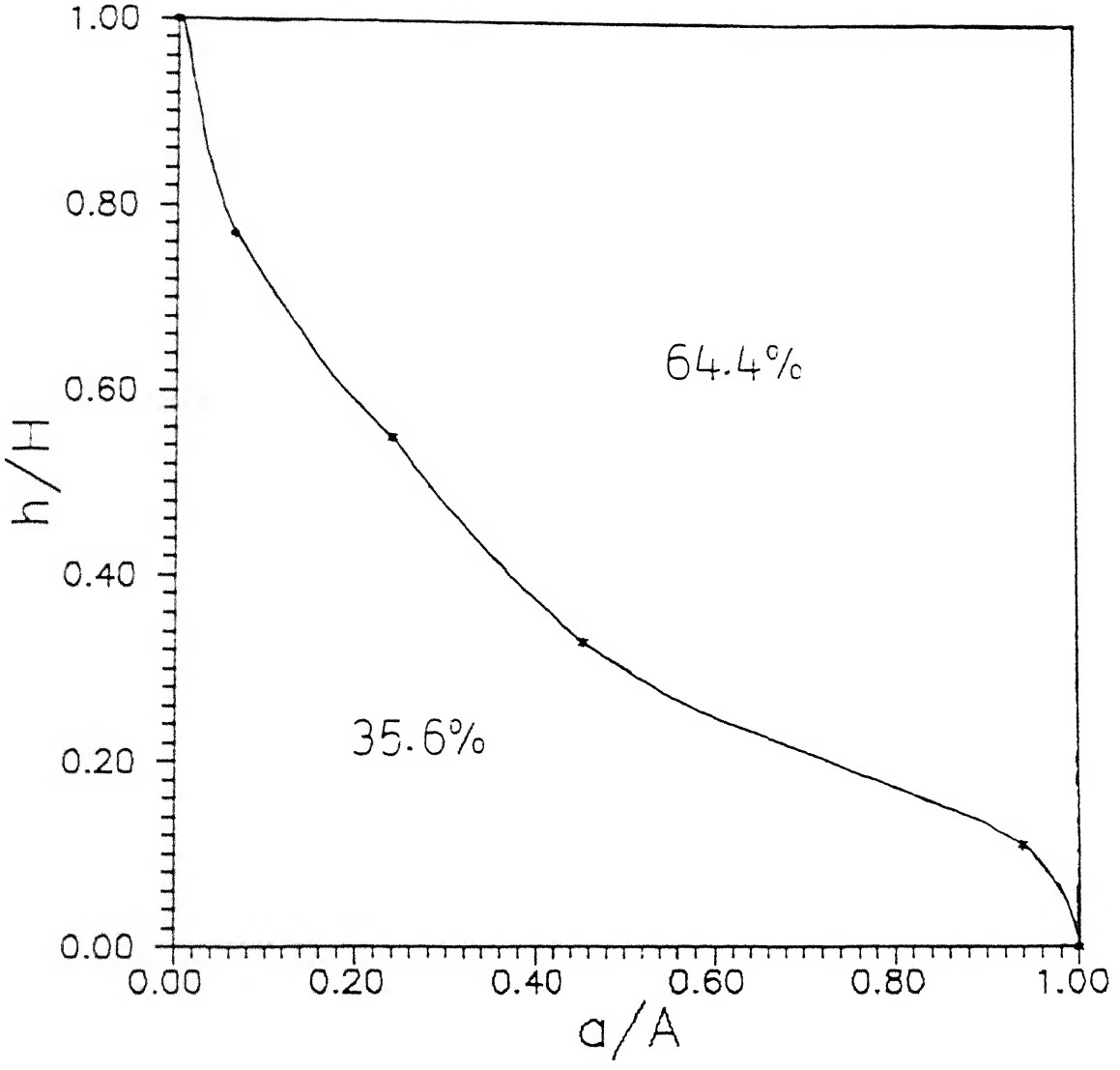

Fig. 4.2 Hypsometric curve for the Turi Nadi

denudation regime as discussed by Stallard and Edmond (1983) are a) weathering limited where rate of transport is faster than that of generation of weathered materials, b) transport limited where rate of transport is less than that of generation of weathered products. A weathering limited denudation regime has the following characteristics : 1) development of thin soil profiles or bare rock surfaces, 2) presence of partially weathered primary minerals in the stream load, 3) availability of less time for soil and water interaction, 4) imprint of weathering of various rock types on the sediment load.

Field observations in the upper part of the Mahanadi basin revealed wide occurrence of limestone exposures without any soil cover. Thin soil profiles are developed on local scales. Mineralogical examination of river suspended sediments show the presence of unweathered felspar and occasionally calcite besides a host of clay minerals [Table 4.2(b)]. This may be due to lack of sufficient time of interaction between physically eroded materials and river water. Size analysis of suspended sediments of four upland tributaries show that about 70% of the material is in the silt fraction [Table 4.2(a)]. These features are consistent with transport dominant or weathering limited condition. This is further validated by a higher suspended load compared with dissolved load carried by the river. Details of

Table 4.2(a) Grain size distribution of suspended sediments(%)

Size (μm)	Sample location			
	Baronda	Rajim	Simga	Andhiyarkore
> 20.66	--	--	--	--
20.66	2.33	--	--	--
16.40	6.30	--	--	1.51
13.01	8.75	1.41	2.21	1.69
10.33	5.16	3.77	3.65	2.45
8.20	4.90	3.54	2.43	3.72
6.51	21.00	10.70	26.19	27.55
5.16	5.51	16.04	15.51	9.13
4.10	5.84	4.58	4.27	8.01
3.25	10.75	6.70	6.18	5.77
2.58	6.91	5.31	7.73	7.06
2.05	5.86	9.24	5.06	8.75
1.63	5.97	13.21	4.35	9.17
1.29	5.31	15.29	11.66	7.27
1.03	2.66	4.93	6.14	3.92
0.81	1.72	3.43	3.08	2.67
0.65	1.05	1.88	1.56	1.34
Mean size (μm)	6.10	4.33	4.33	5.13

'--' = absent

Table 4.2(b) Mineralogy of suspended sediments

1) Baronda : Q + I + K + F	2) Rajim : Q + I + K + F
3) Simga : Q + I	4) Andhiyarkore : Q + Mo + I + K + Chl

Q - Quartz; I - Illite; K - Kaolinite; F - Felspar; Mo - Montmorilloni
Chl - Chlorite; C - Calcite

sediment loads are discussed in the following section.

4.3 Sediment Flux and Erosion Rate

In the Mahanadi river, CWC has 13 gauging stations where measurements for discharge and suspended sediment are carried out on a daily basis. Therefore, available information on basin area, discharge and suspended load for the water year 1980-85 were compiled from CWC sources. These were the latest when this work was started. Annual average suspended load was calculated from daily measurements while annual average dissolved load was estimated from monthly specific conductance measurements. Conductance values were discharge weighted and the average thus obtained was multiplied by a factor of 0.65 to get the discharge weighted total dissolved solids (TDS) in mg/l. Annual suspended loads at 13 sampling stations are presented in Table 4.3. Suspended load carried by the river during monsoon and nonmonsoon periods for the year 1984-85 are listed in Table 4.4. Total physical load was estimated by adding a bed load value equivalent to 10% of the suspended load as suggested by Blatt and Middleton (1972), to the suspended load value. Estimates of physical and chemical erosion rates are given in Table 4.5.

It is obvious from Table 4.4 that almost all of the suspended load is carried during the monsoon period. Since

Table 4.3 Annual suspended load at CWC stations

Location	Suspended load (million tonnes)					
	1980-81	1981-82	1982-83	1983-84	1984-85	Average
1)Baronda	8.04	0.23	0.84	0.84	0.42	2.07
2)Rajim	13.60	1.90	0.74	0.59	0.51	3.47
3)Simga	3.42	1.70	1.35	2.05	2.38	2.18
4)Andhiryarkore	0.93	0.39	0.45	0.49	0.50	0.55
5)Jondhra	0.02	2.55	3.70	5.25	8.08	3.93
6)Rampur	1.07	0.40	0.91	0.35	0.73	0.69
7)Bamnidih	7.09	2.74	4.96	4.58	7.70	5.41
8)Basantpur	36.17	15.24	8.53	16.32	17.07	18.67
9)Kurubhata	2.47	1.58	2.58	2.55	3.14	2.41
10)Sundergarh	2.21	3.09	2.63	2.45	5.73	3.22
11)Salebhata	2.03	0.64	4.02	0.85	1.51	1.81
12)Kantamal	9.71	6.39	5.87	5.20	7.88	7.01
13)Tikarpara	43.79	19.11	42.13	22.23	13.15	28.08

Source: Central Water Commission (CWC)

Table 4.4 Seasonal suspended load distribution (year 1984-85)

Location	Sediment load (tonnes)		Sediment load (%)	
	Monsoon	Premonsoon	Monsoon	Premonsoon
1)Baronda	419816	--	100	--
2)Rajim	506287	--	100	--
3)Simga	2378124	2403	99.9	0.1
4)Andhiryarkore	504211	439	99.9	0.1
5)Jondhra	8082739	1699	99.98	0.02
6)Rampur	729426	--	100	--
7)Bamnidih	7704515	7686	99.9	0.1
8)Basantpur	17069509	19526	99.89	0.11
9)Kurubhata	3141892	8610	99.73	0.27
10)Sundergarh	5732809	4671	99.9	0.1
11)Salebhata	1513251	--	100	--
12)Kantamal	7881677	2595	99.97	0.03
13)Tikarpara	13152194	51441	99.61	0.39

Source: Central Water Commission (CWC); '--' denotes negligible.

Table 4.5 Rate of erosion

Location	Stream	Basin area (sq.km)	Average discharge (m^3/sec)	Sediment load@ (m.t/yr)	Q wtd. TDS (mg/l)	Physical erosion rate (t/sq.km/yr)	Chemical erosion rate (t/sq.km/yr)	Phy : erc
1) Baronda	Pairi	3225	41.20	2.28	40.85	706.98	16.46	43
2) Rajim	Mahanadi	8760	73.95	3.82	50.08	436.07	13.33	32
3) Simga	Seonath	16060	169.58	2.40	145.99	149.44	48.61	3
4) Andhiyarkore	Hamp	2210	10.24	0.60	214.81	271.49	31.39	8
5) Jondhra	Seonath	29645	213.06	4.32	122.65	145.72	27.80	5
6) Rampur	Jonk	2920	47.96	0.76	83.52	260.27	43.26	6
7) Bamnidih	Hasdo	9730	179.39	5.95	59.27	611.51	34.46	17
8) Basantpur	Mahanadi	57780	675.27	20.54	92.46	355.49	34.08	10
9) Kurubhata	Mand	4625	73.63	2.65	39.82	572.97	20.00	28
0) Sundergarh	Ib	5870	99.92	3.54	48.01	603.07	25.77	23
1) Salebhata	Ong	4650	74.36	1.99	87.77	427.96	44.26	9
2) Kantamal	Tel	19600	265.48	7.71	87.82	393.37	37.51	10
3) Tikarpara	Mahanadi	124000	1622.52	30.89	85.05	249.11	35.09	7

Sediment load = Suspended load + Bed load(assumed to be 10% of the suspended load)

monsoon rainfall in the Mahanadi basin constitutes bulk (86%) of the total, sediment yield seems to be strongly correlated with discharge. Figs. 4.3(a) and 4.3(b) constructed from the data in Table 4.3 show that sediment load fluctuates widely with time at most of the sampling stations.

At Tikarpara, the Mahanadi annually carries a total load of 35.24 million tons. Out of this, physical load constitutes 30.89 million tons while chemical load is only 4.35 million tons. However, Chakrapani and Subramanian (1990a) reported a different set of values which might be due to the different sampling and computational technique adopted by them. Erosion rate estimations for each of the tributaries (Table 4.5) show that the ratio of physical to chemical erosion in the entire Mahanadi basin up to Tikarpara is 7.1 : 1. The rate of physical erosion is the highest (707 $t/km^2/yr$) for the upland tributary Pairi followed by Hasdo, Mand and Ib river. This is possibly due to the fact that the relief of these basins is much higher than the base level of erosion compared with other sub-basins. If we consider the ratio of physical to chemical erosion rates, on the other hand, the values are comparatively low for Seonath and Jonk river basins apparently because these rivers drain chemically reactive sedimentary rocks like limestone.

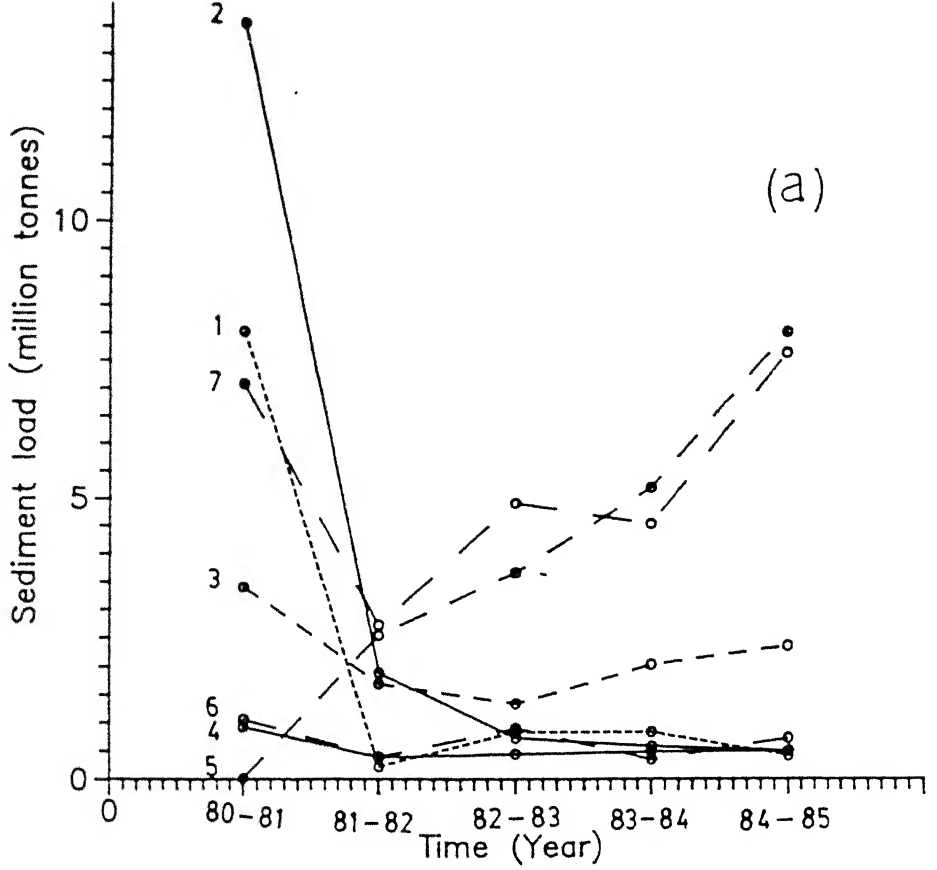
(a)
Sediment load (million tonnes)
0
5
10
2
1
7
3
6
4
5
0
80-81
81-82
82-83
83-84
84-85
Time (Year)

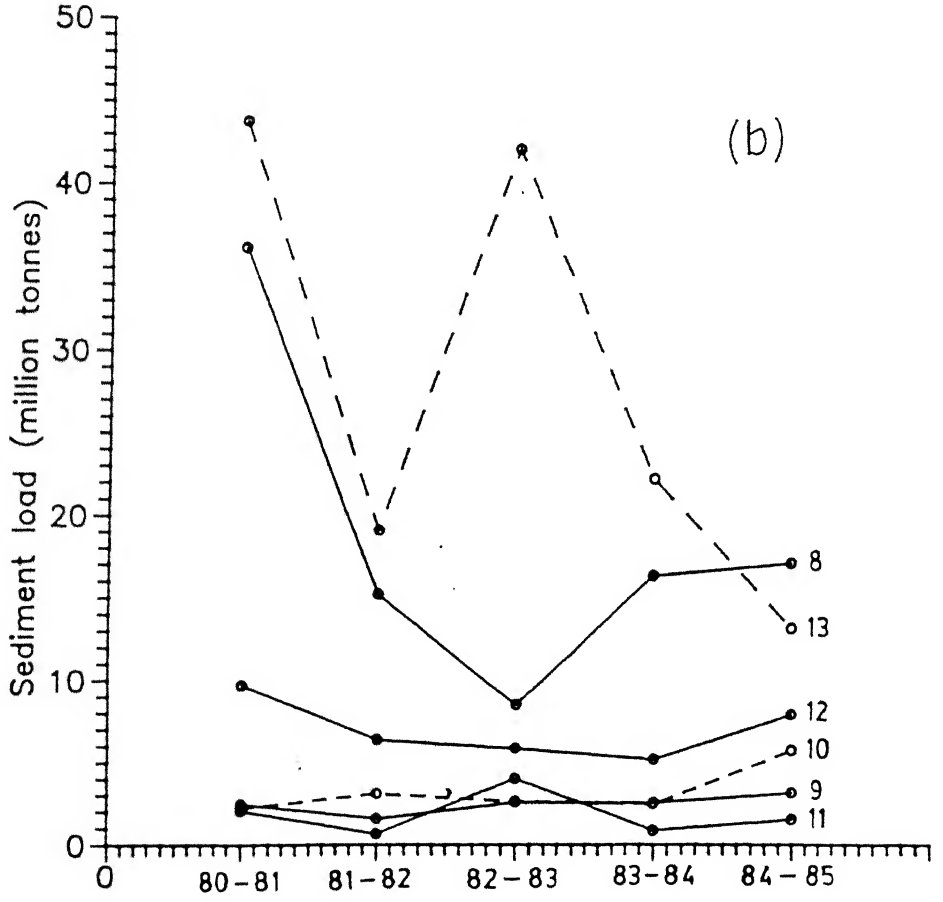
(b)
Sediment load (million tonnes)
0
10
20
30
40
50
8
13
12
10
9
11
0
80-81
81-82
82-83
83-84
84-85

4.4 Grain Size and Mineralogy of Sediments

Sediment size distribution of suspended and bed loads are useful for proper understanding of transport and deposition mechanisms. Size distribution of suspended sediments from stations 1, 2, 3 and 4 during the sampling period January, 1990 is given in Table 4.2(a). It is seen that 5.7 μm fraction dominates over other size populations. Mean size range of suspended sediments is 4.33 to 6.10 μm. As discussed earlier, nearly 70% of the sediment is carried in the silt fraction. Clay fraction (<2μm) constitutes only 16.7% for the Pairi river draining dominantly siliceous rocks compared to 26.8% and 24.4% for the Seonath and Hamp respectively. These rivers drain carbonate rich sedimentary terrains. Mahanadi at Rajim, on the other hand, carries highest percent (38.7) of sediment in clay fraction. It drains both silicate and carbonate rocks in its catchment. Thus it seems grain size is possibly influenced by the rock type in the drainage area.

X-ray study of suspended sediments [Table 4.2(b)] reveals that quartz and illite are present at all the sampling stations. Kaolinite, montmorillonite and chlorite are the other major clay minerals. Minor to trace quantities of felspar and calcite were also identified in some samples.

Table 4.6 Mean size of bed sediments

Location	Average mean diameter (μm)					
	1980 - 81			1981 - 82		
	Pre	Mon	Post	Pre	Mon	Post
1) Baronda	1151	1216	1325	1418	1271	999
2) Rajim	1785	2621	2678	2555	2666	2130
3) Simga	1109	1352	723	793	1468	906
4) Andhiyarkore	7110	3175	2479	5831	1457	1000
5) Jondhra	1579	1282	2018	1536	1869	1545
6) Rampur	1402	1722	2808	2122	1930	2225
7) Bamnidih	709	997	762	1151	694	687
8) Basantpur	955	801	921	902	970	1233
9) Kurubhata	824	992	1058	1099	1032	1330
10) Sundergarh	1400	1479	1942	1674	2027	1885
11) Salebhata	1134	1481	1744	1264	1305	1321
12) Kantamal	1316	922	1225	976	917	1475
13) Tikarpara	2159	940	2044	1743	1513	1964

Pre : May-June samples, Mon : October-November samples,

Post : December samples; Source : CWC

Bed sediment data reported by CWC (Table 4.6) for the year 1980-82 show that average mean size is generally higher than 1000 μm. Lack of significant change in grain size during different sampling seasons indicates that discharge is not a controlling factor for the size of the bed sediments at all the stations except Andhiyarkore. Premonsoon samples of this station, however, record higher grain size.

CHAPTER-5

RIVER WATER COMPOSITION

5.1 Database

Over the years a large amount of water quality data for Indian rivers has been generated by many organisations and individuals. Among them, Central Water Commission (CWC) under the Ministry of Water Resources, Government of India undertakes long term water quality studies for major river basins of India on a regular basis. Water samples collected on the first of every month are analyzed in CWC laboratories and the data are published for restricted circulation in the form of separate books for each water year starting from June of one year to the May of the next.

For the present study, five year CWC water quality database was preferred over periodic short-term water analyses. The reasons for this preference are the following.

a) A continuous period of five years is reasonably long for any water quality assessment study. Hem (1991) suggests that a more intensive investigation of a smaller database can help build useful models compared to a wider database where measurements and analysis become routine.

b) Such a database is capable of deciphering long term trends or lack of trends in water quality. It also takes care of seasonal

variation of dissolved constituents and isolates probable causative factors affecting them.

c) The discharge and silt load data provide scope for better understanding of input-output budgets because it covers both lean and peak flow periods. One is likely to miss these variations and ultimately arrive at doubtful figures in a short term sampling period.

d) The thirteen sampling stations selected are uniformly distributed all over the basin representing all the major tributaries (Fig.3.3).

e) Samples are collected on first of every month and are analyzed within a week.

f) Analysis is carried out for sixteen major and minor chemical parameters e.g. pH, E.C, TDS, HCO_3, Cl, SO_4, NO_3, PO_4, NH_4, SiO_2, Ca, Mg, Na, K, Fe and Al by standard procedures.

Keeping the above merits in view, the CWC data can be safely assumed to provide a representative water analysis for the Mahanadi river. Therefore, in the present study, monthly water analyses were retrieved from CWC water-year books from 1980-1985 for the 13 sampling stations on the major tributaries and the main channel. This was the latest available database when this work was initiated.

5.2 Average Water Composition

The composition of water passing a fixed sampling station varies with time. A series of monthly measurements for five years can provide mean, extreme and standard deviation which summarize the record of the sampling period. Table 5.1 lists the maximum, minimum, mean and standard deviation for concentration of 16 chemical characteristics mentioned earlier. The mean water composition for each of the 13 sampling stations has been separately presented in Table 5.2. This was used for subsequent calculations and various interpretations at different stages of this work.

The mean composition of Mahanadi river water shows certain broad features. Like most Indian rivers, the water is alkaline in nature. Bicarbonate is the most dominant ion followed by calcium, sulphate, silica and sodium. TDS is in the range of 76 to 343 mg/litre.

5.3 Cation-Anion Balance

Charge balance verification of cations and anions on an equivalent basis provides a check for analytical precision and therefore, reliability of a database. For this purpose, the mean concentrations of dissolved species were converted to micro-equivalents per litre. Charge discrepancy was then

Table 5.1 Summary of CWC water analysis data

Station		pH	E.C	TDS	Fe	Al	NH_4	NO_3	PO_4	SiO_2	Na	K	Ca	Mg	HCO_3	Cl	SO_4
1)Baronda	max	8.22	588	343	4.66	0.190	0.20	9.50	0.54	60.00	17.00	19.70	47.00	9.20	153.0	57.00	55.00
	min	5.49	45	40	0.00	0.000	0.00	0.00	0.00	3.00	2.00	1.00	7.10	1.20	8.0	4.00	0.00
	avg	7.23	102	77	0.57	0.009	0.02	0.83	0.06	14.02	4.83	2.05	12.68	2.88	51.3	9.71	10.04
	sd	6.41	73	52	0.83	0.034	0.04	1.76	0.12	9.85	2.40	2.80	5.51	1.73	20.1	7.46	12.44
2)Rajim	max	8.14	305	211	4.66	0.190	0.79	9.50	1.20	45.00	24.00	4.95	32.10	7.90	121.0	26.00	52.50
	min	6.50	47	49	0.00	0.000	0.00	0.00	0.00	2.00	2.00	1.05	7.10	1.20	27.0	4.00	0.00
	avg	7.21	148	106	0.52	0.009	0.05	0.88	0.06	14.28	7.07	1.93	18.35	3.79	74.0	10.05	6.98
	sd	0.35	57	35	0.76	0.034	0.15	1.44	0.18	8.99	3.95	0.75	5.84	1.55	25.0	4.65	9.71
3)Simga	max	8.30	519	352	2.90	0.160	2.40	7.70	2.04	49.00	42.50	21.00	45.70	26.00	199.0	34.00	69.00
	min	6.76	142	93	0.00	0.000	0.00	0.01	0.00	2.50	4.50	1.60	18.40	1.90	69.0	6.00	3.50
	avg	7.75	328	195	0.33	0.006	0.15	1.67	0.89	14.12	19.58	5.01	31.07	10.41	141.7	15.19	21.10
	sd	0.33	91	48	0.45	0.023	0.39	1.42	0.28	8.54	8.51	3.51	6.19	4.43	33.9	5.46	13.56
4)Andhi-yarkore	max	8.70	1076	613	4.80	0.160	1.00	4.80	1.56	72.50	120.00	17.50	64.30	34.10	318.0	33.00	164.00
	min	7.09	116	47	0.00	0.000	0.00	0.03	0.00	2.00	7.50	1.95	4.50	1.60	55.0	5.00	0.50
	avg	7.76	379	343	0.74	0.007	0.06	1.88	1.00	19.16	43.61	4.14	39.56	17.82	222.2	15.28	57.45
	sd	0.34	227	117	0.94	0.025	0.17	1.34	0.24	12.09	26.49	2.42	9.37	7.86	70.9	6.76	29.77
5)Jondhra	max	8.54	740	360	4.44	0.200	0.52	5.20	1.20	40.50	65.50	11.44	64.30	26.00	220.0	78.00	92.50
	min	6.93	81	60	0.00	0.000	0.00	0.00	0.00	2.00	2.00	1.60	9.20	1.90	42.0	4.00	3.00
	avg	7.77	361	213	0.76	0.012	0.03	0.15	0.11	16.40	22.76	3.89	30.85	12.51	143.6	16.55	32.34
	sd	0.47	160	72	1.20	0.038	0.08	1.05	0.21	9.52	12.54	1.91	9.99	5.99	44.7	11.15	17.15
6)Rampur	max	8.14	366	264	2.24	0.120	0.20	4.00	0.72	31.50	26.50	3.20	40.60	11.70	164.0	31.00	51.00
	min	6.69	85	85	0.00	0.000	0.00	0.00	0.00	0.50	4.50	0.72	10.00	1.30	42.0	7.00	0.00
	avg	7.58	238	153	0.44	0.007	0.01	1.27	0.07	14.20	13.62	1.88	26.60	6.64	114.2	11.85	10.35
	sd	0.36	72	36	0.51	0.022	0.04	1.05	0.16	8.26	5.49	0.54	7.09	2.35	32.8	3.82	11.38
7)Bamnidih	max	8.13	431	292	5.40	0.160	0.30	10.00	0.52	50.00	25.00	9.10	42.00	11.90	113.0	47.00	101.50
	min	6.59	51	47	0.00	0.000	0.00	0.00	0.00	2.00	2.50	1.45	7.10	1.20	22.0	4.00	0.00
	avg	7.35	173	126	0.86	0.009	0.03	1.52	0.07	14.75	11.16	3.03	17.64	4.53	73.0	11.40	20.32
	sd	0.38	85	50	1.22	0.029	0.06	1.86	0.13	8.60	6.02	1.61	6.27	1.86	21.9	7.53	21.68
8)Basant-pur	max	8.13	442	252	3.84	0.160	1.64	9.00	0.80	60.00	34.00	5.80	36.40	13.90	163.0	31.00	57.50
	min	6.58	76	71	0.00	0.000	0.00	0.00	0.00	0.50	3.50	1.60	10.20	1.90	33.0	5.00	0.00
	avg	7.73	248	162	0.57	0.012	0.05	1.37	0.07	16.55	15.49	3.13	23.50	7.73	110.2	12.83	18.93
	sd	0.41	90	42	0.84	0.033	0.22	1.96	0.17	11.57	8.27	1.10	6.02	3.11	34.2	5.31	11.02
9)Kuru-bhata	max	7.87	1301	1089	5.50	0.400	0.50	5.20	0.86	52.50	24.50	3.45	20.00	5.70	110.0	16.00	73.00
	min	6.46	39	44	0.00	0.000	0.00	0.00	0.00	3.50	1.50	1.25	5.10	0.60	18.0	4.00	0.00
	avg	7.33	124	109	0.96	0.011	0.03	0.47	0.14	17.24	5.71	2.22	11.49	3.77	55.3	8.37	15.36
	sd	0.37	169	180	1.29	0.036	0.05	0.79	0.24	9.69	3.46	0.53	2.68	1.39	16.1	16.06	2.41
10)Sunder-garh	max	8.22	214	130	5.40	0.250	1.45	27.50	0.95	55.00	22.50	3.72	21.40	11.90	120.0	15.00	74.00
	min	5.35	43	56	0.00	0.000	0.00	0.00	0.00	1.50	2.00	0.95	7.50	1.20	22.0	3.00	0.00
	avg	7.39	129	94	0.73	0.008	0.06	1.21	0.08	15.91	9.76	1.48	13.64	4.02	67.7	8.70	13.28
	sd	0.49	43	21	1.19	0.035	0.21	3.59	0.18	10.30	4.21	0.52	3.27	1.90	20.1	2.95	15.11
11)Sale-bhata	max	8.40	412	254	2.32	0.160	0.40	2.70	1.31	28.00	38.00	3.00	34.60	13.20	189.0	26.00	50.50
	min	6.97	82	110	0.00	0.000	0.00	0.00	0.00	2.50	7.00	1.00	12.20	1.20	41.0	5.00	0.00
	avg	7.83	281	175	0.42	0.005	0.05	0.71	0.06	14.65	22.32	1.76	26.39	7.90	137.5	11.86	9.00
	sd	0.33	85	35	0.49	0.023	0.09	0.68	0.19	6.56	7.89	0.45	6.04	2.70	38.5	4.30	11.84
12)Kanta-mal	max	8.57	360	230	4.76	0.640	0.50	6.50	1.24	53.00	48.00	3.40	29.90	11.90	155.0	25.00	52.00
	min	6.67	94	70	0.00	0.000	0.00	0.00	0.00	3.00	5.50	1.34	10.70	1.90	47.0	4.00	0.00
	avg	7.64	212	141	0.79	0.015	0.04	0.98	0.09	18.19	14.80	2.19	20.66	6.29	102.2	10.85	10.42
	sd	0.43	52	36	1.11	0.087	0.09	1.91	0.24	10.44	6.65	0.48	3.49	2.17	22.1	3.81	13.02
13)Tikar-para	max	8.10	416	270	5.00	1.850	0.35	11.40	1.34	35.50	14.50	3.26	40.70	17.60	211.0	21.00	61.00
	min	6.67	87	75	0.00	0.000	0.00	0.00	0.00	1.50	3.00	0.86	11.20	1.30	37.0	5.00	0.00
	avg	7.47	178	117	0.81	0.040	0.03	2.21	1.00	14.48	7.87	1.73	20.18	4.91	87.5	10.80	9.83
	sd	0.36	59	36	1.11	0.239	0.07	2.72	0.21	7.74	2.63	0.45	4.43	2.30	32.0	3.11	1.21

Table 5.2 Average water composition of the Mahanadi at different stations.

Station	pH	E.C	TDS	Fe	Al	NH_4	NO_3	PO_4	SiO_2	Na	K	Ca	Mg	HCO_3	Cl	SO_4
1) Baronda	7.23	102	77	0.57	0.009	0.02	0.83	0.06	14.03	4.83	2.05	12.68	2.88	51.3	9.71	10.04
2) Rajim	7.21	149	106	0.52	0.009	0.05	0.88	0.06	14.28	7.07	1.93	18.34	3.79	74.0	10.05	6.98
3) Simga	7.75	328	195	0.34	0.006	0.15	1.67	0.09	14.12	19.58	5.01	31.07	10.41	141.7	15.19	21.11
4) Andhiyarkore	7.76	579	343	0.74	0.007	0.06	1.88	0.10	19.16	43.61	4.14	39.56	17.82	222.2	15.28	57.45
5) Jondhra	7.77	361	213	0.76	0.012	0.03	1.15	0.11	16.40	22.76	3.89	30.85	12.51	143.6	16.55	32.34
6) Rampur	7.58	238	153	0.44	0.007	0.02	1.27	0.07	13.20	14.62	1.88	26.60	6.64	114.2	11.85	10.35
7) Bamnidih	7.35	173	125	0.86	0.009	0.03	1.52	0.07	14.75	11.17	3.03	17.64	4.53	73.0	11.40	20.52
8) Basantpur	7.73	248	162	0.57	0.012	0.05	1.37	0.07	16.55	15.49	3.13	23.50	7.73	110.2	12.83	18.95
9) Kurubhata	7.33	124	109	0.96	0.011	0.03	0.47	0.14	17.24	5.71	2.22	11.49	3.77	55.3	8.37	15.36
10)Sundergarh	7.39	129	94	0.73	0.008	0.06	1.21	0.08	15.91	9.76	1.48	13.64	4.02	67.7	8.70	13.28
11)Salebhata	7.83	281	175	0.42	0.005	0.05	0.71	0.06	14.65	22.32	1.76	26.39	7.90	137.5	11.86	9.00
12)Kantamal	7.64	212	141	0.79	0.015	0.04	0.98	0.09	18.19	14.80	2.19	20.66	6.29	102.2	10.85	10.42
13)Tikarpara	7.47	178	117	0.81	0.040	0.03	2.21	0.10	14.48	7.87	1.73	20.18	4.91	87.5	10.80	9.83

E.C (Electrical conductivity) in micro-mhos/cm, all other parameters except pH are in mg/l.

estimated for water of each stations using the formula

$$D = \frac{[TZ^+]-[TZ^-]}{[TZ^+]+[TZ^-]} \times 100$$

where TZ^+ is total cations, TZ^- is total anions and D is percent of discrepancy. Table 5.3 shows that the maximum discrepancy is 8.4 percent which is well within the tolerable limit. A plot (Fig.5.1) of TZ^+ versus TZ^- resulted in a linear regressional relationship between them. The equation of regression line by best fit method is $TZ^-(\mu eq/l) = 1.11\ TZ^+(\mu eq/l) - 258.75$.

Before finally adopting the CWC data, spot checks for water composition were carried out by collecting samples at a few CWC stations located in the upper part of the Mahanadi basin during the field season of January-February, 1989. These waters were analyzed for some major ions like HCO_3, Ca, Mg, Na, K and Cl so that an order of magnitude of reported values could be assessed. It was seen that most of the parameters analyzed during the present study fell within the concentration ranges reported by CWC (Figs.5.2).

5.4 Expression of Water Analyses

Various terms and units are commonly used for reporting water composition. Table 5.2 shows average water analyses in

Table 5.3 Cation - anion balance

Station	Na	K	Ca	Mg	NH_4	Al	Fe	HCO_3	Cl	NO_3	PO_4	SO_4	TZ^+	TZ^-	Discrepancy (%)
1) Baronda	210	52	634	240	1.0	0.97	30	840	273	13	3.0	208	1168	1337	6.7
2) Rajim	307	50	916	314	2.0	0.99	28	1213	283	14	2.0	146	1618	1658	1.2
3) Simga	852	128	1552	866	8.0	0.66	18	2323	428	27	3.0	440	3424	3221	3.0
4) Andhiyarkore	1896	106	1978	1484	3.0	0.81	39	3643	430	30	3.0	1196	5466	5302	1.5
5) Jondhra	989	100	1542	1042	1.0	1.32	40	2352	466	18	3.5	674	3715	3513	2.8
6) Rampur	592	48	1330	552	0.9	0.78	24	1872	334	20	2.2	216	2547	2444	2.1
7) Bamnidih	486	78	882	378	1.0	1.02	46	1197	321	24	2.2	426	1872	1970	2.5
8) Basantpur	674	80	1174	644	2.0	1.35	30	1807	361	22	2.3	394	2605	2586	0.0
9) Kurubhata	248	57	574	314	1.0	1.17	51	907	236	07	4.5	320	1246	1475	8.4
10) Sunderhgarh	424	38	682	334	3.0	0.81	39	1110	245	19	2.5	276	1521	1652	4.1
11) Salebhata	970	45	1320	658	2.0	0.57	22	2254	336	11	1.5	188	3017	2791	3.9
12) Kantamal	643	56	1032	524	2.0	1.60	42	1675	306	16	3.0	216	2301	2216	1.9
13) Tikarpara	342	44	1008	410	1.7	4.50	43	1435	304	36	3.0	204	1853	1982	3.4

TZ^+- total cations, TZ^-- total anions, all concentrations in micro-equivalents/litre

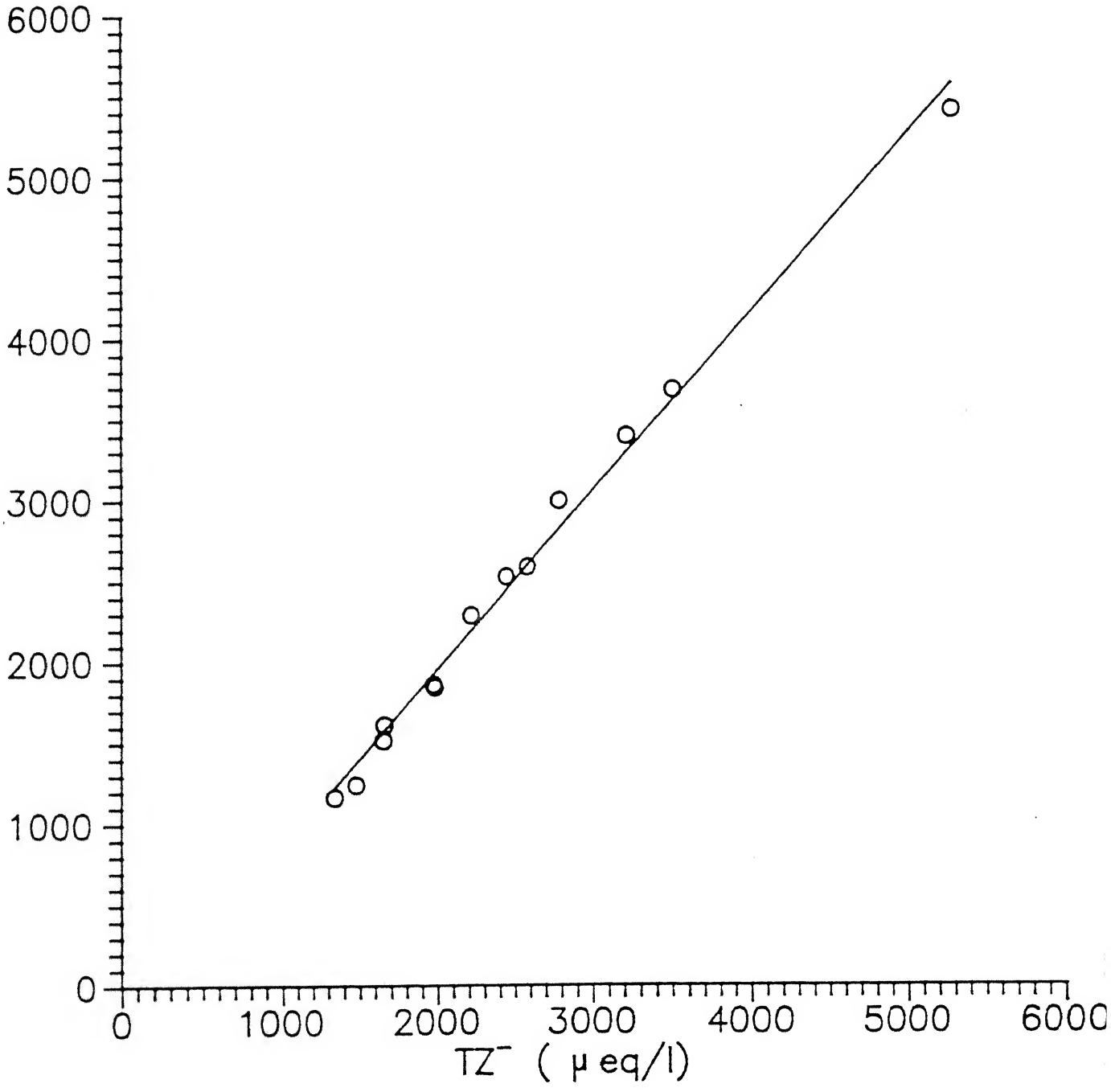

Fig. 5.1 Balance of total cations (TZ^+) and total anions (TZ^-)

Fig. 5.2 CWC vs Present water analysis (Baronda)

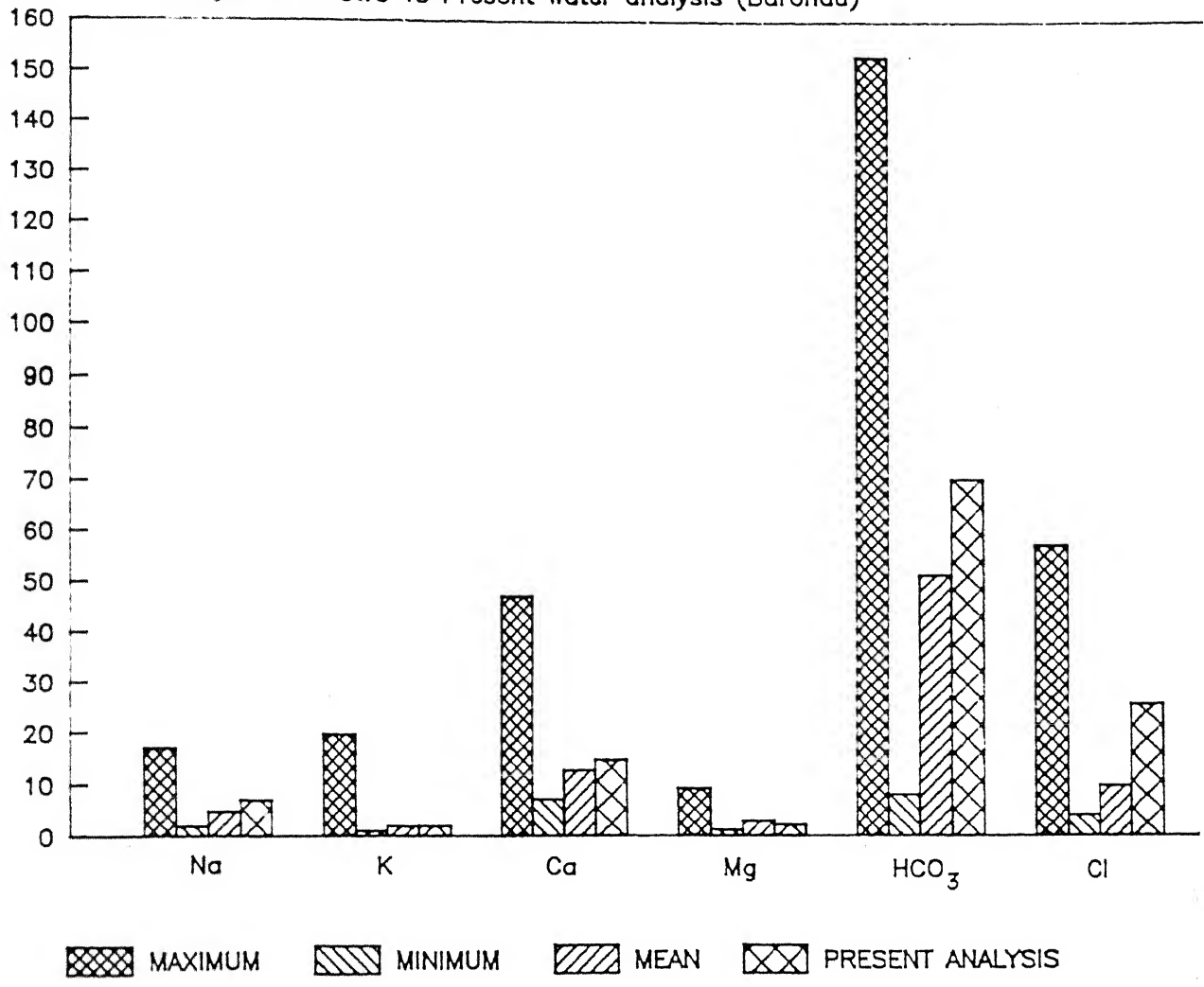

cont

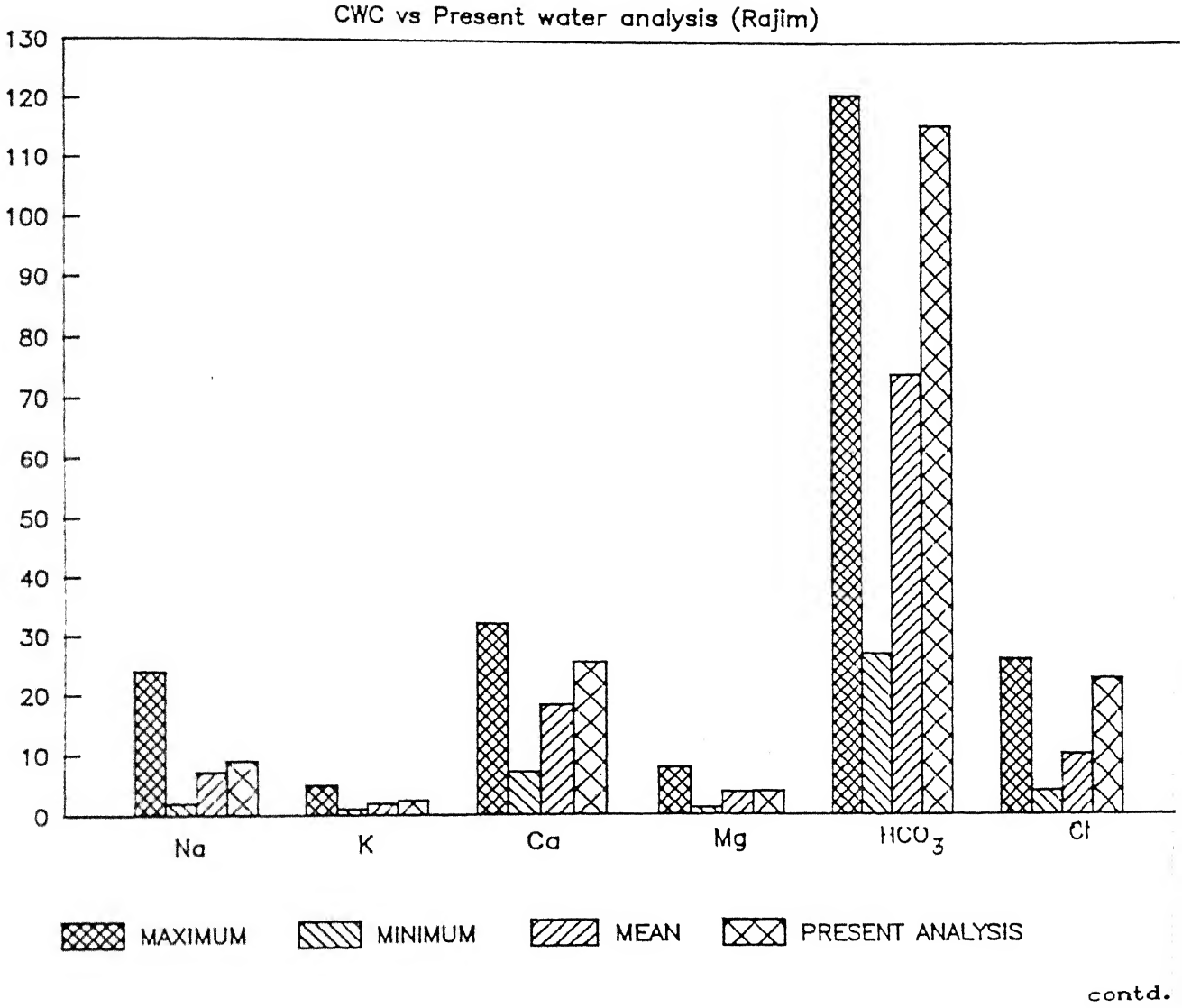
CWC vs Present water analysis (Rajim)
130
120
110
100
90
80
70
60
50
40
30
20
10
0
Na
K
Ca
Mg
HCO3
Cl
MAXIMUM
MINIMUM
MEAN
PRESENT ANALYSIS

contd.

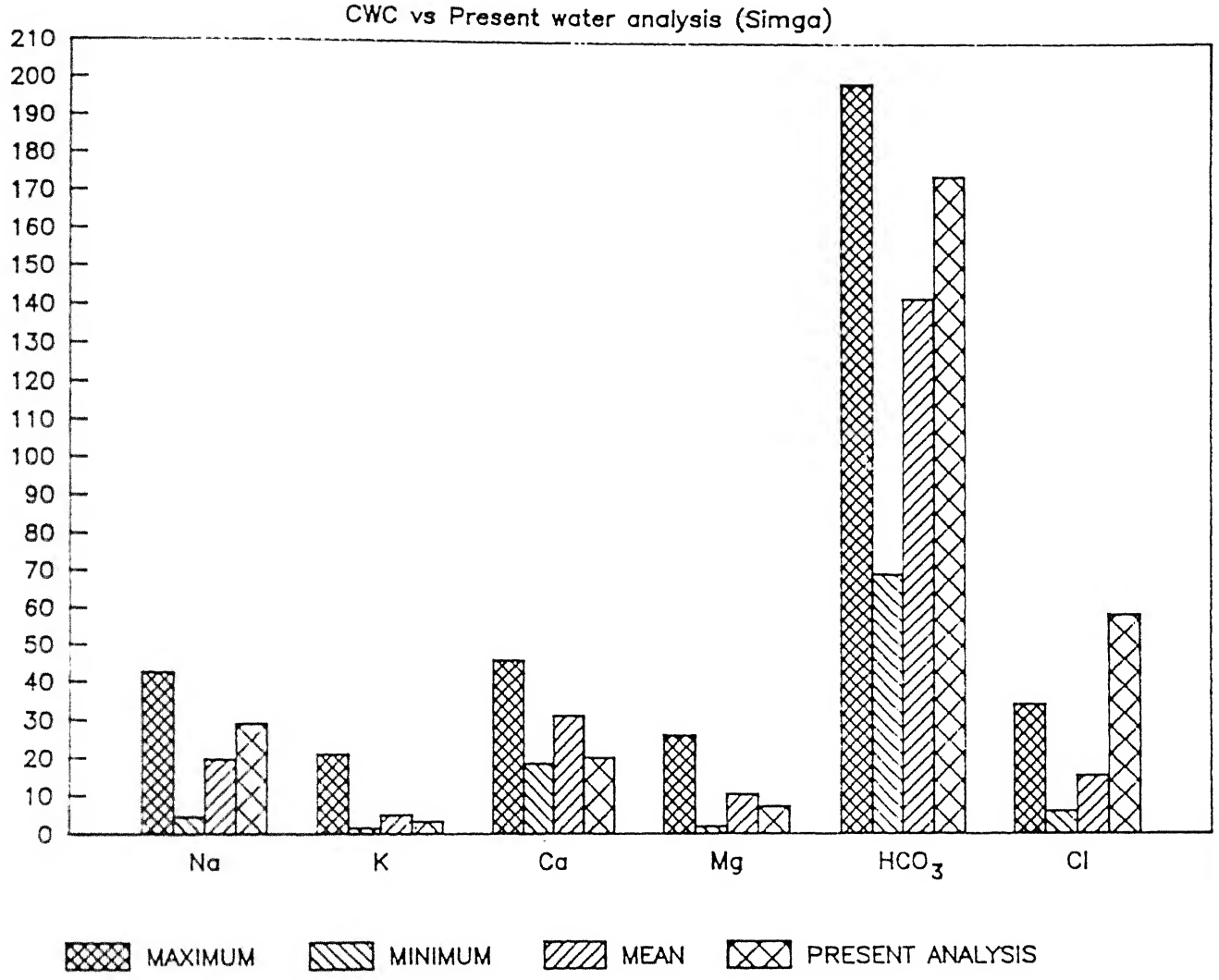
CWC vs Present water analysis (Simga)
210
200
190
180
170
160
150
140
130
120
110
100
90
80
70
60
50
40
30
20
10
0
Na
K
Ca
Mg
HCO3
Cl
MAXIMUM
MINIMUM
MEAN
PRESENT ANALYSIS

contd.

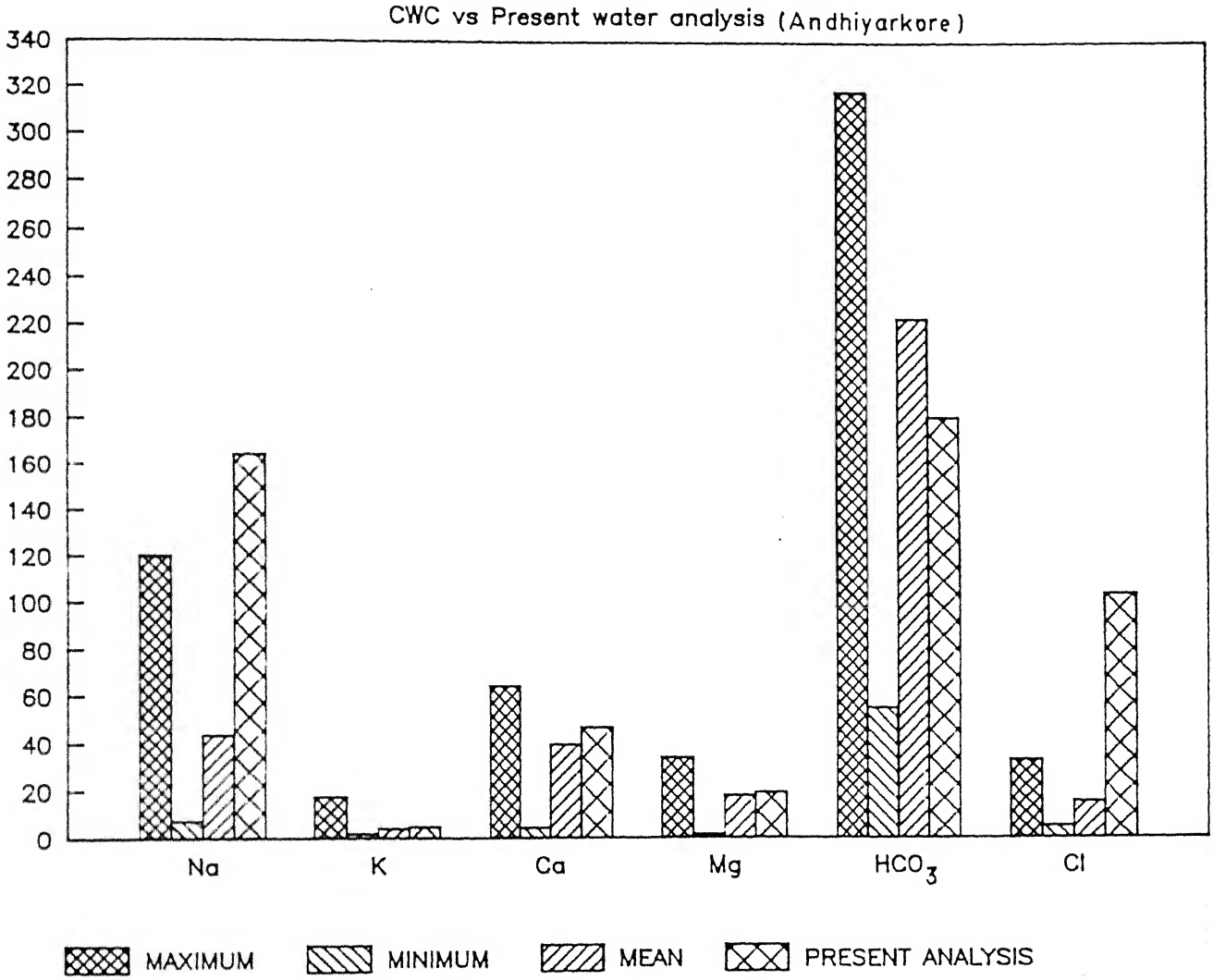
CWC vs Present water analysis (Andhiyarkore)
340
320
300
280
260
240
220
200
180
160
140
120
100
80
60
40
20
0
Na
K
Ca
Mg
HCO3
Cl
MAXIMUM
MINIMUM
MEAN
PRESENT ANALYSIS

parts per million (ppm) at 13 sampling stations. It is assumed that ppm values are equal to milligrams per litre because dilute river water has a density value practically equal to 1 gm/cm^3. Conversion of mg/litre values to mole/litre, estimation of ionic strengths, activity co-efficients and ion activities, were carried out by a user friendly computer program (Appendix I) written in TURBO-PASCAL using the following relations :

$$\text{mole/litre } (m_i) = \frac{\text{mg/litre}}{\text{formula weight}} \times 10^{-3} \qquad (1)$$

where 'i' is any dissolved species.

$$\text{ionic strength } (I) = \frac{1}{2} \Sigma\, m_i . Z_i^2 \qquad (2)$$

where Z_i is the charge of the species.

$$\log \gamma_i = - A . Z_i^2 \left[\frac{\sqrt{I}}{1+\sqrt{I}} - 0.2I \right] \qquad (3)$$

where γ_i is the activity co-efficient of the species and A is dielectric constant equal to 0.5085 at $25^{o}C$.

Table 5.4 Concentration of dissolved species (milli-moles/litre)

Station	Na	K	Ca	Mg	HCO_3	Cl	SO_4	SiO_2	NO_3	PO_4	NH_4	Al	Fe
1) Baronda	0.210	0.052	0.317	0.120	0.840	0.273	0.104	0.233	0.013	0.00063	0.001	0.00033	0.010
2) Rajim	0.307	0.050	0.458	0.157	1.213	0.283	0.073	0.238	0.014	0.00066	0.002	0.00033	0.009
3) Simga	0.852	0.128	0.776	0.433	2.323	0.428	0.220	0.235	0.027	0.00094	0.008	0.00022	0.006
4) Andhiyarkore	1.896	0.106	0.989	0.742	3.643	0.430	0.598	0.319	0.030	0.00101	0.003	0.00027	0.013
5) Jondhra	0.989	0.100	0.771	0.521	2.352	0.466	0.337	0.273	0.018	0.00116	0.001	0.00044	0.014
6) Rampur	0.592	0.048	0.665	0.276	1.872	0.334	0.108	0.237	0.020	0.00074	0.001	0.00026	0.008
7) Bamnidih	0.486	0.078	0.441	0.189	1.197	0.321	0.213	0.246	0.024	0.00074	0.001	0.00034	0.015
8) Basantpur	0.674	0.080	0.587	0.322	1.807	0.361	0.197	0.276	0.022	0.00078	0.003	0.00045	0.010
9) Kurubhata	0.248	0.057	0.287	0.157	0.907	0.236	0.160	0.287	0.007	0.00147	0.001	0.00039	0.017
10) Sunderhgarh	0.424	0.038	0.341	0.167	1.110	0.245	0.138	0.265	0.019	0.00083	0.003	0.00027	0.013
11) Salebhata	0.970	0.045	0.660	0.329	2.254	0.336	0.094	0.244	0.011	0.00058	0.002	0.00018	0.007
12) Kantamal	0.643	0.056	0.516	0.262	1.675	0.306	0.108	0.303	0.016	0.00099	0.002	0.00055	0.014
13) Tikarpara	0.342	0.044	0.504	0.205	1.435	0.304	0.102	0.241	0.036	0.00101	0.002	0.00150	0.014

Table 5.5 Ionic strengths and activity coefficients

Station	Ionic strength	Ionic activity coefficient		
		Univalent	Bivalent	Trivalent
1) Baronda	0.0018	0.9539	0.8278	0.6537
2) Rajim	0.0023	0.9483	0.8088	0.6203
3) Simga	0.0053	0.9248	0.7313	0.4946
4) Andhiyarkore	0.0077	0.9115	0.6904	0.4345
5) Jondhra	0.0053	0.9247	0.7313	0.4946
6) Rampur	0.0036	0.9366	0.7697	0.5549
7) Bamnidih	0.0028	0.9434	0.7923	0.5923
8) Basantpur	0.0037	0.9359	0.7672	0.5509
9) Kurubhata	0.0020	0.9516	0.8203	0.6405
10) Sundergarh	0.0023	0.9483	0.8088	0.6204
11) Salebhata	0.0040	0.9336	0.7597	0.5388
12) Kantamal	0.0031	0.9408	0.7834	0.5774
13) Tikarpara	0.0028	0.9435	0.7924	0.5923

Table 5.6 Activity of dissolved species (x 10^3)

Station	Na	K	Ca	Mg	HCO_3	Cl	SO_4	SiO_2	NO_3	PO_4	NH_4	Al	Fe
1) Baronda	0.200	0.050	0.262	0.099	0.801	0.260	0.099	0.233	0.012	0.00041	0.0009	0.00021	0.0065
2) Rajim	0.291	0.047	0.370	0.127	1.150	0.268	0.039	0.238	0.012	0.00041	0.0019	0.00021	0.0038
3) Simga	0.788	0.118	0.567	0.317	2.148	0.396	0.161	0.235	0.025	0.00046	0.0074	0.00011	0.0030
4) Andhiyarkore	1.728	0.097	0.683	0.512	3.320	0.392	0.413	0.319	0.027	0.00044	0.0027	0.00012	0.0057
5) Jondhra	0.914	0.092	0.564	0.381	2.175	0.431	0.246	0.273	0.017	0.00057	0.0009	0.00022	0.0067
6) Rampur	0.554	0.045	0.512	0.212	1.753	0.313	0.083	0.237	0.019	0.00041	0.0009	0.00014	0.0044
7) Bamnidih	0.458	0.074	0.349	0.150	1.129	0.303	0.169	0.246	0.023	0.00044	0.0009	0.00020	0.0091
8) Basantpur	0.631	0.075	0.450	0.247	1.691	0.338	0.151	0.276	0.020	0.00042	0.0028	0.00025	0.0056
9) Kurubhata	0.236	0.054	0.235	0.129	0.863	0.225	0.131	0.287	0.007	0.00094	0.0009	0.00025	0.0109
10) Sunderhgarh	0.402	0.036	0.276	0.135	1.052	0.232	0.112	0.265	0.018	0.00051	0.0028	0.00017	0.0081
11) Salebhata	0.906	0.042	0.501	0.250	2.104	0.314	0.071	0.244	0.010	0.00031	0.0019	0.00010	0.0040
12) Kantamal	0.605	0.053	0.404	0.205	1.576	0.288	0.085	0.303	0.015	0.00057	0.0019	0.00032	0.0081
13) Tikarpara	0.323	0.042	0.399	0.162	1.354	0.287	0.081	0.241	0.034	0.00060	0.0019	0.00089	0.0085

$$a_i = m_i \cdot \gamma_i \qquad (4)$$

here a_i is the activity of the ion. Table 5.4 lists conversions n mole/litre. Ionic strengths and activity co-efficients are iven in Table 5.5 while ion activities are presented in Table .6.

.5 Seasonal Variation

Effect of season on physical and chemical parameters is mportant to the assessment of surface water composition. One of he advantages of a long term database lies in its ability to ecord seasonal variations, if any. Based on the distribution of ainfall (Table 3.1), three seasons can be identified in the lahanadi basin. They cover the periods 1) January to May (7.6% of otal rainfall), 2) June to September (86.2%) and 3) October to lecember (6.2%). These periods can be termed as `pre-monsoon', monsoon' and `post-monsoon' respectively. Accordingly, all major arameters and discharge values from the CWC raw database have een averaged. These are given in Table 5.7.

Certain broad features are easily discernible from he diagrams (Fig.5.3) constructed using the data in Table 5.7. s usual, the effect of dilution is observed as a marked decrease n the conductivity value. pH is largely constant during

ıble 5.7 Seasonal variation of water composition

Station	Season	Discharge	pH	E.C	SiO_2	Na	K	Ca	Mg	HCO_3	Cl	SO_4
	Pre	0.55	7.44	135.7	11.1	5.3	2.0	14.0	3.3	58.4	11.7	4.0
) Baronda	Mon	61.65	7.08	86.7	18.3	4.4	1.8	12.0	2.0	47.7	8.4	16.0
	Post	14.03	7.15	86.9	11.6	4.3	2.6	12.0	3.5	46.6	9.1	10.6
	Pre	2.99	7.15	199.7	13.7	9.9	2.4	23.4	4.8	93.1	12.7	3.3
) Rajim	Mon	93.30	7.09	103.6	17.6	5.2	2.1	13.9	2.8	54.4	9.0	11.7
	Post	30.61	7.37	130.8	10.6	5.8	1.6	16.4	3.6	69.1	7.5	5.5
	Pre	10.70	7.84	392.2	12.1	24.4	6.2	32.9	12.6	161.9	18.0	19.7
) Simga	Mon	144.97	7.53	252.0	17.4	16.6	5.0	22.9	7.9	111.6	13.3	29.7
	Post	143.62	7.85	321.0	11.7	15.3	2.2	35.3	10.1	149.0	12.7	10.9
	Pre	2.06	7.81	642.8	16.3	54.4	4.3	42.9	22.4	247.2	16.6	59.6
) Andhi-	Mon	11.38	7.63	480.9	24.7	37.4	4.3	34.1	12.6	188.8	13.6	59.3
yarkore	Post	39.63	7.83	499.2	15.3	29.7	2.9	41.0	16.6	210.8	13.9	48.5
	Pre	14.65	7.91	482.7	14.2	31.6	4.5	35.0	16.1	170.1	20.1	38.5
) Jondhra	Mon	339.65	7.54	278.3	20.5	18.8	4.1	26.0	10.7	112.4	22.3	32.6
	Post	204.50	7.73	311.9	13.9	14.8	2.5	34.7	10.1	145.1	13.5	16.2
	Pre	0.41	7.76	290.5	11.2	14.7	1.8	31.5	8.3	137.8	10.7	5.8
) Rampur	Mon	87.33	7.36	167.5	18.2	10.9	2.0	18.4	4.9	86.4	12.9	16.9
	Post	29.78	7.68	248.5	11.3	13.7	1.6	28.5	6.6	117.9	11.2	8.6
	Pre	14.50	7.45	208.2	11.9	12.2	3.3	20.0	5.2	82.6	13.7	13.7
) Bamnidih	Mon	410.60	7.12	137.3	19.7	10.7	3.1	14.1	3.2	58.7	9.7	40.4
	Post	76.86	7.40	151.6	12.3	8.5	2.4	16.6	5.1	71.2	10.0	8.6
	Pre	33.86	7.80	296.3	14.3	20.1	3.5	24.9	9.0	123.4	13.8	18.2
) Basant-	Mon	1235.60	7.53	194.1	21.4	13.6	3.2	19.4	6.4	86.8	12.0	24.5
pur	Post	806.20	7.82	236.0	13.7	10.8	2.3	26.9	7.0	114.8	11.6	12.3
	Pre	6.31	7.52	175.4	14.1	7.0	2.4	12.3	4.1	53.4	9.3	6.5
) Kuru-	Mon	206.10	7.02	73.9	22.6	3.7	2.2	9.2	3.1	44.5	7.0	31.2
bhata	Post	43.40	7.45	109.2	15.3	5.1	2.0	12.4	4.2	61.8	8.2	11.0
	Pre	5.50	7.59	155.1	13.7	12.6	1.4	15.5	4.4	76.1	10.0	7.1
0) Sunder-	Mon	296.20	7.05	92.8	20.5	7.4	1.8	11.4	2.4	52.2	7.3	26.3
garh	Post	37.90	7.56	138.5	12.7	8.9	1.2	13.7	5.8	74.6	8.5	14.5
	Pre	1.79	7.94	348.6	13.5	27.3	1.7	30.4	10.0	167.6	14.0	4.7
1) Sale-	Mon	157.00	7.55	179.7	17.5	17.7	1.9	19.3	4.5	90.8	9.9	20.8
bhata	Post	31.28	7.91	270.8	11.9	19.2	1.6	27.0	7.9	135.3	10.1	4.4
	Pre	6.00	7.82	243.2	14.4	17.8	2.4	22.1	7.1	111.6	11.4	4.4
2) Kanta-	Mon	687.20	7.27	159.4	24.0	12.0	2.2	17.4	4.8	83.2	9.8	19.4
mal	Post	170.80	7.75	209.8	17.5	11.8	1.9	21.8	6.5	108.3	11.7	13.1
	Pre	276.80	7.63	201.3	11.9	9.1	1.6	18.8	5.7	100.0	10.7	5.1
3) Tikar-	Mon	3048.20	7.24	149.0	19.8	7.5	2.1	18.6	4.2	77.9	9.5	14.1
para	Post	1443.00	7.51	181.4	11.9	6.5	1.5	18.9	4.7	87.3	12.2	11.5

ischarge in cubic metres/sec. E.C (Electric Conductivity) in micro-mhos/cm. all other oncentratins in mgs/litre except pH

Fig. 5.3(a) SEASONAL VARIATION OF pH

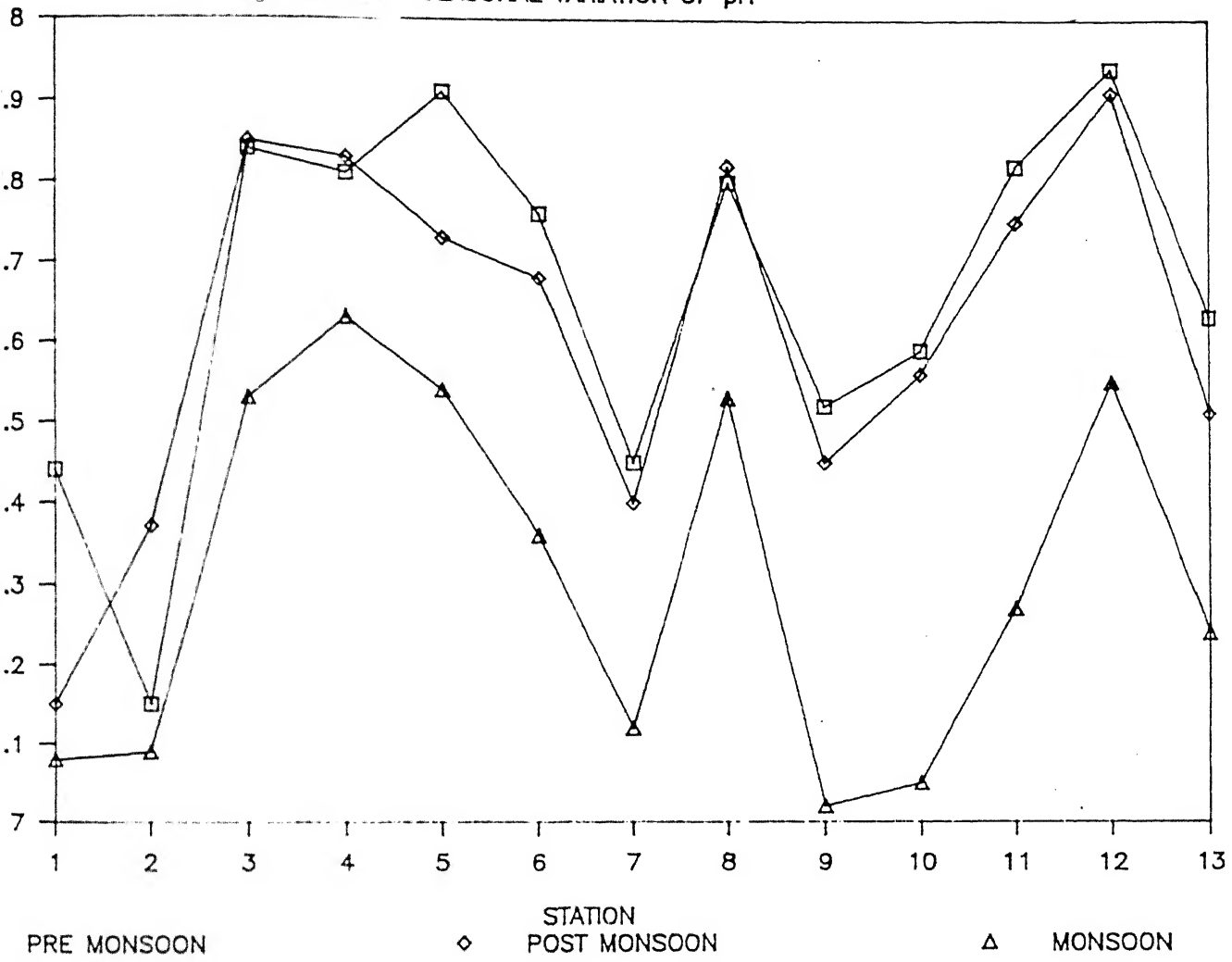

Fig. 5.3(b) SEASONAL VARIATION OF CONDUCTIVITY

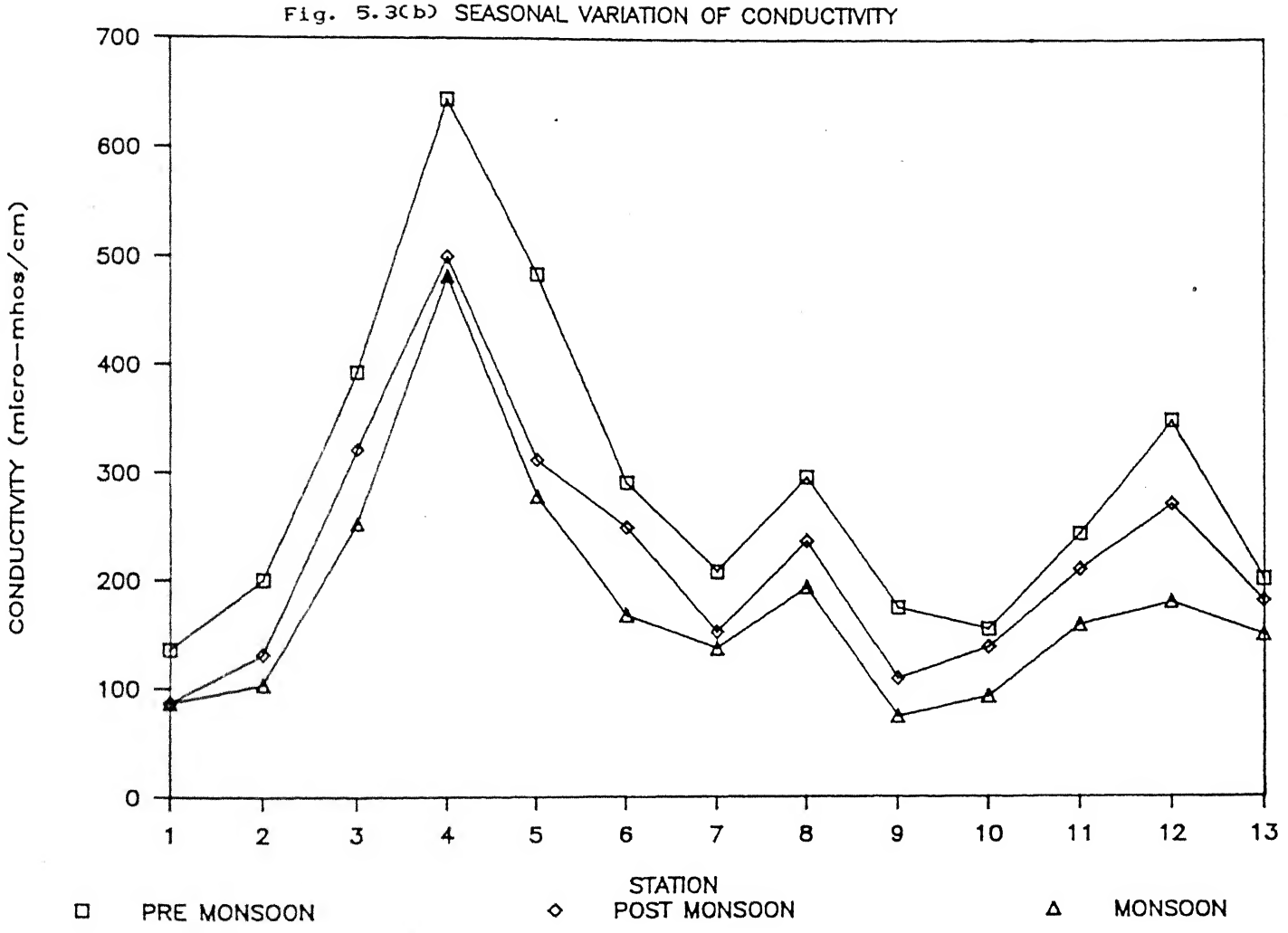

Fig. 5.3(c) SEASONAL VARIATION OF SiO_2

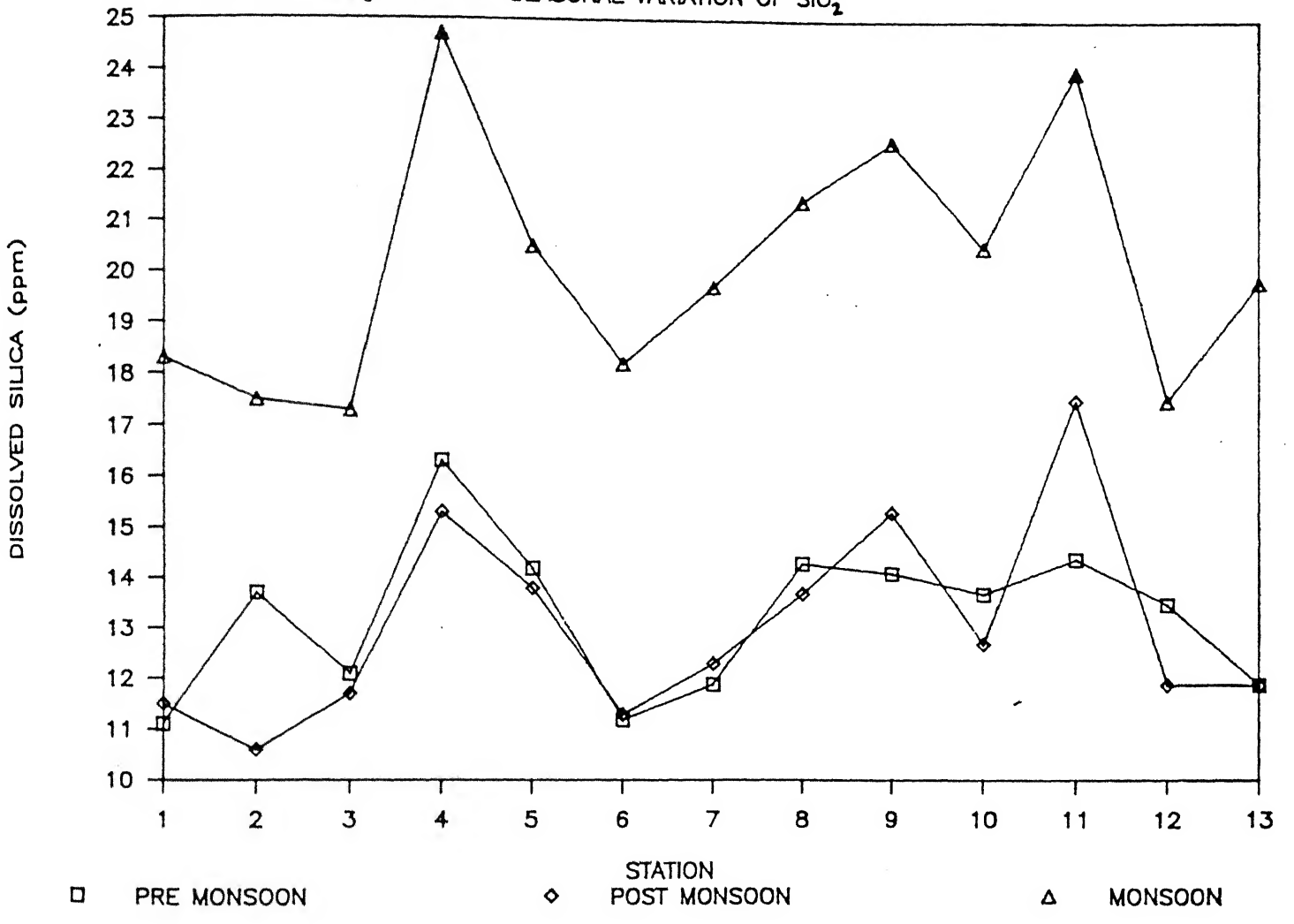

Fig. 5.3(d) SEASONAL VARIATION OF SULPHATE

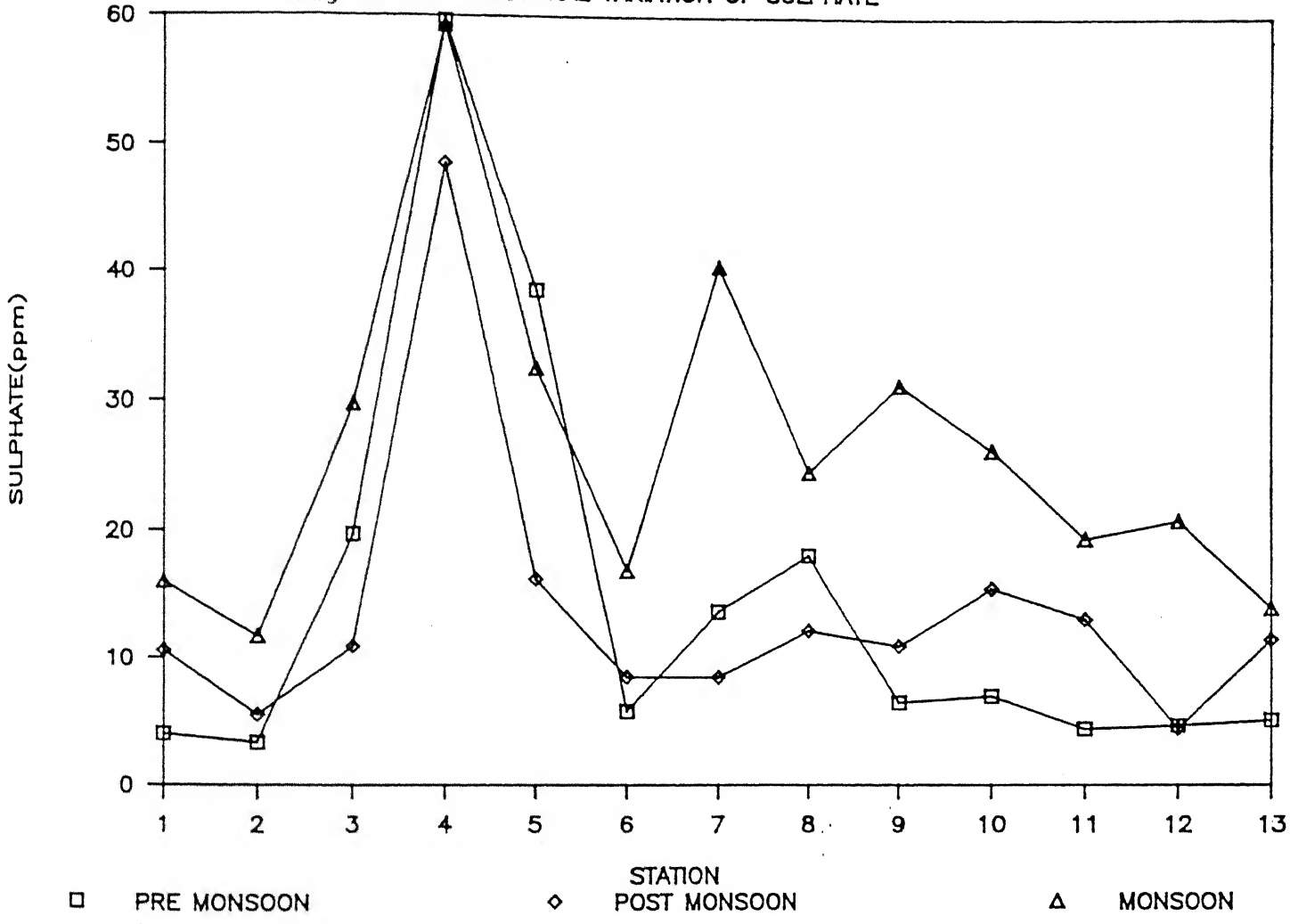

Fig. 5.3(e) SEASONAL VARIATION OF CALCIUM

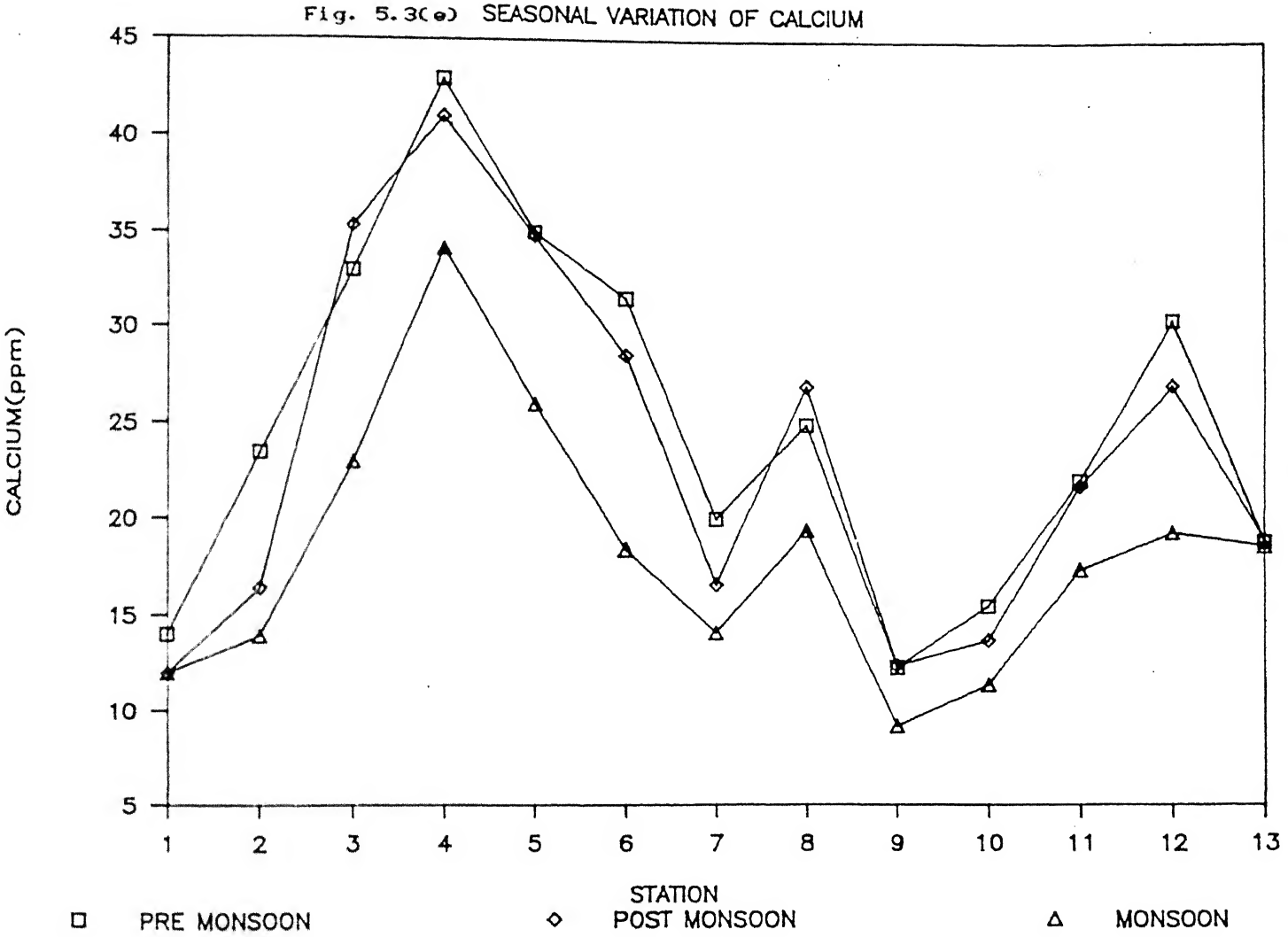

Fig. 5.3(f) SEASONAL VARIATION OF MAGNESIUM

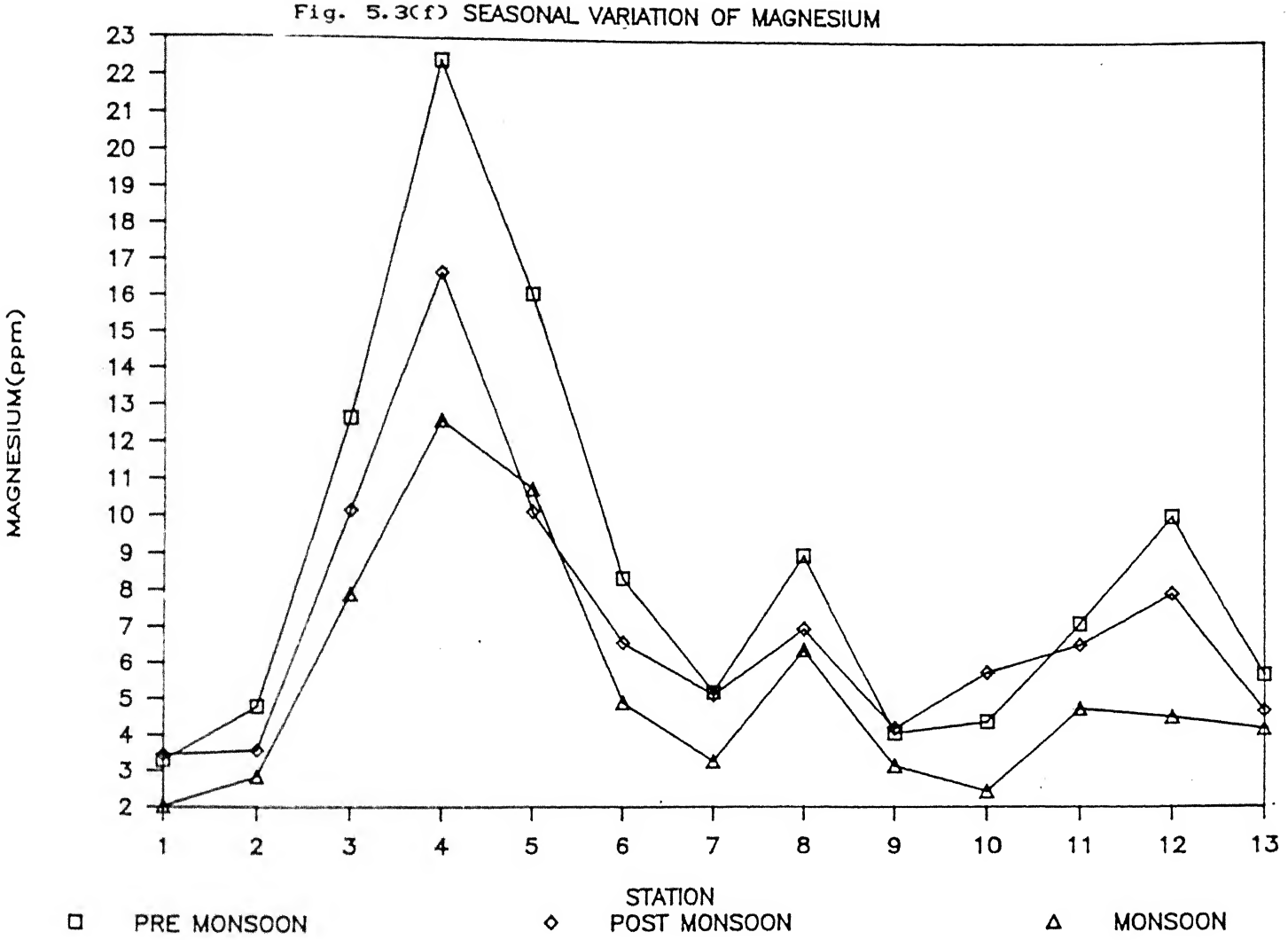

Fig. 5.3(g) SEASONAL VARIATION OF BICARBONATE

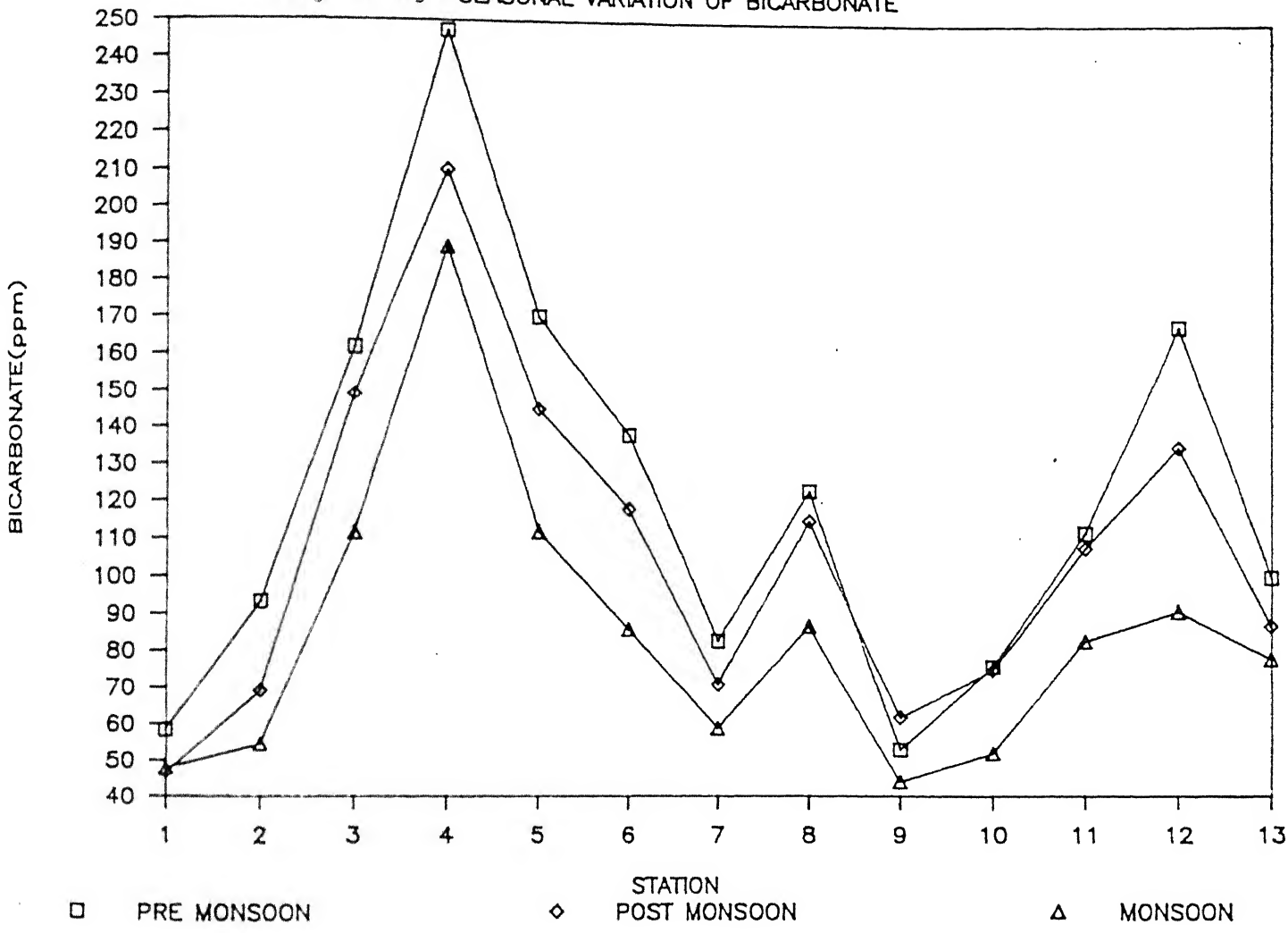

pre-monsoon and post-monsoon periods but is relatively low during peak flow periods. Calcium, magnesium and bicarbonate also show a similar trend of lowest concentrations during monsoon where as highest concentrations are observed in the lean season. Post-monsoon period is characterized by moderate values for the above ions. High values during monsoon period may be attributed to ground water recharge which is a usual feature in carbonate terrains. Sulphate shows highest concentrations during monsoon, invariably moderate during post-monsoon and low in the dry period. However, the Seonath river waters at the upstream region (stations 4 and 5) do not follow this trend. Such notable deviation may be due to the bed-rock geology. This part of the basin consists of evaporite deposits at the subsurface and surface levels (Chapter 3).

Silica seems to be directly related to discharge. It consistently maintains high concentrations during monsoon. Davis (1964) suggests that this may be due to rapid dissolution of silica during storm run-off which exposes much larger surface area of suspended silt and clay size particles than during the periods of low discharge. In addition, much run-off, during and shortly after the monsoon, passes through the upper part of the soil profile which may contain silica leached from the soil.

5.6. Spatial Variation

An attempt has been made to find out whether the Mahanadi waters show any definite trend in major dissolved constituents with respect to location of sampling stations. Two pathways of water flow through sampling stations 1, 2, 8, 13 and 3, 5, 8, 13 along the downstream direction of the Mahanadi river channel were considered. Average concentration of two groups of dissolved species Ca-Mg-HCO_3 and Na-K-Cl-SO_4-SiO_2 along these routes have been examined for any possible spatial variation. Figs. 5.4 and 5.5 plot the concentration of the above species against distance downstream. It is observed (Fig. 5.4a,b) that water compositions at stations 1, 2 and 13 do not reflect any marked change. It is seen from the geologic map (Fig.3.3) that waters at stations 1 and 2 drain mostly crystalline rocks in their catchments. Station 13 is located farthest downstream where crystalline rocks are dominant. This partly explains their similar water compositions. At Basantpur (station 8), all the constituents registered highest level of concentration. The increase in Ca, Mg and HCO_3 values may be due to contribution of the Seonath tributary which drains predominantly carbonate and associated rocks. In addition, Jonk and Hasdo tributaries which drain mostly crystalline rocks, could possibly supply silicate derived ions and SiO_2.

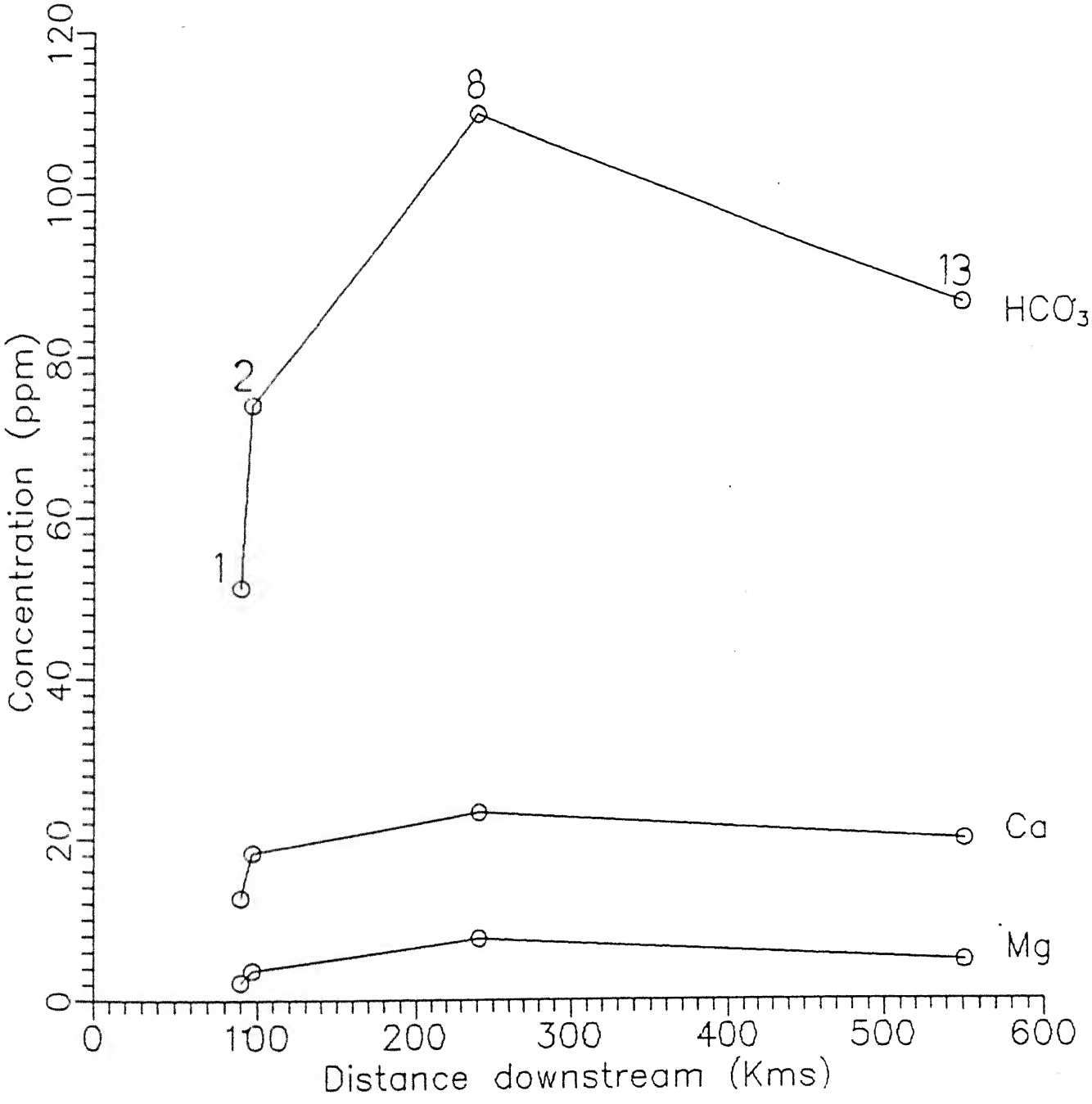

Fig. 5.4(a) Spatial variation of Ca, Mg and HCO_3 along sampling stations 1, 2, 8 and 13

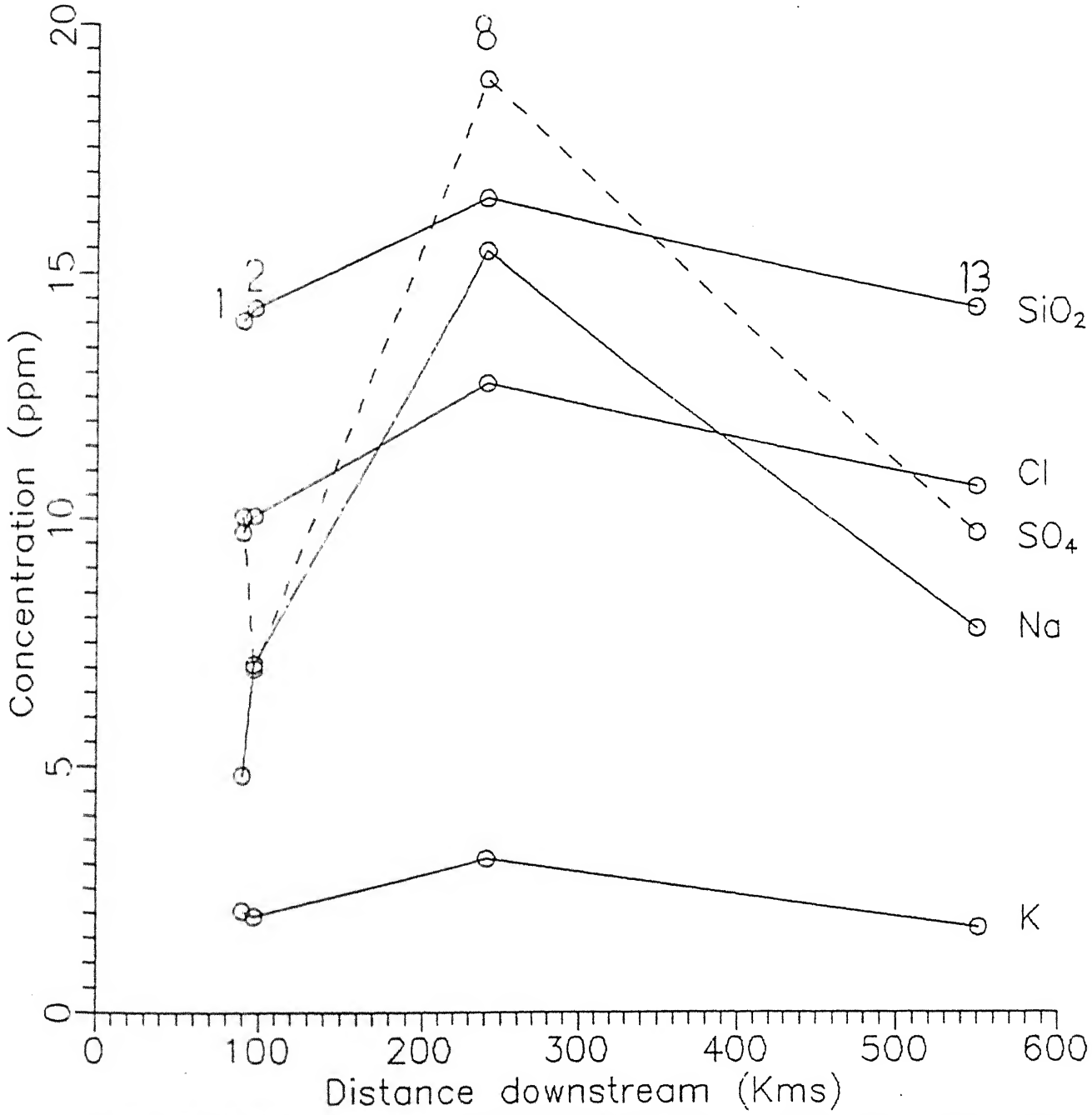

Fig. 5.4(b) Spatial variation of Na, K, Cl, SO_4 and SiO_2 along sampling stations 1, 2, 8 and 13

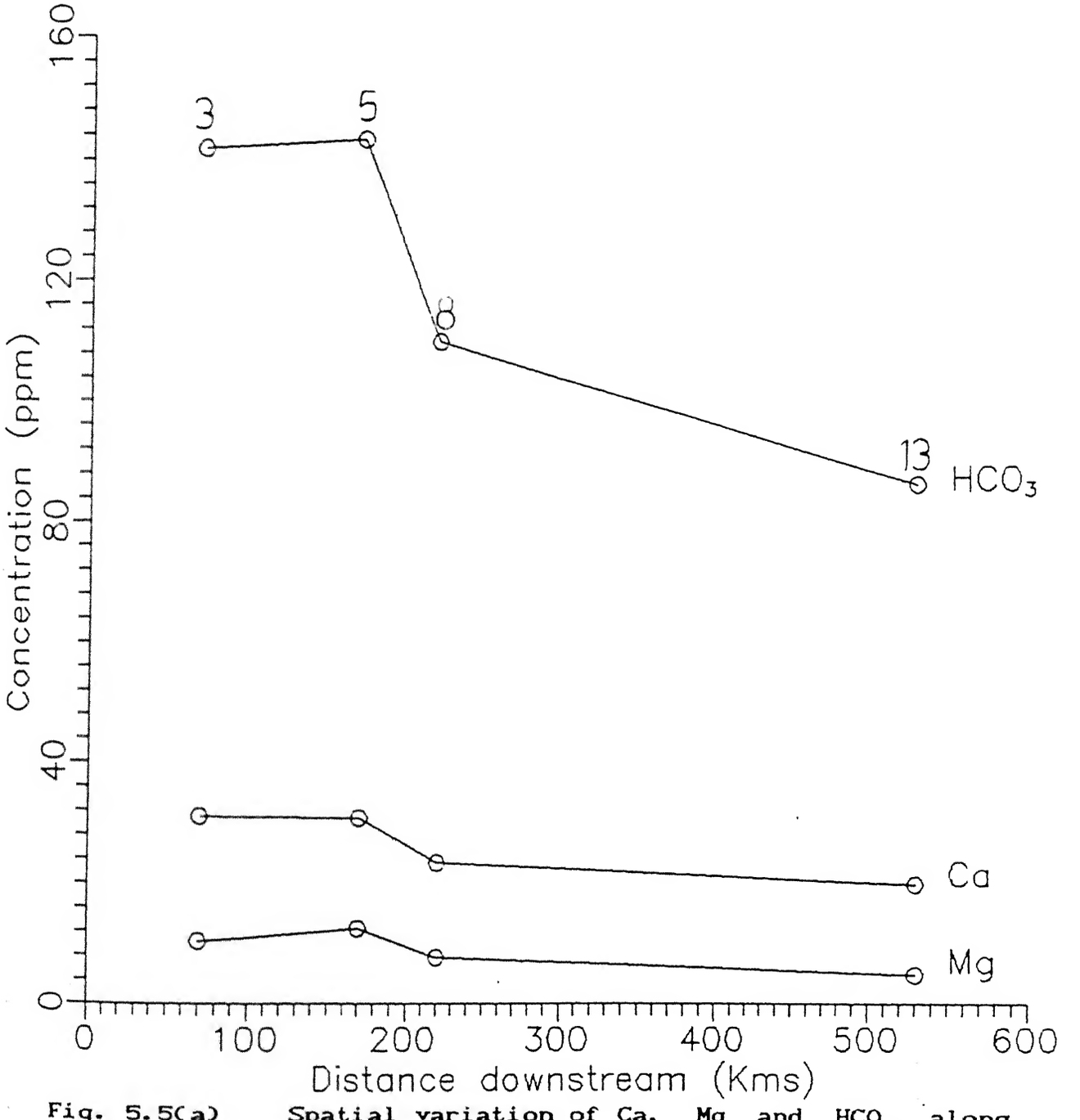

Fig. 5.5(a) Spatial variation of Ca, Mg and HCO_3 along sampling stations 3, 5, 8 and 13

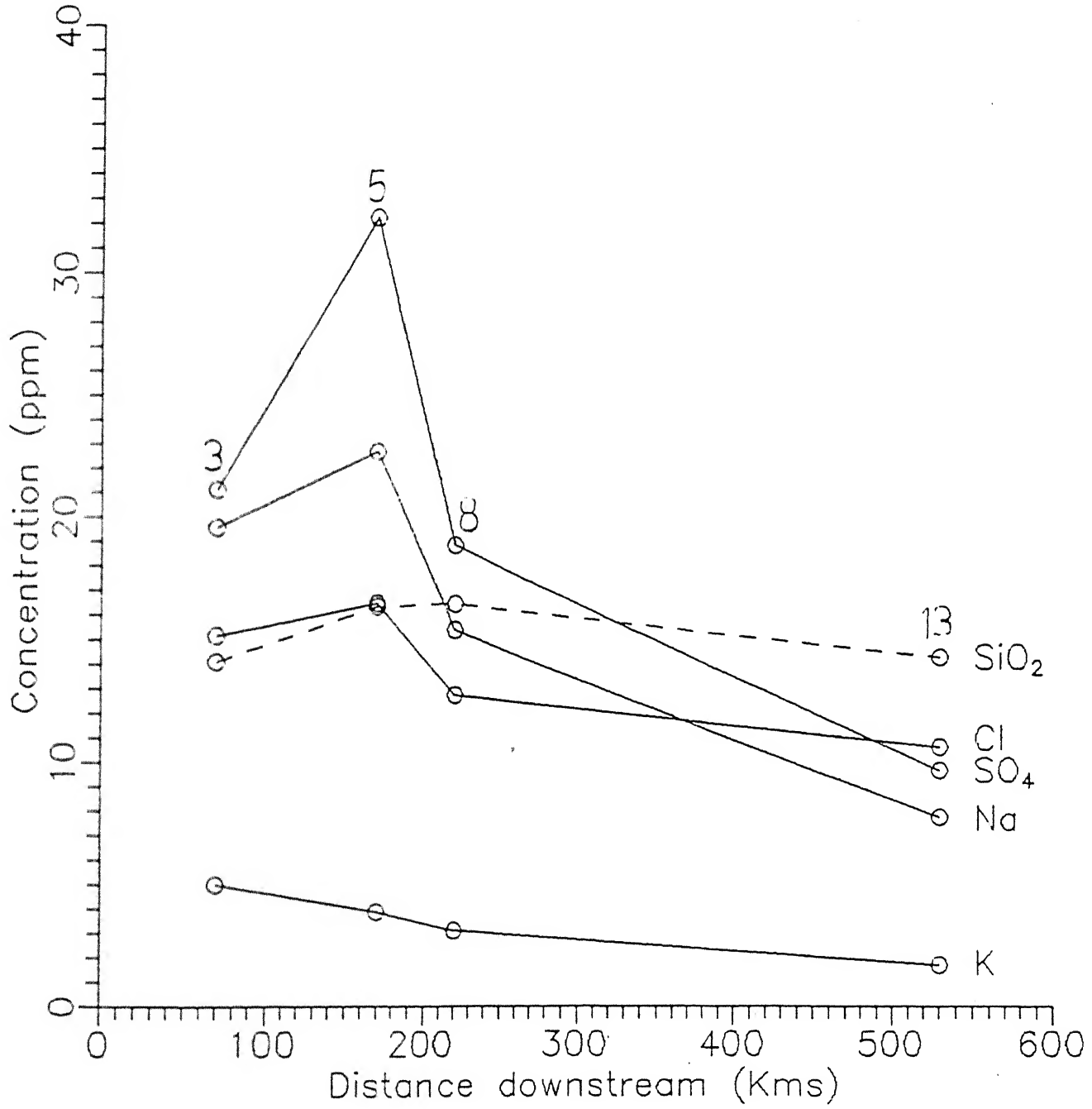

Fig. 5.5(b) Spatial variation of Na, K, Cl, SO_4 and SiO_2 along sampling stations 3, 5, 8 and 13

Figs.5.5(a) and 5.5(b) show that at Jondhra (station 5), the river water records highest concentration of Na, Cl, SO_4 and SiO_2 while Ca, Mg and HCO_3 concentration levels are maintained with respect to those at Simga (station 3). Further downstream, concentration of all the dissolved constituents except SiO_2 decrease. The sharp rise in the concentrations of Na and SO_4 at station 5 may be due to the contributions from the Hamp tributary which has high concentrations of Na and SO_4 compared to waters from other parts in the Mahanadi basin.

5.7 Correlation Analysis

Correlation analysis is a statistical tool to help establish some degree of association among a set of variables in a manner unaffected by their measurement units. In this analysis, correlation co-efficient (r) which is the ratio of the co-variance of two variables to the product of their standard deviations, is estimated for all the variables. This was carried out by taking mean values of 16 chemical parameters for all the sampling stations listed in Table 5.2. Computer processing of this data with SPSS (Statistical Package for Social Sciences) resulted in a correlation co-efficient matrix (Table 5.8). As seen from the matrix, a strong positive correlation (r = 0.995) exists between electrical conductivity and total dissolved solids. Sodium,

Table 5.8 Correlation coefficient matrix (confidence level 95%)

	pH	E.C	TDS	Fe	Al	NH_4	NO_3	PO_4	SiO_2	Na	K	Ca	Mg	HCO_3	Cl	SO_4
pH	1.000	0.764	0.740	-0.434	-0.109	0.388	0.273	0.085	0.343	0.761	0.531	0.819	0.772	0.822	0.774	0.458
E.C		1.000	0.995	-0.524	-0.191	0.329	0.437	0.155	0.496	0.979	0.703	0.955	0.991	0.987	0.850	0.869
TDS			1.000	-0.487	-0.204	0.302	0.412	0.197	0.545	0.980	0.694	0.932	0.985	0.976	0.816	0.889
Fe				1.000	0.453	0.523	-0.166	0.534	0.215	-0.513	-0.330	-0.629	-0.469	-0.594	-0.460	-0.219
Al					1.000	-0.228	0.510	0.276	-0.045	-0.267	-0.247	-0.158	-0.188	-0.188	-0.136	-0.185
NH_4						1.000	0.311	-0.021	-0.085	0.298	0.600	0.387	0.321	0.361	0.388	0.176
NO_3							1.000	0.003	-0.002	0.363	0.396	0.478	0.409	0.425	0.448	0.420
PO_4								1.000	0.571	0.090	0.272	0.024	0.220	0.760	0.089	0.340
SiO_2									1.000	0.550	0.245	0.287	0.527	0.440	0.192	0.626
Na										1.000	0.617	0.908	0.965	0.974	0.769	0.855
K											1.000	0.688	0.730	0.640	0.838	0.740
Ca												1.000	0.940	0.973	0.907	0.715
Mg													1.000	0.970	0.873	0.885
HCO_3														1.000	0.836	0.783
Cl															1.000	0.690
SO_4																1.000

calcium, magnesium and bicarbonate seem to be strongly correlated among themselves. The correlation co-efficient is greater than 0.9 in each pair of ions, thus indicating a common source for them.

5.8 Water Quality-Discharge Relationship

It is well established that the concentration of dissolved constituents in water is strongly related to river discharge. A consistent relationship is expected between average water discharge and solute concentration of streams in a conceptual dilution or mixing model. Dissolved solute concentration of a set of tributary waters add up at a downstream point. Solute concentration at this point represents the diluted version of all the earlier waters. If discharge factor is significant, then the predicted value provides a good comparison with the analytical value. Predicted solute concentration of mixed water derived by dilution can be given by the equation

$$C_p = \frac{Q_1C_1 + Q_2C_2 + \ldots\ldots\ldots\ldots\ldots + Q_nC_n}{Q_{n+1}}$$

where C_1, C_2.....C_n are average solute concentrations of different tributaries at stations 1, 2 ....n where Q_1, Q_2 ....Q_n are corresponding discharge values. C_p is the predicted

concentration of mixed water whose discharge value is Q_{n+1}.

The above model was put to test in the upper part of the Mahanadi river. Waters of stations 2, 5, 6 and 7 mix up near sampling station 8 (Fig.3.3). Mean discharges for the above stations were calculated from CWC water quality database. Average water compositions of 2, 5, 6 and 7 were used to predict the composition at station 8. A bar diagram (Fig. 5.6) was constructed based on the results of the calculations presented in Table 5.9. It is seen that observed concentrations of dissolved species such as Ca, Mg, HCO_3, Na, K, Cl, SO_4 and SiO_2 is generally higher than the predicted values. Observed TDS is 20% higher than the predicted value. This surplus TDS of 20% (which is largely due to the bicarbonate species) may be derived from the weathering of carbonate rocks in the upper part of the Mahanadi catchment area.

5.9 Water Quality-Catchment Area Relationship

A broad approach towards deciphering the relationship between water quality and catchment area is based on a principle similar to that outlined in the earlier section. Such a model takes into account the area weighted average water composition of tributaries to predict the solute composition at a downstream point of the main river. If only lithologic factors are

Table 5.9 Estimation of Q-weighted concentration (ppm) of solutes in mixed water

Dissolved solute	Predicted concentration $= \left[\frac{Q_2C_2 + Q_5C_5 + Q_6C_6 + Q_7C_7}{Q_8} \right]$	Observed concentration
Ca	19.84	23.50
Mg	6.79	7.73
HCO_3	88.39	110.23
Na	13.27	15.49
K	2.59	3.13
Cl	10.98	12.83
SO_4	19.29	18.95
SiO_2	12.32	16.55
TDS	173.47	208.41

Note : Q_2, Q_5, Q_6, Q_7 and Q_8 are average discharge values at stations 2, 5, 6, 7 and 8 respectively where C_2, C_5, C_6, C_7, and C_8 are corresponding solute concentrations.

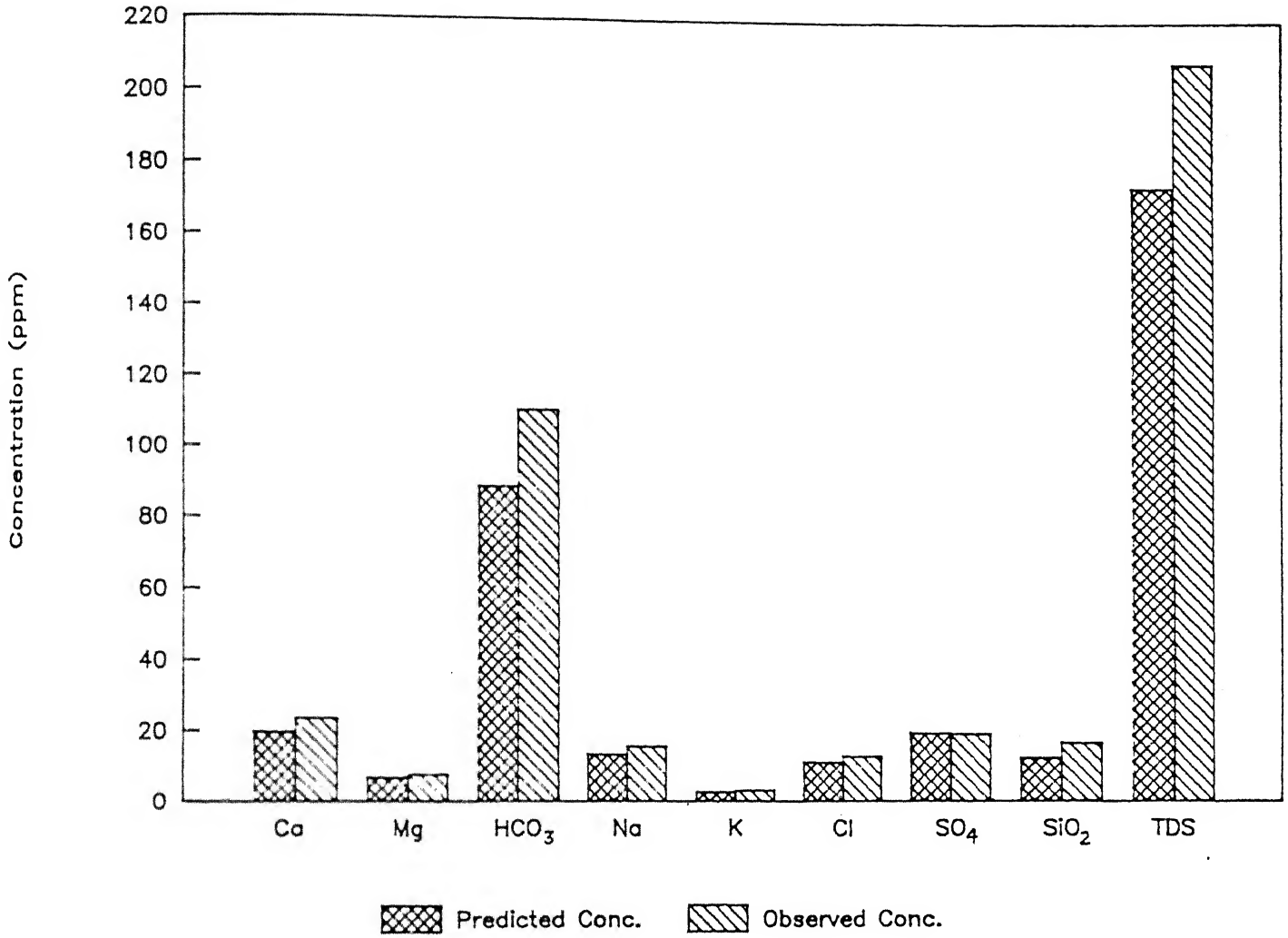

Fig. 5.6 Comparison of Q-weighted concentration with observed concentration

significant, then this predicted value provides a good comparison with the analytical value. Predicted solute concentration of mixed water derived from upstream tributaries can be given by the equation

$$C_p = \frac{A_1C_1 + A_2C_2 + \ldots\ldots\ldots + A_nC_n}{A_{n+1}}$$

where C_1, C_2.....C_n are average solute concentrations of tributaries with catchment areas A_1, A_2.....A_n respectively. C_p is the predicted solute concentration at the downstream station where the catchment area is A_{n+1}.

In the upper part of the Mahanadi basin (Fig.3.3), waters from upper Mahanadi, Seonath, Jonk and Hasdo tributaries add up near Basantpur (station 8). Average solute concentrations at stations 2, 5, 6 and 7 of above tributaries were used along with their catchment areas to predict the concentration at station 8. Fig.5.7 based on the calculations listed in Table 5.10, shows that observed concentration of most of the rock-derived cations like Ca, Mg, Na and K are equal to the predicted values. Magnitudes of observed bicarbonate and silica are found to be slightly higher while sulphate is lower than the predicted ones. Analytical TDS (200 ppm) is about 4% higher than the area weighted TDS (208 ppm). Therefore, it seems that the theoretical area weighted water composition is a fairly good approximation of the analytical one.

Table 5.10 Estimation of area weighted predicted concentration (ppm) of solutes in mixed water

Dissolved solute	Predicted concentration $= \left[\frac{A_2C_2 + A_5C_5 + A_6C_6 + A_7C_7}{A_8} \right]$	Observed concentration
Ca	22.92	23.50
Mg	8.09	7.73
HCO_3	102.94	110.23
Na	15.32	15.49
K	2.90	3.13
Cl	12.49	12.83
SO_4	21.63	18.95
SiO_2	13.78	16.55
TDS	200.07	208.41

Note : A_2, A_5, A_6, A_7 and A_8 are catchment areas (up to stations 2,5,6,7 and 8) whose values are 8760, 29645, 2920, 9730 and 57780 sq. kms. respectively. C_2, C_5, C_6, C_7 and C_8 are corresponding average concentration of solutes at stations 2, 5, 6, 7 and 8.

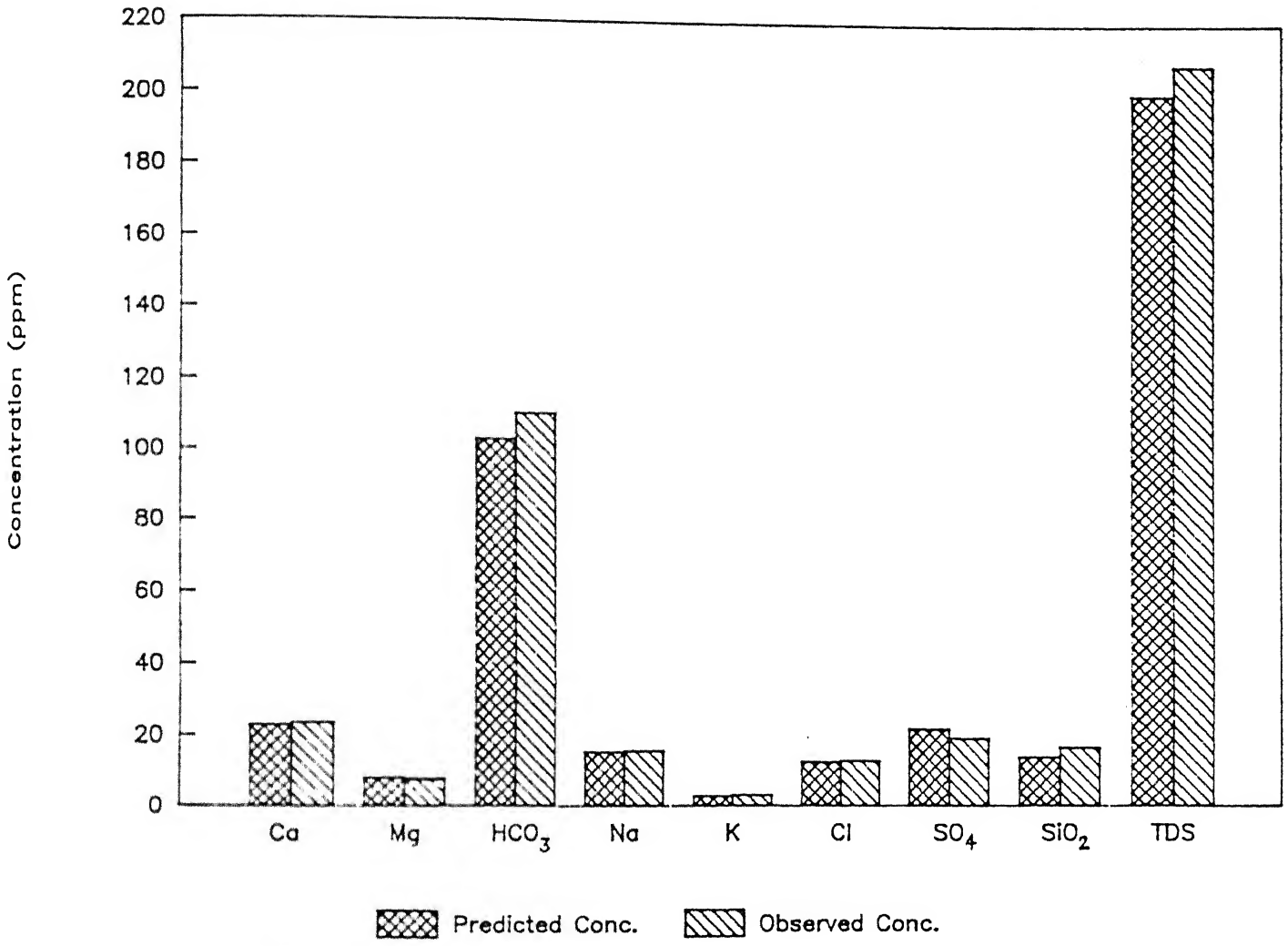

Fig. 5.7 Comparison of area weighted concentration with observed concentration

CHAPTER-6

ROCK-WATER INTERACTION

6.1 Introduction

Chemical weathering of rocks is an expression of rock-water interaction at relatively low temperature and pressure which prevail at the earth's surface environment. Extensive field and laboratory work has established that natural water is the principal weathering agent for rocks. Commonly observed rock-water reactions can be classified into three major groups. These are i) Congruent dissolution of carbonate rocks, ii) Incongruent decomposition of silicate rocks, iii) Oxidation-Reduction which is important in specific cases.

The rocks exposed in the upper part of the Mahanadi basin offer an opportunity to study all three types of reactions between rock and water. Following the approaches listed by Drever (1988), available data on mineralogy and water composition were used to test existing models based on Mass Balance, Thermodynamics and Statistical Methods.

6.2 Role of Carbon Dioxide

It is interesting to note that much of the weathering capability of natural water is due to the mild acidity produced by dissolved carbon dioxide. The principal source of CO_2 is the earth's atmosphere with additional supply from decay of organic matter in the soil zone. The chemistry of dissolved carbon

dioxide can be described with the help of the following reactions.

a) Solubility of carbon dioxide :

$$CO_2 + H_2O = H_2CO_3$$

$$K_{CO_2} = a_{H_2CO_3} / P_{CO_2} \qquad (1)$$

b) First dissociation of carbonic acid, H_2CO_3 :

$$H_2CO_3 = H^+ + HCO_3^-$$

$$K_1 = a_{H^+} \cdot a_{HCO_3^-} / a_{H_2CO_3} \qquad (2)$$

c) Second dissociation of HCO_3^-:

$$HCO_3^- = H^+ + CO_3^{2-}$$

$$K_2 = a_{H^+} \cdot a_{CO_3^{2-}} / a_{HCO_3^-} \qquad (3)$$

The equilibrium constants of the above reactions have values $K_{CO_2} = 10^{-1.5}$, $K_1 = 10^{-6.4}$ and $K_2 = 10^{-10.3}$ at 25°C (after Garrels and Christ, 1965).

Combining equations (1) and (2)

$$a_{H^+} \cdot a_{HCO_3^-} = 10^{-7.9} \times P_{CO_2}$$

Taking logarithm,

$$\log P_{CO_2} = 7.9 + \log a_{HCO_3^-} - pH \qquad (4)$$

Equation 4 can be used to calculate the value of partial pressure of CO_2 from pH and bicarbonate content of river water at an average temperature of 25°C. This CO_2 pressure can be defined as 'apparent CO_2' of river water consistent with the given temperature, pH and bicarbonate alkalinity.

The results of this calculation for the sampling points along the Mahanadi river have been given in Table 6.1. Log $a_{HCO_3^-}$ was calculated from the analysis listed in Chapter 5. These calculations show that the apparent CO_2 pressure in each of the tributaries and the main Mahanadi river is higher than the atmospheric $P_{CO_2} = 10^{-3.5}$ atm. with an average log P_{CO_2} =-2.464 ± 0.1. This is in agreement with the global trend described by Garrels and Mackenzie (1971) where average P_{CO_2} of major world rivers is about ten times higher than that of the earth's atmosphere. Holland (1978) and Stumm and Morgan (1981) have discussed the possible reasons for the apparent P_{CO_2} being higher than the atmospheric value. Two possibilities are 1) A perennial river like Mahanadi contains a significant fraction of high CO_2 ground water, 2) The rate of release of excess CO_2 for re-equilibrium with the atmosphere is slower than the rate of solubility of CO_2 gas.

Fig. 6.1 which is a plot of apparent P_{CO_2} versus TDS shows that the apparent CO_2 pressure remains fairly constant all

Table 6.1 Calculated values of apparent P_{CO_2} at 25°c

Station	TDS	HCO_3^-	$\gamma_{HCO_3^-}$	Log $a_{HCO_3^-}$	pH	Log P_{CO_2}
1.	76.7	0.640	0.9539	-3.096	7.23	-2.426
2.	105.9	1.213	0.9465	-3.061	7.21	-2.249
3.	194.7	2.323	0.9248	-3.332	7.75	-2.516
4.	343.4	3.643	0.9115	-3.521	7.76	-2.339
5.	212.9	2.352	0.9247	-3.387	7.77	-2.533
6.	152.9	1.672	0.9366	-3.244	7.57	-2.426
7.	124.5	1.197	0.9434	-3.053	7.35	-2.397
8.	161.6	1.807	0.9359	-3.228	7.72	-2.592
9.	109.3	0.957	0.9516	-3.064	7.33	-2.494
10.	93.9	1.110	0.9483	-3.022	7.39	-2.466
11.	174.5	2.254	0.9366	-3.323	7.83	-2.607
12.	140.5	1.675	0.9408	-3.197	7.64	-2.543
13.	117.4	1.435	0.9435	-3.132	7.47	-2.438

TDS is in mg/lit. and HCO_3^- in milli-mol/lit.

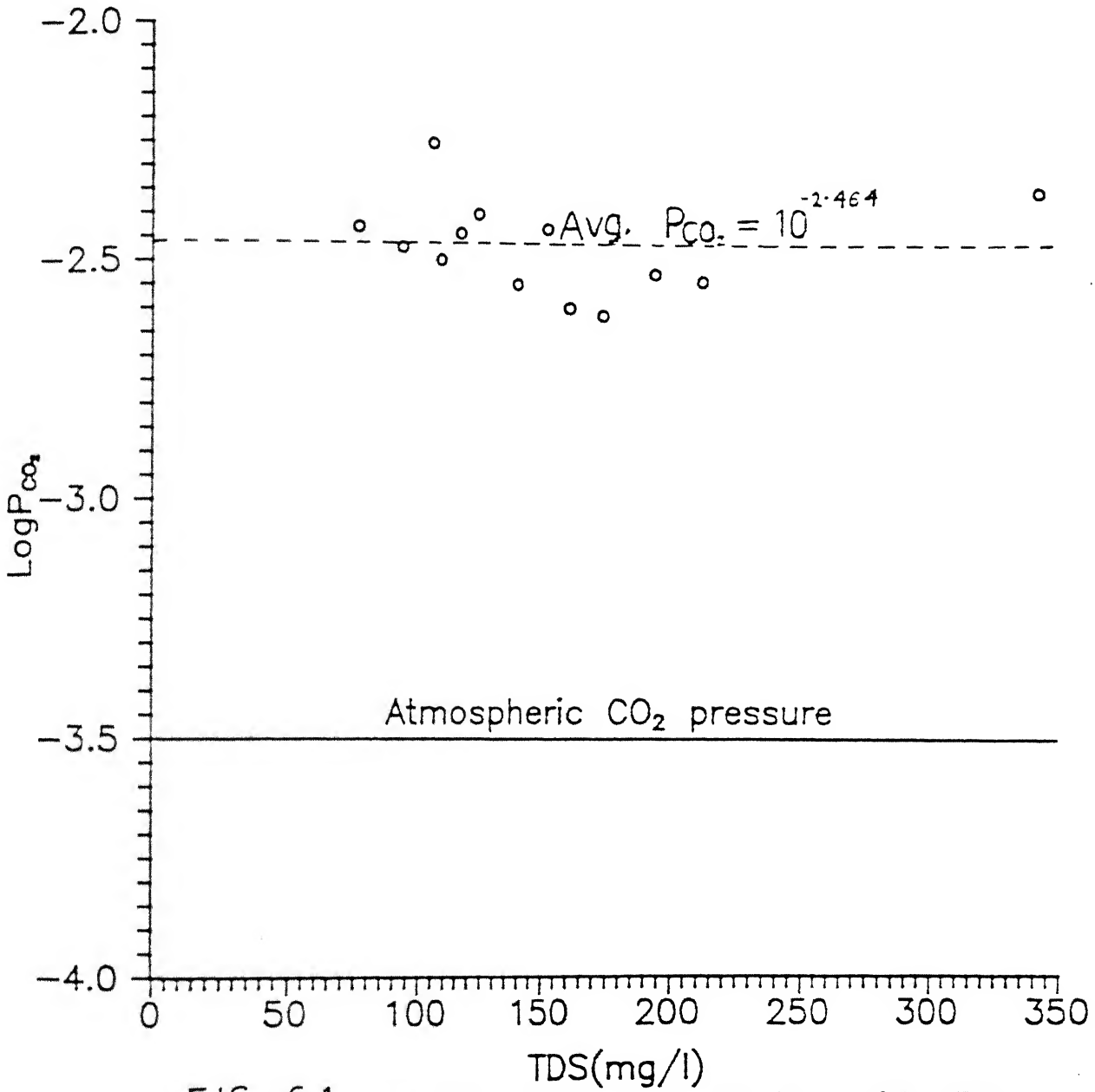

FIG 6.1 Variation of apparent P_{CO_2} with TDS

over the basin, independent of dissolved load along the course of the river. On the other hand, subtle variations from station to station indicate that samples from the upper part of the basin where limestone and calcareous shales are dominant (Fig. 3.4) have relatively higher P_{CO_2}

6.3 Silicate versus Carbonate Rocks

As discussed earlier, the Chhattisgarh basin occupying the upper part of the Mahanadi river is dominated by dolomitic limestone with intercalations of calcareous shale and sandstone (Fig. 3.4). The basin is fringed by basement rocks of granitic composition near the source of the river. On the other hand, in the lower reaches, the river passes through sandstone, granite, khondalite and other metamorphic rocks which are covered by lateritic soils and recent alluvium. Thus it will be reasonable to expect that a dual weathering scheme of carbonate and silicate rocks will influence the river water composition.

6.3.1 Sources of Ca and Mg

The main source of Ca and Mg in river water is the weathering of rock-forming minerals. Minor amounts can be derived from cyclic sea salts and pollution (Berner and Berner, 1987). The important Ca-bearing minerals are calcite and dolomite in limestones; gypsum and anhydrite in evaporite beds; plagioclase and other silicates in igneous and metamorphic rocks. Similarly, Mg in river water can be derived by the weathering of dolomite,

biolite, amphibole, pyroxene and olivine.

Holland (1978) attempted to estimate the contribution of Ca and Mg from rock weathering by a comprehensive review of rock and river water composition. He concluded that 86% of the TDS in average river water is derived from sedimentary terrains. On the other hand, 85 ± 8% of total Ca and 50 ± 20% of total Mg in sedimentary rocks are present in carbonate minerals. Details of this estimation are presented in the Appendix-II. It follows that in river water,

Ca from carbonate minerals

$$= (0.85 \pm 0.08) \times 0.86 \times Ca_{total}$$

$$= 0.73 \pm 0.08 \cong 74 \pm 10\%$$

Mg from carbonate minerals

$$= (0.50 \pm 0.20) \times 0.86 \times Mg_{total}$$

$$= 0.43 \pm 0.20 \cong 40 \pm 20\%$$

The remainder of Ca and Mg in river water is derived largely from silicate minerals, neglecting the minor contribution of sulphates and other evaporite minerals.

Meybeck (1987) arrived at a similar distribution of Ca and Mg in river water on a global scale based on a study of chemical weathering in selected rivers of France. His distribution of Ca was 67% from carbonates, 26% from silicates and 7% from evaporites. The values for Mg were 42% from carbonates, 48% from silicates and 10% from evaporites. It is obvious that this distribution may change from basin to basin depending on the proportion of different rock types. However, Holland's original

estimate that 74% of Ca and 40% of Mg in river water are derived from carbonate weathering appears to be a reasonable approximation. Therefore, this fractionation was adopted for estimating the source of bicarbonate as discussed in the next section.

6.3.2 Source of HCO_3

The main sources of HCO_3 in river water are i) atmospheric CO_2, ii) CO_3^{2-} in carbonate minerals and iii) CO_2 produced by oxidation of organic matter and carbon present in the rocks (Holland, 1978). As discussed in the earlier section, the second dissociation constant of H_2CO_3 has the value $K_2 = 10^{-10.3}$. It follows that at the pH value of river water which is much less than 10.3, CO_3^{2-} is relatively negligible compared to HCO_3^-. Therefore, among the dissolved carbonate species derived from the solubility of atmospheric CO_2 gas, HCO_3^- is dominant in river water.

The weakly acidic H_2CO_3 derived from atmospheric CO_2 weathers carbonate and silicate minerals according to the following two representative reactions.

a) Congruent dissolution of dolomite :

$$CaMg(CO_3)_2 + 2CO_2 + 2H_2O = Ca^{2+} + Mg^{2+} + 4HCO_3^-$$

Ca^{2+} and Mg^{2+} are balanced by HCO_3^- on an equivalent basis.

b) In congruent decomposition of K-felspar :

$$2K\text{-felspar} + 2CO_2 + 11H_2O = \text{Kaolinite} + 2K^+ + 2HCO_3^- + 4H_4SiO_4$$

Therefore, the HCO_3^- in river water has two fractions viz.

i) HCO_3^- derived from the weathering of primary carbonate minerals as well as calcareous cement.

ii) HCO_3^- derived from the weathering of silicate minerals.

The total Ca and Mg in river water also have the same two sources, neglecting the weathering of evaporites. Hence the proportion of the carbonate and silicate fraction of total HCO_3^- can be calculated by the following steps suggested by Raymahashay (1986).

1. $(HCO_3)_{tot} = (HCO_3)_c + (HCO_3)_{si}$
2. $(HCO_3)_c = (Ca)_c + (Mg)_c$
3. $(Ca)_{tot} = (Ca)_c + (Ca)_{si}$
4. $(Mg)_{tot} = (Mg)_c + (Mg)_{si}$
5. $(HCO_3)_c = 0.74(Ca)_{tot} + 0.4(Mg)_{tot}$
6. $(HCO_3)_{si} = (HCO_3)_{tot} - (HCO_3)_c$

where all concentrations are in milli-equivalents per litre and the subscripts `c', `si' and `tot' stand for carbonate, silicate and total respectively.

The results of this calculation for the Mahanadi river have been presented in Table 6.2. It is realized that the estimate of the proportion of HCO_3 derived from carbonate weathering can be improved if factors for Ca and Mg specific to the Mahanadi basin are determined to replace the global average of 0.74 and 0.40 adopted from Holland (1978).

The ratio $(HCO_3)_c/(HCO_3)_{si}$ serves as an index of carbonate versus silicate weathering in different parts of the

Table : 6.2 Bicarbonate derived from rock weathering in the Mahanadi basin (All concentrations are in milliequivalents per litre)

Parameter	Ca_{tot}	Mg_{tot}	$(HCO_3)_{tot}$	$(HCO_3)_c$	$(HCO_3)_{si}$	$(HCO_3)_c/(HC$
Stn-1	0.63	0.24	0.84	0.56	0.28	2.00
Stn-2	0.91	0.31	1.21	0.80	0.41	1.95
Stn-3	1.55	0.87	2.32	1.49	0.83	1.79
Stn-4	1.98	1.48	3.64	2.06	1.58	1.30
Stn-5	1.54	1.04	2.35	1.56	0.79	1.97
Stn-6	1.33	0.55	1.87	1.20	0.67	1.79
Stn-7	0.88	0.38	1.20	0.80	0.40	2.00
Stn-8	1.17	0.64	1.81	1.12	0.69	1.62
Stn-9	0.57	0.31	0.91	0.55	0.36	1.53
Stn-10	0.68	0.33	1.11	0.64	0.47	1.36
Stn-11	1.32	0.66	2.25	1.24	1.01	1.23
Stn-12	1.03	0.52	1.68	0.97	0.71	1.37
Stn-13	1.01	0.41	1.44	0.91	0.53	1.72

basin. For example, the relatively high values of this ratio at stations 1, 2, 3 ,5 and 6 probably reflect the dominance of carbonate weathering over silicate weathering. The geologic map (Fig. 6.2) and lithologic data (Table 6.3) support this conclusion. The high ratio at station 7 is at least partly due to the occurrence of carbonaceous shale in the drainage area. As discussed earlier, oxidation of carbonaceous matter in rocks is one of the sources of bicarbonate in river water. In contrast, the relatively low values at stations 9, 10, 11 and 12 may be due to the weathering of shale, sandstone, granite, khondalite, charnockite and similar silicate dominated rocks occurring in the drainage area. The low value at station 4 located within the limestone rich Chhattisgarh basin requires special attention. The main rock type in this area happens to be a reddish brown shale in contact with argillaceous dolomitic limestone (Das et al., 1990). The X-ray pattern of this rock did not show any carbonate peaks. It appears that the weathering of the silicate rich shale surpasses the effect of carbonate weathering at this location. The $(HCO_3)_c/(HCO_3)_{si}$ ratio at stations 8 and 13 has a value intermediate between the range of carbonate weathering and silicate weathering. These two stations are located on the main Mahanadi river channel. Therefore, it is highly probable that the river water composition at these stations reflect a combined influence of weathering of carbonate and silicate rocks which occur in the drainage basins of the tributaries.

Table 6.3 Lithology around CWC sampling stations along the Mahanadi river

Station	Inferred rock types in the catchment area
1.	Limestone, granite and sandstone
2.	Granite, limestone and sandstone
3.	Dolomitic limestone, calcareous shale, sandstone and granite.
4.	Shale, dolomitic limestone and sandstone
5.	Dolomitic limestone, shale, sandstone and granite
6.	Granite, limestone and sandstone
7.	Carbonaceous shale, sandstone, granite and limestone
8.	Dolomitic limestone, shale, granite and sandstone
9.	Sandstone, shale and limestone
10.	Granite, sandstone and shale
11.	Granite and charnockite
12.	Granite, khondalite and charnockite
13.	All the above rocks with alluvium.

6.3.3 Balance of (Ca + Mg) and HCO_3

As discussed above, Ca, Mg and HCO_3 in river water have two major sources namely, carbonate and silicate weathering. Therefore,

$$(Ca + Mg)_{tot} = (Ca + Mg)_c + (Ca + Mg)_{si}$$

and $$(HCO_3)_{tot} = (HCO_3)_c + (HCO_3)_{si}.$$

On the other hand, the stoichiometry of carbonate weathering reactions demands that $(Ca + Mg)_c = (HCO_3)_c$. However, the data presented in Table 6.4 shows that in the Mahanadi river basin, $(Ca + Mg)_{tot}$ is not very different from $(HCO_3)_{tot}$. Fig. 6.3 also shows that the water compositions fall very close to the equiline $(Ca + Mg)_{tot} = (HCO_3)_{tot}$. It is interesting to note that Stallard and Edmond (1983) drew a similar conclusion for the Amazon basin. The near-equality of $(Ca + Mg)_{tot}$ and $(HCO_3)_{tot}$ can be achieved in the equation

$$(Ca + Mg)_c + (Ca + Mg)_{si} = (HCO_3)_c + (HCO_3)_{si}$$

if the following two conditions are satisfied :

i) $(Ca + Mg)_c > (Ca + Mg)_{si}$ and $(HCO_3)_c > (HCO_3)_{si}$

i.e. carbonate weathering dominates over silicate weathering.

ii) $(Ca + Mg)_{si} = (HCO_3)_{si}$

The estimation of carbonate weathering fraction of (Ca + Mg) and HCO_3 from Holland's global factor of $(Ca)_c = 0.74(Ca)_{tot}$ and $(Mg)_c = 0.4(Mg)_{tot}$ indicates that the first condition is satisfied for each of the water samples of the Mahanadi river basin. In other words, carbonate weathering is relatively more important than silicate weathering throughout the Mahanadi basin.

Table 6.4 : Fractionation of Ca, Mg and HCO_3 in water

Parameter	$(Ca+Mg)_{tot}$	$(HCO_3)_{tot}$	$(Ca+Mg)_c = (HCO_3)_c$	$(Ca+Mg)_{si}$	$(HCO_3)_{si}$
Stn-1	0.87	0.84	0.56	0.31	0.28
Stn-2	1.23	1.21	0.80	0.43	0.41
Stn-3	2.42	2.32	1.49	0.93	0.83
Stn-4	3.46	3.64	2.06	1.40	1.58
Stn-5	2.58	2.35	1.56	1.02	0.79
Stn-6	1.88	1.87	1.20	0.68	0.67
Stn-7	1.26	1.20	0.80	0.46	0.40
Stn-8	1.82	1.81	1.13	0.69	0.68
Stn-9	0.88	0.91	0.55	0.33	0.36
Stn-10	1.01	1.11	0.64	0.37	0.47
Stn-11	1.98	2.25	1.24	0.74	1.01
Stn-12	1.55	1.68	0.97	0.58	0.71
Stn-13	1.42	1.44	0.91	0.51	0.53

(All concentrations are in milliequivalents per litre)

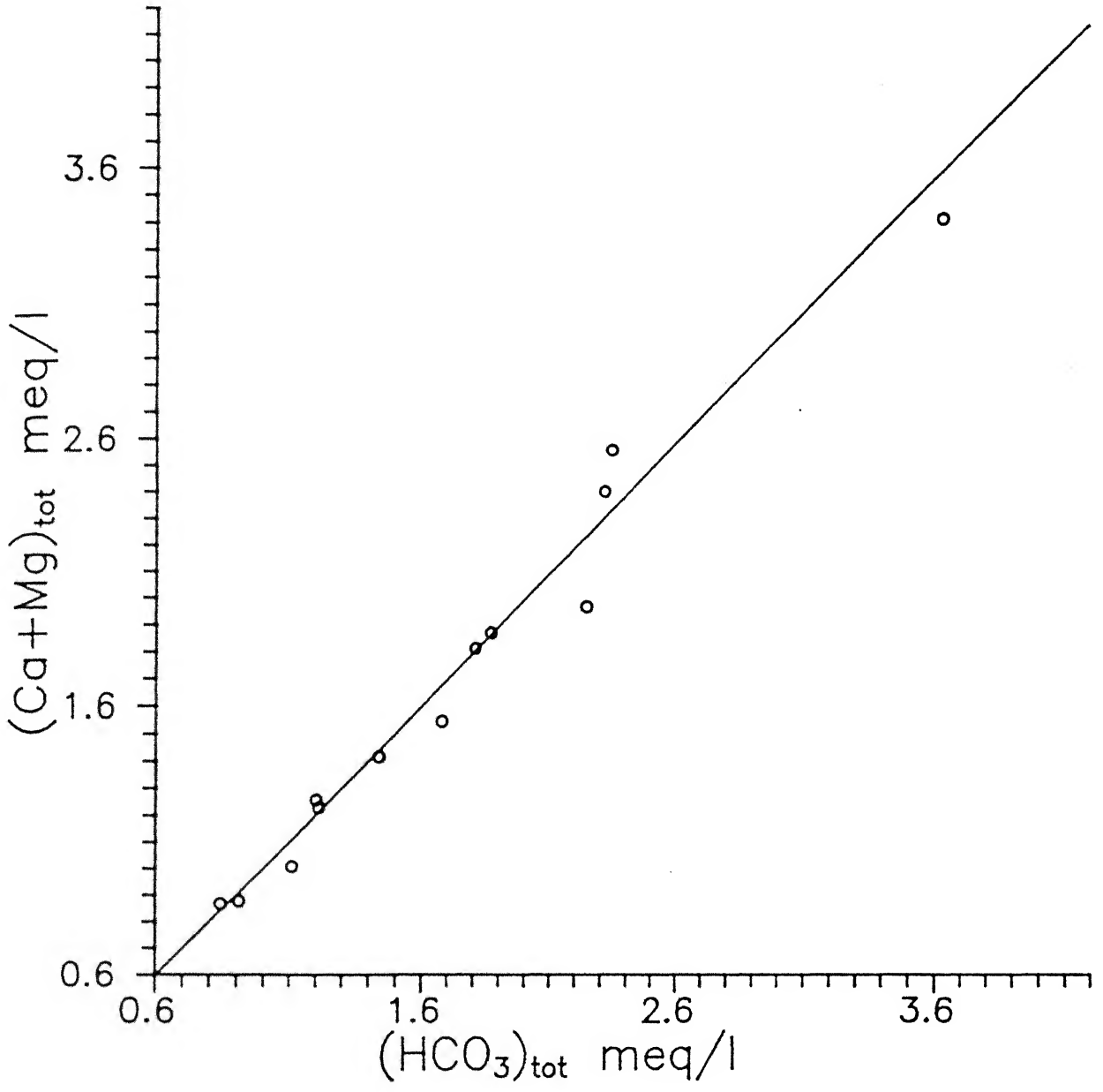

Fig. 6.2 Balance of $(Ca+Mg)_{total}$ and $(HCO_3)_{total}$

There are two local factors which might explain the small deviations from the equiline in Fig. 6.3. For example, the weathering of evaporite beds has been neglected in these calculations. However, it has been realized that the small excess of $(Ca + Mg)_{tot}$ over $(HCO_3)_{tot}$ at stations 3 and 5 can be produced by this extra source of Ca and Mg. In fact gypsum occurs as cementing material in surface exposures of shale and mudstone in the Seonath river section. It has been observed in bore hole sections within calcareous and non-calcareous shales of this area (Das et al., 1990). Similarly, the small deficiency in $(Ca + Mg)_{tot}$ at stations 4, 10, 11 and 12 can be produced by ion-exchange between Na-clays and Ca^{2+} in water (Cerling et al., 1989). This mechanism is feasible in the silicate dominated drainage areas corresponding to these stations.

6.3.4 Ternary Diagrams

The relative role of carbonate, silicate and evaporite weathering in influencing river water composition can be evaluated through a ternary diagram (Fig. 6.3) similar to that developed by Stallard and Edmonds (1983). The relevant percentages of HCO_3, SiO_2 and SO_4 are given in Table 6.5. In the diagram, the Mahanadi river waters plot near the bicarbonate vertex. This indicates that the weathering of carbonate rocks has the maximum influence on river water composition.

The charge balance of $(Ca^{2+} + Mg^{2+})_{tot}$ by HCO_3^- or SO_4^{2-} can be further verified by another ternary plot of these

Table 6.5 Relative percentages of HCO_3, SiO_2 and SO_4 on an equivalent basis

Sampling stations	HCO_3	SiO_2	SO_4
1.	65.57	18.19	16.24
2.	75.95	14.90	9.15
3.	77.48	7.84	14.68
4.	70.63	6.18	23.19
5.	71.29	8.28	20.43
6.	80.52	10.19	9.29
7.	64.40	13.16	22.79
8.	72.95	11.14	15.91
9.	59.91	18.96	21.13
10.	67.23	16.05	16.72
11.	83.92	9.08	7.00
12.	76.34	13.81	9.85
13.	76.33	12.82	10.85

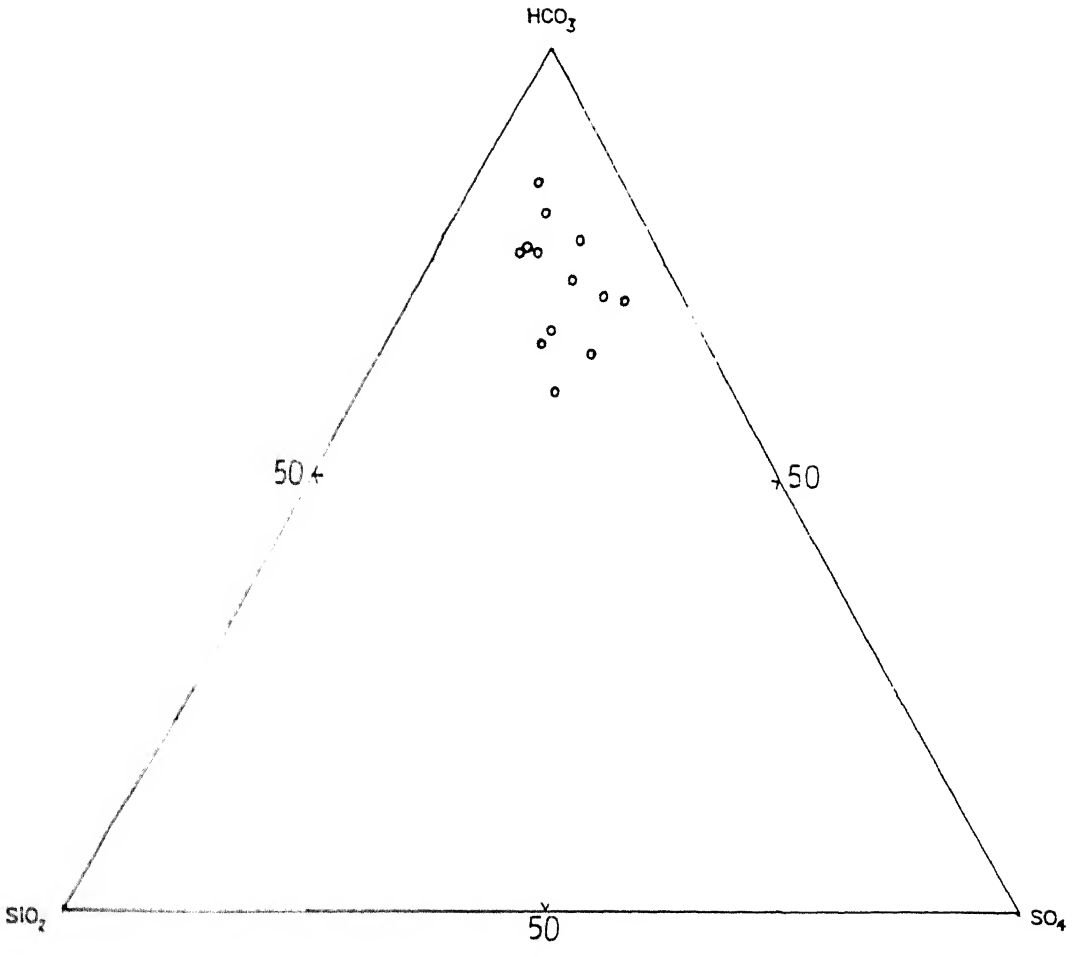

6.3 Ternary plot of bicarbonate, silica and sulphate

parameters (Fig. 6.4). The relevant percentages are given in Table 6.6. It is clearly seen that water compositions from the Mahanadi river fall along the line $(Ca^{2+} + Mg^{2+}) = HCO_3^-$ which once again confirms that weathering of carbonates is the dominant process.

6.4 Carbonate Mineral Equilibria

The broad geochemical trends discussed in the earlier sections indicate that weathering of dolomitic limestone has a pronounced influence on water chemistry in the upper part of the Mahanadi river basin. Therefore, it would be important to evaluate the state of saturation of river water in terms of the solubility products of the two minerals calcite and dolomite. The relevant reactions are

i) $CaCO_3 = Ca^{2+} + CO_3^{2-}$

$K_c = a_{Ca^{2+}} \cdot a_{CO_3^{2-}} = 10^{-8.4}$ at 25°C.

ii) $CaMg(CO_3)_2 = Ca^{2+} + Mg^{2+} + 2CO_3^{2-}$

$K_d = a_{Ca^{2+}} \cdot a_{Mg^{2+}} \cdot (a_{CO_3^{2-}})^2 = 10^{-17.0}$ at 25°C.

At the first instance, the ionic activity product (IAP) in river water was calculated using pH, $(a_{Ca^{2+}})_{tot}$, $(a_{Mg^{2+}})_{tot}$ and $(a_{HCO_3^-})_{tot}$ listed in Table 6.7. The activity of CO_3^{2-} ion was calculated from $(a_{HCO_3^-})_{tot}$ from the relationship

Table 6.6 Relative percentages of (Ca+Mg), HCO_3 and SO_4 on equivalent basis

Sampling	(Ca+Mg)	HCO_3	SO_4
1.	45.47	43.71	10.82
2.	47.51	46.85	5.64
3.	46.67	44.84	8.49
4.	41.71	44.17	14.52
5.	46.08	41.92	12.00
6.	47.41	47.15	5.44
7.	43.70	41.52	14.78
8.	45.24	44.96	9.80
9.	41.99	42.88	15.13
10.	42.30	46.21	11.49
11.	44.75	51.00	4.25
12.	45.14	48.59	6.27
13.	46.39	46.94	6.67

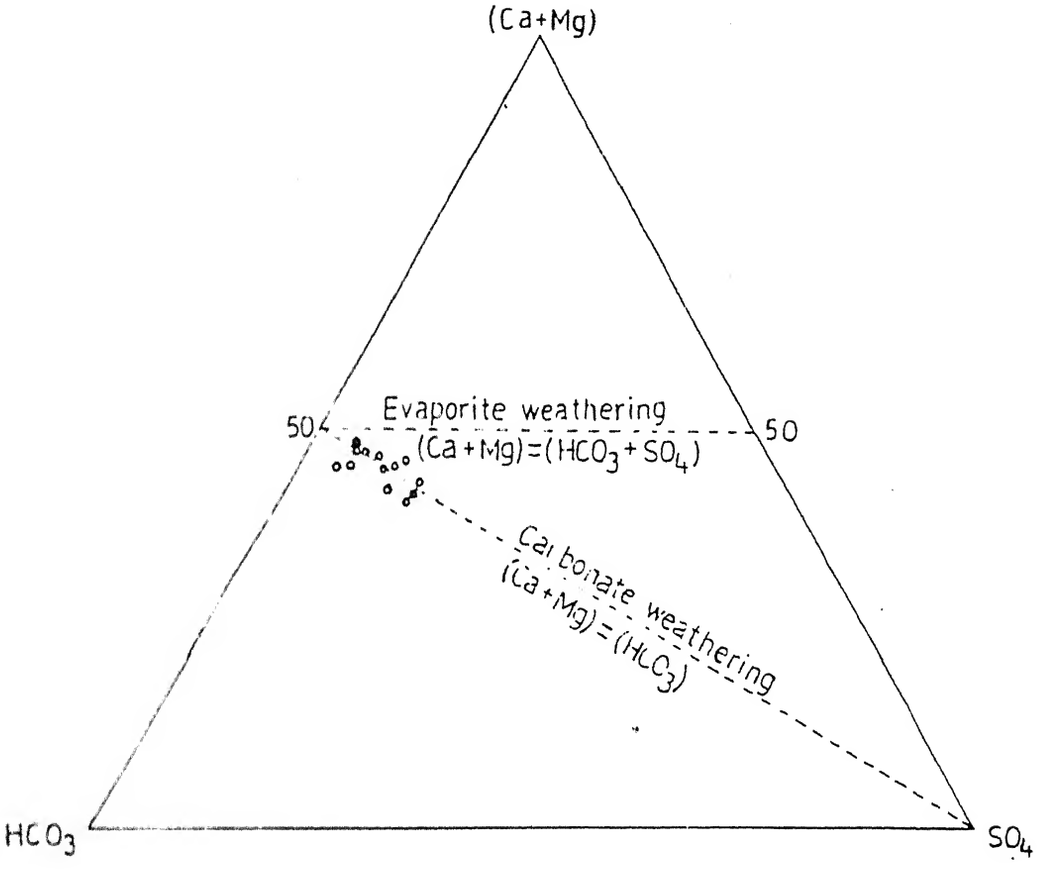

Fig. 6.4 Ternary plot of (Ca+Mg), HCO_3 and SO_4

$$K_2 = \frac{a_{CO_3^{2-}} \cdot a_{H^+}}{(a_{HCO_3^-})_{tot}} = 10^{-10.3} \text{ at } 25^{\circ}C.$$

The calculated values of IAP are also listed in Table 6.7. It is clear that the river water at all stations is undersaturated with respect to calcite and dolomite with the exception of station 4. This should account for the aggressive weathering of dolomitic limestone throughout the river basin.

An attempt was made to refine this calculation by considering the fraction of Ca and Mg derived from carbonate weathering instead of total Ca and Mg. As before on an equivalent basis

$$(Ca)_c = 0.74(Ca)_{tot}$$

$$(Mg)_c = 0.4(Mg)_{tot}$$

Therefore, $(HCO_3)_c = (Ca)_c + (Mg)_c$

and $$a_{CO_3^{2-}} = \frac{K_2 \cdot (a_{HCO_3^-})_c}{a_{H^+}}$$

The revised calculations are presented in Table 6.8. This revision confirms the earlier conclusion that except at station 4, the river water is undersaturated with respect to calcite and dolomite throughout the basin. This trend is presented graphically in Figs. 6.5(a) and 6.5(b) where the logarithmic values of IAP for calcite and dolomite are plotted against TDS. It is obvious that at high values of dissolved ion concentration, the water approaches saturation with calcite and

Table 6.8 Estimation of calcite and dolomite saturation from carbonate derived Ca^{2+}, Mg^{2+} and HCO_3^- in water

Stn.	pH	$\log(a_{HCO_3^-})_c$	$\log a_{CO_3^{2-}}$	$\log(a_{Ca^{2+}})_c$	$\log(a_{Mg^{2+}})_c$	$\log\left[a_{Ca^{2+}}.a_{CO_3^{2-}}\right]$	$\log\left[a_{Ca^{2+}}.a_{Mg^{2+}}(a_{CO_3^{2-}}\right]$	TDS (mg/l)
1.	7.23	-3.195	-6.265	-3.712	-4.402	-9.977	-20.640	76.7
2.	7.21	-3.041	-6.131	-3.562	-4.294	-9.693	-20.120	105.9
3.	7.75	-2.757	-5.307	-3.377	-3.897	-8.684	-17.890	194.7
4.	7.76	-2.564	-5.104	-3.296	-3.688	-8.400	-17.190	343.4
5.	7.77	-2.774	-5.274	-3.379	-3.817	-8.653	-17.740	212.9
6.	7.57	-2.854	-5.314	-3.421	-4.085	-8.735	-18.130	152.9
7.	7.35	-3.042	-5.992	-3.588	-4.223	-9.580	-19.790	124.5
8.	7.73	-2.863	-5.433	-3.477	-4.005	-8.910	-18.350	161.6
9.	7.33	-3.156	-6.126	-3.760	-4.287	-9.886	-20.300	109.3
10.	7.39	-3.075	-5.985	-3.690	-4.268	-9.675	-19.930	93.9
11.	7.83	-2.775	-5.245	-3.431	-4.000	-8.676	-17.920	174.5
12.	7.64	-2.898	-5.558	-3.524	-4.086	-9.082	-18.730	140.5
13.	7.47	-2.967	-5.797	-3.530	-4.188	-9.327	-19.310	117.4

Note : 1. $a_{CO_3^{2-}}$ calculated from pH, $(a_{HCO_3^-})_c$ and

$K_2 = 10^{-10.3}$ at 25°C

2. $K_c = 10^{-8.4}$ and $K_d = 10^{-17}$ at 25°C.

Table 6.7 Estimation of calcite and dolomite saturation from total Ca^{2+}, Mg^{2+} and HCO_3^- in water

Stn.	pH	$\log(a_{HCO_3^-})_{tot}$	$\log a_{CO_3^{2-}}$	$\log(a_{Ca^{2+}})_{tot}$	$\log(a_{Mg^{2+}})_{tot}$	$\log\left[a_{Ca^{2+}}.a_{CO_3^{2-}}\right]$	$\log\left[a_{Ca^{2+}}.a_{Mg^{2+}}.(a_{CO_3^{2-}}\right.$
1.	7.23	-3.096	-6.166	-3.582	-4.004	-9.748	-19.918
2.	7.21	-2.939	-6.029	-3.432	-3.896	-9.461	-19.386
3.	7.75	-2.667	-5.217	-3.246	-3.499	-8.463	-17.179
4.	7.76	-2.479	-5.019	-3.165	-3.219	-8.184	-16.494
5.	7.77	-2.662	-5.192	-3.249	-3.419	-8.441	-17.052
6.	7.57	-2.756	-5.486	-3.291	-3.674	-8.777	-17.937
7.	7.35	-2.947	-5.897	-3.547	-3.824	-9.354	-19.075
8.	7.72	-2.772	-5.352	-3.347	-3.607	-8.699	-17.658
9.	7.33	-3.064	-6.304	-3.629	-3.889	-9.663	-19.586
10.	7.39	-2.978	-5.888	-3.559	-3.870	-9.447	-19.205
11.	7.83	-2.667	-5.137	-3.300	-3.602	-8.437	-17.176
12.	7.64	-2.802	-5.462	-3.394	-3.688	-8.856	-18.006
13.	7.47	-2.868	-5.698	-3.399	-3.790	-9.097	-18.585

Note : 1. $a_{CO_3^{2-}}$ calculated from pH, $(a_{HCO_3^-})_{tot}$ and

$K_2 = 10^{-10.3}$ at 25°C

2. $K_c = 10^{-8.4}$ and $K_d = 10^{-17}$ at 25°C.

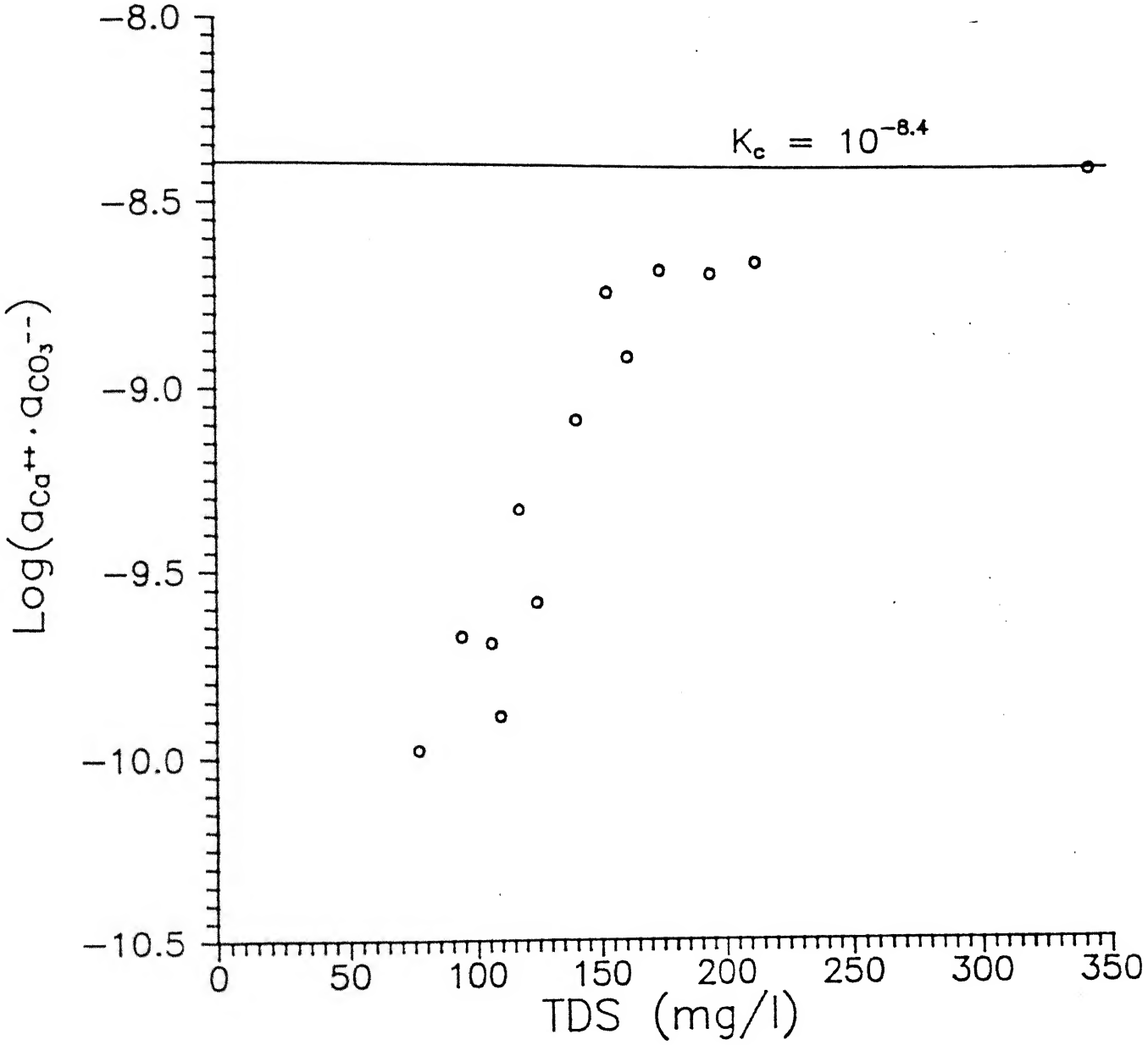

Fig. 6.5(a) TDS versus log $IAP_{calcite}$

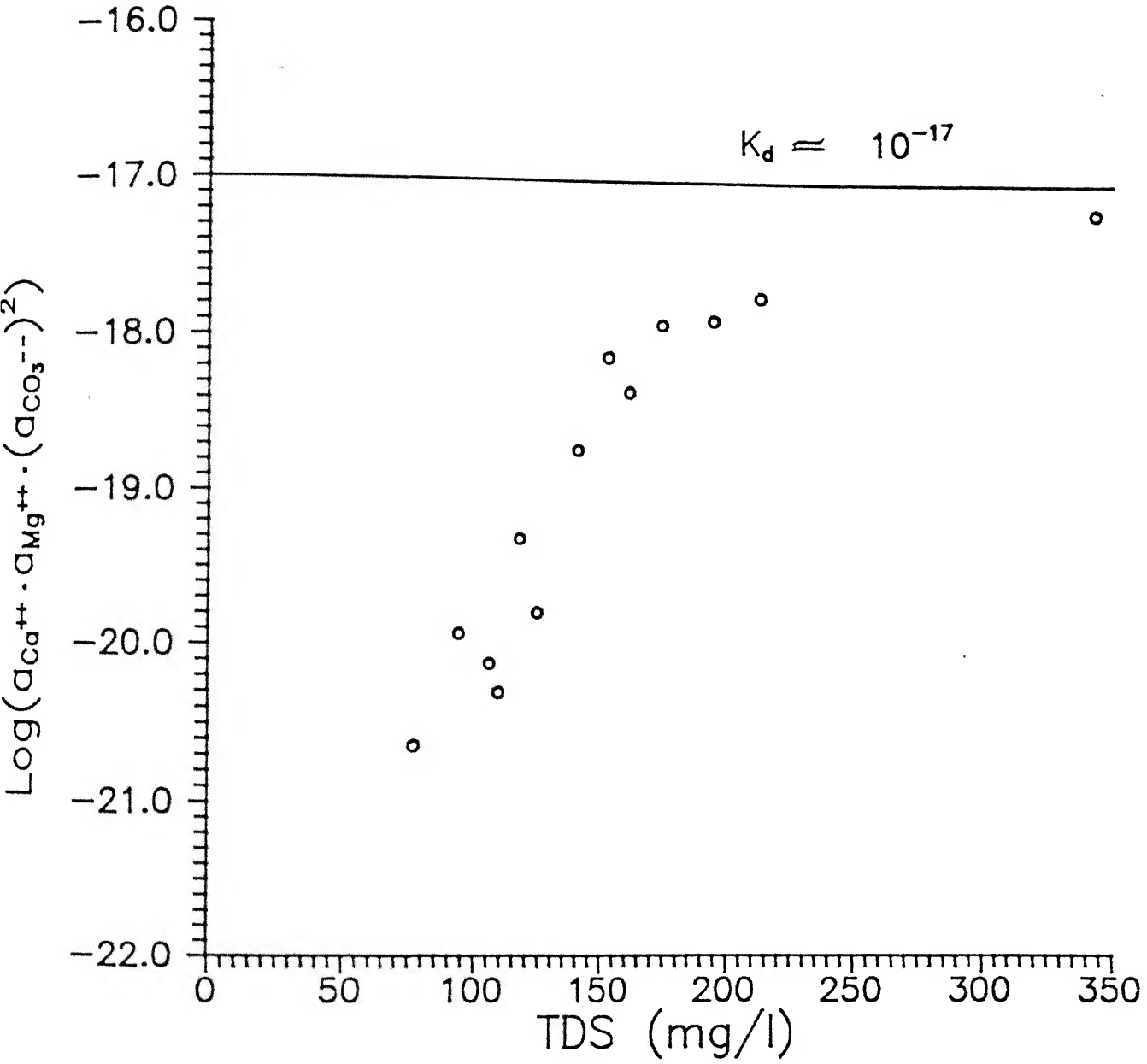

Fig. 6.5(b) TDS versus log $IAP_{dolomite}$

dolomite. For example, TDS is maximum at station 4 and this may be the reason why the river water is practically saturated with respect to calcite and dolomite at this location.

Similar conclusions can be drawn by evaluating a Saturation Index (SI) defined as

$$SI_{calcite} = \log \left[\frac{(a_{Ca^{2+}})_c \cdot (a_{CO_3^{2-}})_c}{K_{calcite}} \right]$$

and

$$SI_{dolomite} = \log \left[\frac{(a_{Ca^{2+}})_c \cdot (a_{Mg^{2+}})_c \cdot (a_{CO_3^{2-}})_c^2}{K_{dolomite}} \right]$$

It is obvious that a value of SI = 0 indicates saturation. The SI values have been presented in Table 6.9 and the same plotted in Fig. 6.6. The general undersaturation of the river water simultaneously with respect to calcite and dolomite is clear from this figure.

The calcium and magnesium concentration in river water can also be used to evaluate the possibility of dolomitization of calcite by limestone-water interaction. Calcite can be converted to dolomite by the reaction

$$2CaCO_3 + Mg^{2+} = CaMg(CO_3)_2 + Ca^{2+}$$

The equilibrium constant of this reaction is expressed as

$$K_{cal\text{-}dol} = \frac{a_{Ca^{2+}}}{a_{Mg^{2+}}}$$

Table 6.9 Estimation of Saturation Index (SI) of calcite and dolomite

Station	$SI_{calcite}$	$SI_{dolomite}$
1.	-1.58	-3.64
2.	-1.29	-3.12
3.	-0.28	-0.89
4.	0.00	-0.19
5.	-0.25	-0.74
6.	-0.34	-1.13
7.	-1.18	-2.79
8.	-0.51	-1.35
9.	-1.49	-3.30
10.	-1.28	-2.90
11.	-0.28	-0.92
12.	-0.68	-1.73
13.	-0.93	-2.31

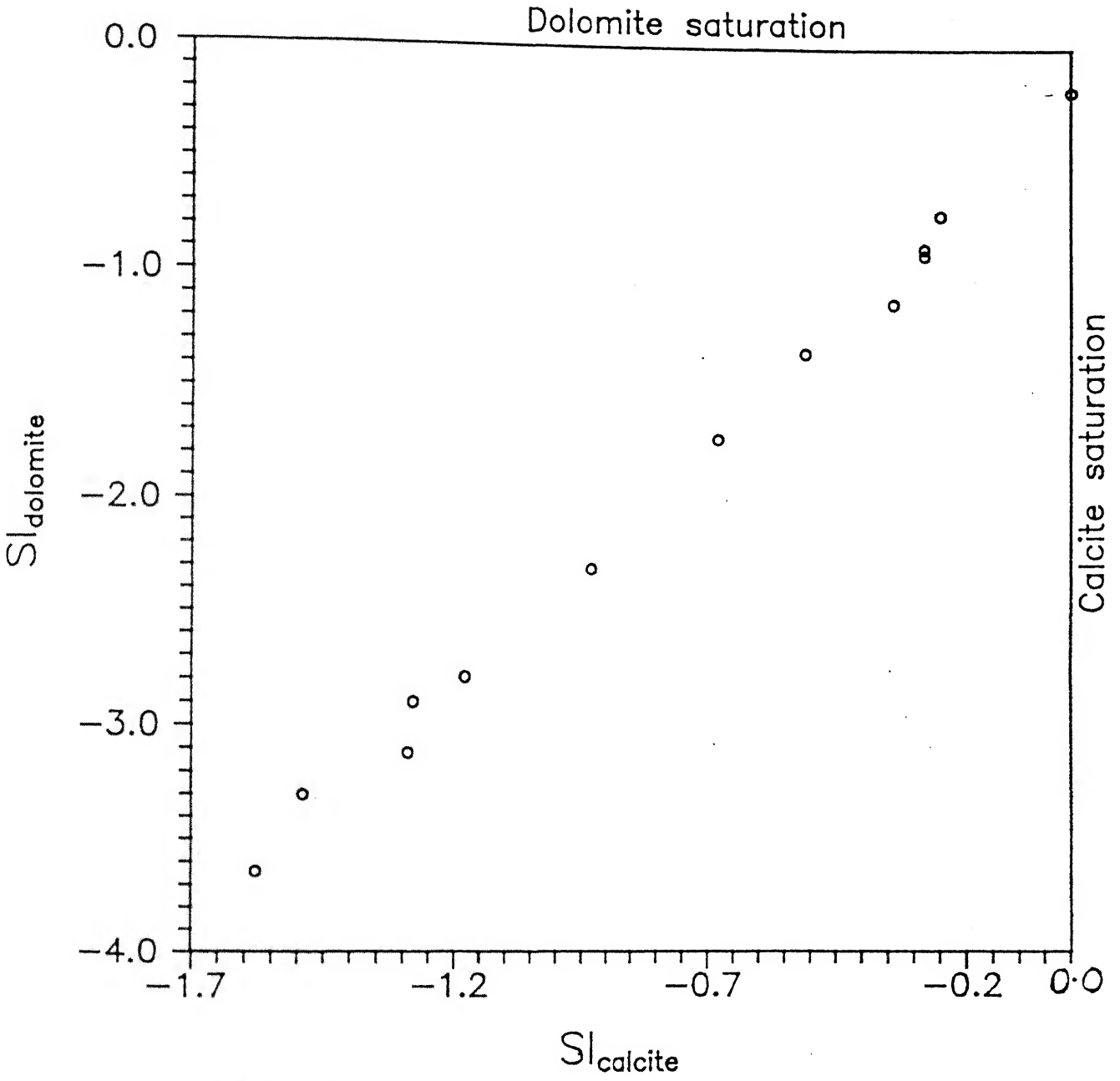

Fig. 6.6 Saturation indices for calcite and dolomite with respect to river water samples

This is numerically equal to

$$\frac{K_c^2}{K_d} = \frac{(10^{-8.4})^2}{(10^{-17.0})} = 10^{0.20}$$

In other words calcite can be converted to dolomite only if the value of $a_{Ca}{}^{2+}/a_{Mg}{}^{2+}$ is less than $10^{0.20}$. The value of this ratio at various stations along the Mahanadi river have been listed in Table 6.10. It is clear that the river water is not capable of dolomitization except at station 4 and 5.

6.5 Thermodynamics of Silicate-Water Equilibria

Thermodynamic data allow us to verify whether a given water environment is suitable for stability of silicate minerals found in weathered rocks, soils and sediments.

To start with, we need a set of weathering reactions involving primary minerals, secondary minerals and dissolved ions. It is assumed that these reactions approach equilibrium in the weathering environment. In that case, the equilibrium constant (K) of these reactions can be estimated as discussed below.

For a reversible reaction such as

$$bB + cC \rightleftharpoons dD + eE$$

$$K = \frac{a_D{}^d \cdot a_E{}^e}{a_B{}^b \cdot a_C{}^c}$$

where the symbol 'a' stands for activity or effective

Table 6.10 Calculation for dolomitization of calcite

Station	$\log \left[(a_{Ca^{2+}})_{tot} / (a_{Mg^{2+}})_{tot} \right]$
1.	0.42
2.	0.46
3.	0.25
4.	0.05
5.	0.17
6.	0.38
7.	0.28
8.	0.26
9.	0.26
10.	0.31
11.	0.30
12.	0.29
13.	0.39

concentration of the species taking part in the reaction. For pure minerals and liquid H_2O, activity is assumed to be equal to unity.

This constant is related to the change in Gibbs free energy during reaction (ΔG_r^o) under standard conditions (298.16°K and 1 atmosphere pressure) through the equation

$$\Delta G_r^o = -RT \ln K$$

or $$\Delta G_r^o = -2.303\ RT \log K \qquad (1)$$

where R is universal gas constant equal to 1.98×10^{-3} kcal/deg.mole or 8.28×10^{-3} kJ/deg.mole. ΔG_r^o for a given weathering reaction can be calculated from the relationship

$$\Delta G_r^o = \Sigma \Delta G_{f\ product}^o - \Sigma\ \Delta G_{f\ reactant}^o$$

The symbol ΔG_f^o stands for standard state Gibbs free energy of formation of various species participating in the reaction.

At 25°C, the above equation (1) reduces to

$$\Delta G_r^o = -\ 1.364 \log K$$

in kcal

or $$\Delta G_r^o = -\ 5.707 \log K$$

in kJ

6.5.1 Construction of Stability Diagrams

Sufficient information are now available for the construction of stability diagrams in the four systems :

a) $K_2O - Al_2O_3 - SiO_2 - H_2O$

b) $Na_2O - Al_2O_3 - SiO_2 - H_2O$

c) $CaO - Al_2O_3 - SiO_2 - H_2O$

d) $MgO - Al_2O_3 - SiO_2 - H_2O$

As illustrated below, equilibrium constants of relevant weathering reactions are simple functions of cation to hydrogen ion activity ratio and silica activity. By convention, these weathering reactions are written with the 'conservation of Al principle' i.e all Al is locked up in the weathering products and the solution does not contain dissolved Al. Thus stability diagrams can be constructed with logarithmic axes ashowing a_{K^+} / a_{H^+}, a_{Na^+} / a_{H^+}, $a_{Ca^{2+}} / (a_{H^+})^2$, $a_{Mg^{2+}} / (a_{H^+})^2$ and $a_{H_4SiO_4}$.

Three constant silica lines are common to the four diagrams (Fig. 6.7, 6.8, 6.9 and 6.10). These are

1) Solubility of quartz, 6 ppm SiO_2 at 25^oC

$$\text{Quartz} + 2H_2O = H_4SiO_4$$

$$\log K_1 = \log a_{H_4SiO_4} = -4.0$$

2) Solubility of amorphous silica, 120 ppm SiO_2 at 25°C

$$SiO_2 + 2H_2O = H_4SiO_4$$
$$\log K_2 = \log a_{H_4SiO_4} = -2.7$$

3) Gibbsite-Kaolinite boundary

$$Al_2Si_2O_5(OH)_4 + 5H_2O = Al_2(OH)_6 + 2H_4SiO_4$$
$$1/2 \log K_3 = \log a_{H_4SiO_4}$$

The value of silica activity can be calculated from ΔG_r^o of this reaction. However, it has been observed (Drever, 1988) that large uncertainty prevails in the reported values of free energy of silicate minerals involved in weathering reactions. Therefore, those thermodynamic values have been selected which match with equilibrium constants independently estimated from experimental works and field observations. For example, accepting quartz solubility of 6 ppm and ΔG_f^o of quartz and H_2O as -856.29 and 237.14 kJ/mole (Robie et al., 1978) respectively, ΔG_f^o of H_4SiO_4 can be calculated as follows :

$$\text{Quartz} + 2H_2O = H_4SiO_4$$
$$\therefore \quad \log K = -\log a_{H_4SiO_4} = -4.0$$
$$\Delta G_r^o = 4 \times 5.707 = 22.83 \text{ kJoules}$$
$$\therefore \quad \Delta G_f^o \, H_4SiO_4 = -1307.74 \text{ kJ/mole.}$$

This value differs from - 1316.6 kJ/mole used by Drever (1988) to construct the stability diagram. On the other hand, it matches closely with majority of values listed by Woods and Garrels (1987) including -1308.0 reported by Robie et al. (1978).

Using this value of ΔG^o_f H_4SiO_4 and-2309.78 kJ/mole for gibbsite -3799.36 kJ/mole for kaolinite (Robie et al., 1978), ΔG^o_r for the gibbsite-kaolinite reaction is 59.80.

$$\therefore \quad \frac{1}{2} \log K_3 = \frac{59.8}{2(-5.707)} = -5.24$$

This value of $a_{H_4SiO_4} = 10^{-5.24}$ for gibbsite-kaolinite equilibrium obviously differs from $10^{-4.4}$ used by Drever (1988) but is close to 10^{-5} derived by Krauskopf (1979) from a different set of free-energy values.

K_2O-Al_2O_3-SiO_2-H_2O SYSTEM

The boundaries of the stability diagrams for the K-system have been drawn by calculating equilibrium constants for the following reactions.

4) Muscovite-Kaolinite boundary

$$2KAl_3Si_3O_{10}(OH)_2 + 2H^+ + 3H_2O = 3Al_2Si_2O_5(OH)_4 + 2K^+$$

From the data in Table 6.11

$$\Delta G^o_r = -50.3 \text{ kJoules}$$

Table 6.11 Free energy values (kJ/mole) for various minerals and solutes at 25°C temperature and 1 atmosphere

Gibbsite [$Al_2(OH)_6$]	-2309.78
Kaolinite [$Al_2Si_2O_5(OH)_4$]	-3799.36
Muscovite [$KAl_3Si_3O_{10}(OH)_2$]	-5600.67
K-felspar [$KAlSi_3O_8$]	-3742.33
Na-smectite [$Na_{0.33}Al_{2.33}Si_{3.67}O_{10}(OH)_2$]	-5368.39 (1)
Ca-smectite [$Ca_{0.167}Al_{2.33}Si_{3.67}O_{10}(OH)_2$]	-5376.96 (2)
Chlorite [$Mg_5Al_2Si_3O_{10}(OH)_8$]	-8207.75 (3)
Quartz [SiO_2]	- 856.29
Na^+	- 261.90
K^+	- 282.49
Ca^{2+}	- 553.54
Mg^{2+}	- 454.80
H_4SiO_4	-1307.74 (4)
H_2O	- 237.14

(1) Calculated by extrapolation of Hemley's data (Hess, 1966)

(2) Calculated from log K = -18.4 for Ca smectite-kaolinite equilibrium (Norton, 1974)

(3) Helgeson et al. (1978)

(4) Calculated from 6 ppm SiO_2 for quartz solubility

All other values from Robie et al (1978).

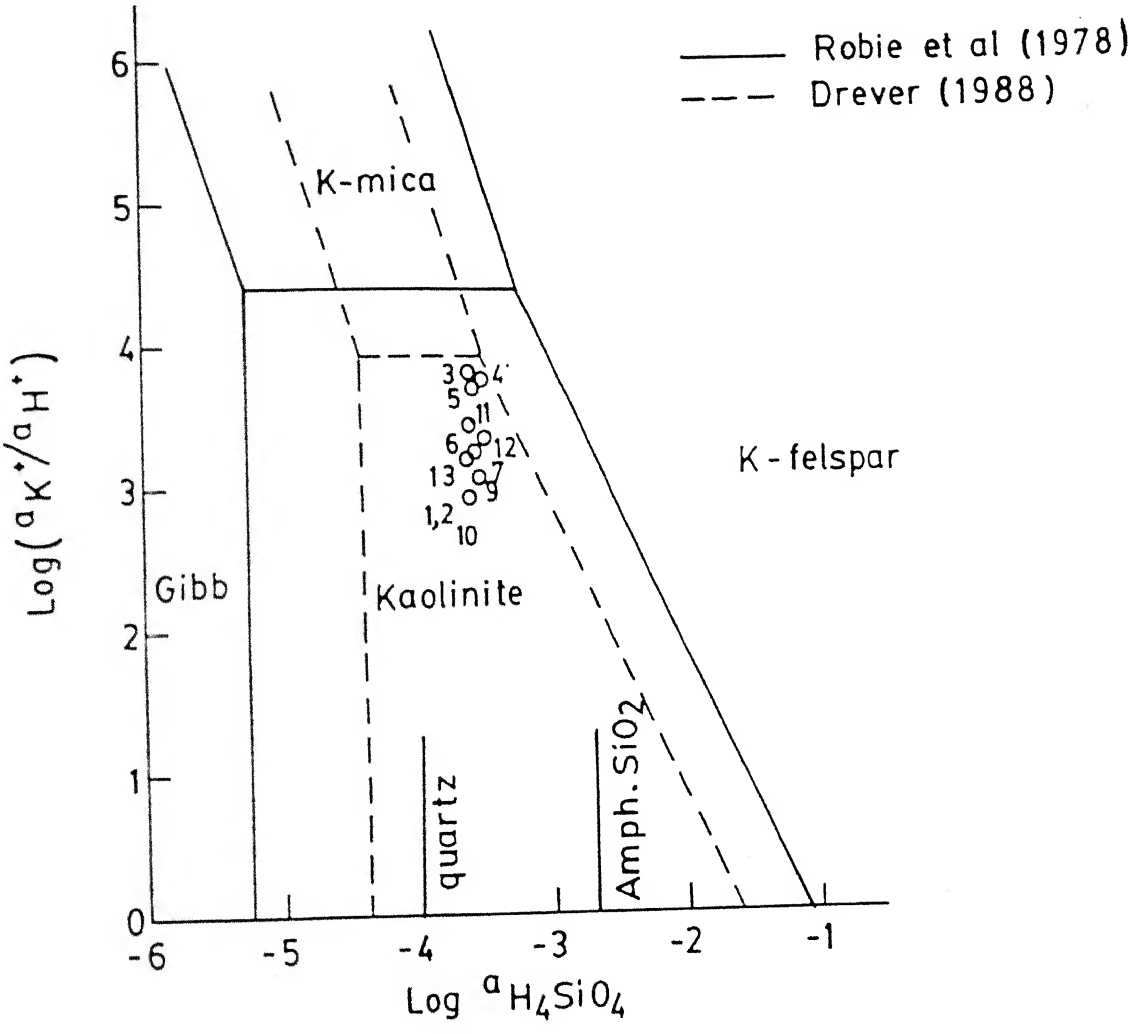

FIG 6.7 Stability diagram: $K_2O - Al_2O_3 - SiO_2 - H_2O$ System

$$\log K_4 = 2 \log (a_{K^+}/a_{H^+}) = 8.81$$

$$\therefore \log (a_{K^+}/a_{H^+}) = 4.40$$

5)Muscovite-Gibbsite boundary

$$2KAl_3Si_3O_{10}(OH)_2 + 2H^+ + 18H_2O = 3Al_2(OH)_6 + 2K^+ + 6H_4SiO_4$$

A line of slope -3:1 passes through the point of intersection of line (3) and (4).

6) K-felspar-Kaolinite boundary

$$2KAlSi_3O_8 + 2H^+ + 9H_2O = Al_2Si_2O_5(OH)_4 + 2K^+ + 4H_4SiO_4$$

$$\Delta G_r^o = 23.62 \text{ kJoules}$$

$$\log K_6 = -4.14$$

$$\therefore 1/2 \log K_6 = \log (a_{K^+}/a_{H^+}) + 2 \log a_{H_4SiO_4} = -2.07$$

7) K-felspar-Muscovite boundary

$$3KAlSi_3O_8 + 2H^+ + 12H_2O = KAl_3Si_3O_{10}(OH)_2 + 6H_4SiO_4 + 2K^+$$

A line of slope -3:1 passes through the point of intersection of (4) and (6).

Na_2O-Al_2O_3-SiO_2-H_2O SYSTEM

Stability diagram of the Na-system contains a new line representing equilibrium between kaolinite and an ideal

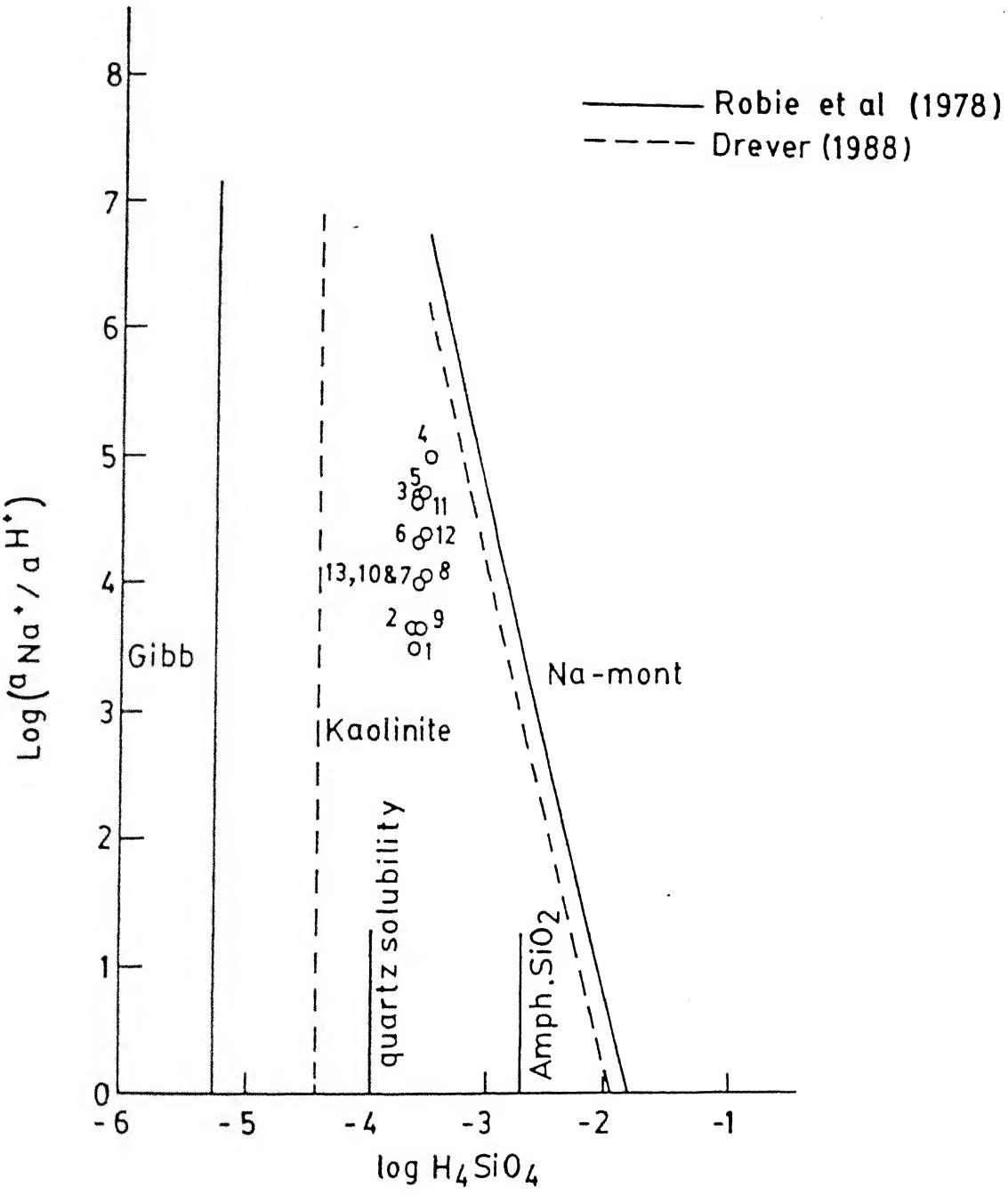

FIG 6.8 Stability diagram: $Na_2O - Al_2O_3 - SiO_2 - H_2O$ System

Na-montmorillonite with structural formula $Na_{0.33}Al_{2.33}Si_{3.67}O_{10}(OH)_2$. On the other hand, there is a great deal of confusion about the ΔG_f^o value of this phase as well as the exact composition of montmorillonite formed in weathering environment. Some of these aspects have been discussed by Drever (1988). Therefore, the equilibrium constant for kaolinite-Na montmorillonite reaction was estimated in the following way.

8) Na montmorillonite-Kaolinite boundary

$$6Na_{0.33}Al_{2.33}Si_{3.67}O_{10}(OH)_2 + 2H^+ + 23H_2O = 7Al_2Si_2O_5(OH)_4 + 8H_4SiO_4 + 2Na^+$$

$$\log K_8 = 2\log (a_{Na^+}/a_{H^+}) + 8\log a_{H_4SiO_4}$$

Hess (1966) extrapolated Hemley's high temperature experimental data to 25°C and estimated $\log (a_{Na^+}/a_{H^+}) = 5.9$ and $\log a_{H_4SiO_4} = -3.3$ for the above equilibrium.

$\therefore \log K_8 = -14.6$

The equation for Na montmorillonite-kaolinite boundary is

$$\log (a_{Na^+}/a_{H^+}) + 4\log a_{H_4SiO_4} = 1/2 \log K_8 = -7.3$$

ΔG_r^o = 83.32 kJoules. Knowing the ΔG_f^o of other species (Table 6.11), ΔG_f^o of Na-montmorillonite corresponding to the above equilibrium constant can be calculated as -5368.39 kJ/mole.

Table 6.12 Values of ΔG_f^o of Na-montmorillonite as reported in recent literature

1)	Raymahashay (1968)	:	-1277.4 kcal/mole
		=	-5344.64 kJ/mole
2)	Helgeson (1969)	:	-1278.9 kcal/mole
		=	-5350.92 kJ/mole
3)	Nriagu (1975)	:	-1277.76 kcal/mole
		=	-5350.92 kJ/mole
4)	Woods & Garrels (1987)	:	-5346.1 kJ/mole
5)	Drever (1988)	:	-5382.0 kJ/mole
6)	Karathanasis (1989)	:	-5080.5 to -5262.0 kJ/mole (soil smectite)
7)	This report @	:	-5368.39 kJ/mole

@ Calculated by extrapolation of Hemley's data (Hess, 1966)

This value has been compared with those reported in recent literature (Table 6.12). In the resulting stability diagram (Fig. 6.8), the kaolinite field is slightly wider compared with the diagram recommended by Drever (1988).

$CaO-Al_2O_3-SiO_2-H_2O$ SYSTEM

Stability diagram for the calcium system contains the boundary between kaolinite and an ideal Ca-montmorillonite [$Ca_{0.167}Al_{2.33}Si_{3.67}O_{10}(OH)_2$] in the manner similar to the sodium system. The equilibrium consant for Ca montmorillonite-kaolinite reaction was calculated in the following way.

9) Ca montmorillonite-Kaolinite boundary

$$6Ca_{0.167}Al_{2.33}Si_{3.67}O_{10}(OH)_2 + 2H^+ + 23H_2O = 7Al_2Si_2O_5(OH)_4 + 8H_4SiO_4 + Ca^{2+}$$

$$\log K_9 = \log \left[a_{Ca^{2+}}/(a_{H^+})^2\right] + 8\log a_{H_4SiO_4}$$

From his study of river water and sediments in the Rio Tanama system, Puerto Rico, Norton (1974), calculated the value for log K as -18.4 ± 0.8. Therefore, the Ca montmorillonite-kaolinite boundary can have the equation

$$\log \left[a_{Ca^{2+}}/(a_{H^+})^2\right] + 8\log a_{H_4SiO_4} = -18.4$$

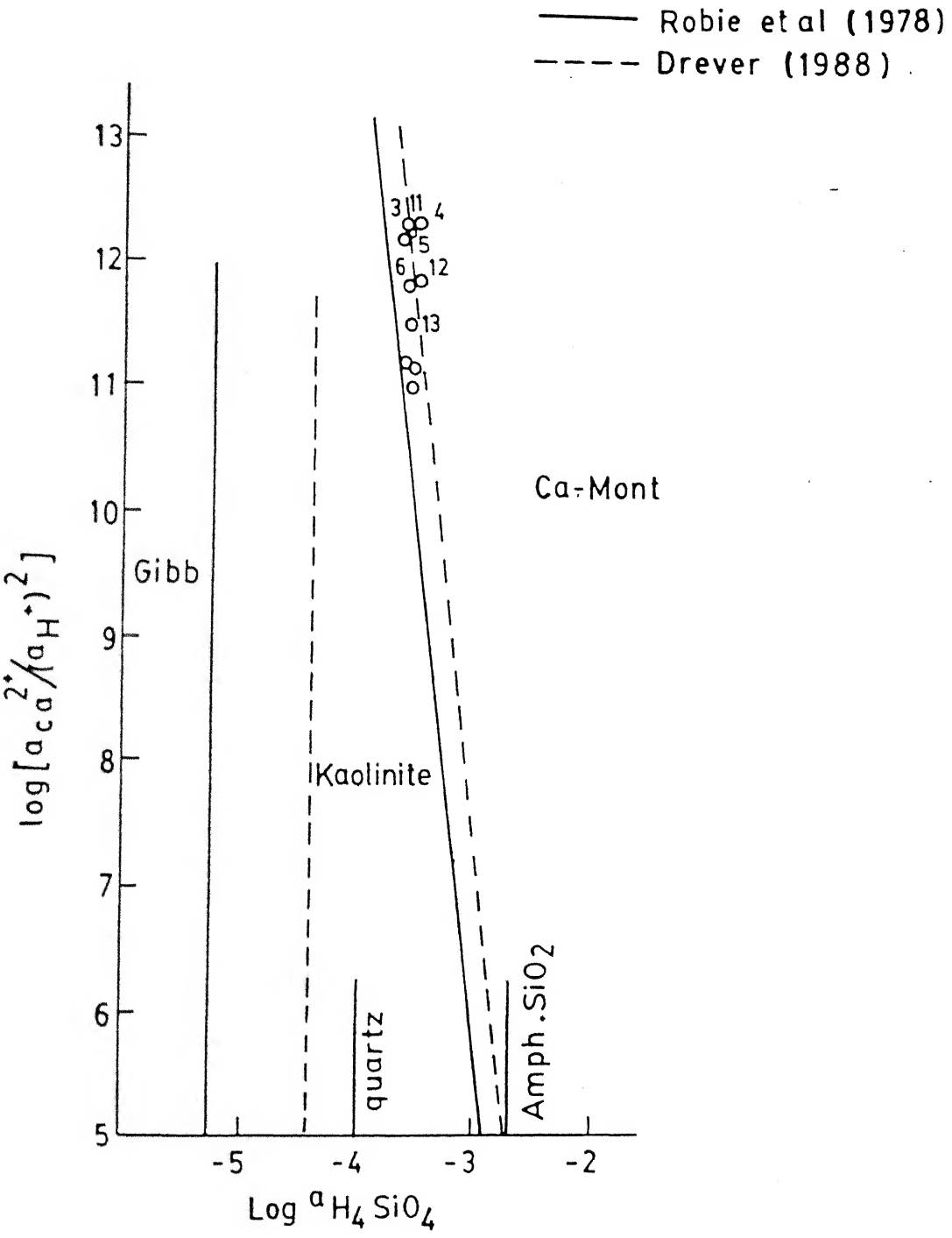

FIG 6.9 Stability diagram: $CaO - Al_2O_3 - SiO_2 - H_2O$ System

Table 6.13 Values of ΔG_f^o Ca-montmorillonite as reported in recent literature

1.	Helgeson (1969)	:	-1279.24 kcal/mole
		=	-5352.34 kJ/mole
2)	Nriagu (1975)	:	-1280.9 kcal/mole
		=	-5359.28 kJ/mole
3)	Raymahashay (1984)*1	:	-1278.84 kcal/mole
		=	-5350.67 kJ/mole
4)	Woods & Garrels (1987)	:	-5349.1 to -5354.9 kJ/mole
5)	Drever (1988)	:	-5388.0 kJ/mole
6)	Karathanasis (1989)	:	-5374.0 kJ/mole (soil smectite)
7)	This report *2	:	-5376.96 kJ/mole

*1 Calculated from log K = -15.7 for Ca montmorillonite-kaolinite equilibrium (Tardy, 1971).

*2 Calculated from log K = -18.4 for Ca-montmorillonite-kaolinite equilibrium (Norton, 1974).

Using the above log K,

ΔG_r^o = 105.0 kJoules.

Knowing the ΔG_f^o of other species (Table 6.11), ΔG_f^o of Ca-montmorillonite can be calculated as -5376.96 kJ/mole. This value has been compared with other sources in Table 6.13. As is seen from the resulting stability diagram (Fig. 6.11), the kaolinite field has slightly narrower width compared with that recommended by Drever (1988).

$MgO-Al_2O_3-SiO_2-H_2O$ SYSTEM

Stability diagram for the magnesium system shows two new boundaries i) between kaolinite and chlorite, $Mg_5Al_2Si_3O_{10}(OH)_8$ and ii) between gibbsite and chlorite. The diagram has been constructed in the following way.

10) Chlorite-Kaolinite boundary

$$Mg_5Al_2Si_3O_{10}(OH)_8 + 10H^+ = Al_2Si_2O_5(OH)_4 + 5Mg^{2+} + H_4SiO_4 + 5H_2O$$

From the ΔG_f^o values listed in the Table 6.11,

ΔG_r^o = -359.05 kJoules

$\log K_{10}$ = 62.91

or $$5 \log K = \log \left[a_{Mg^{2+}}/(a_{H^+})^2\right] + \log a_{H_4SiO_4} = 62.91$$

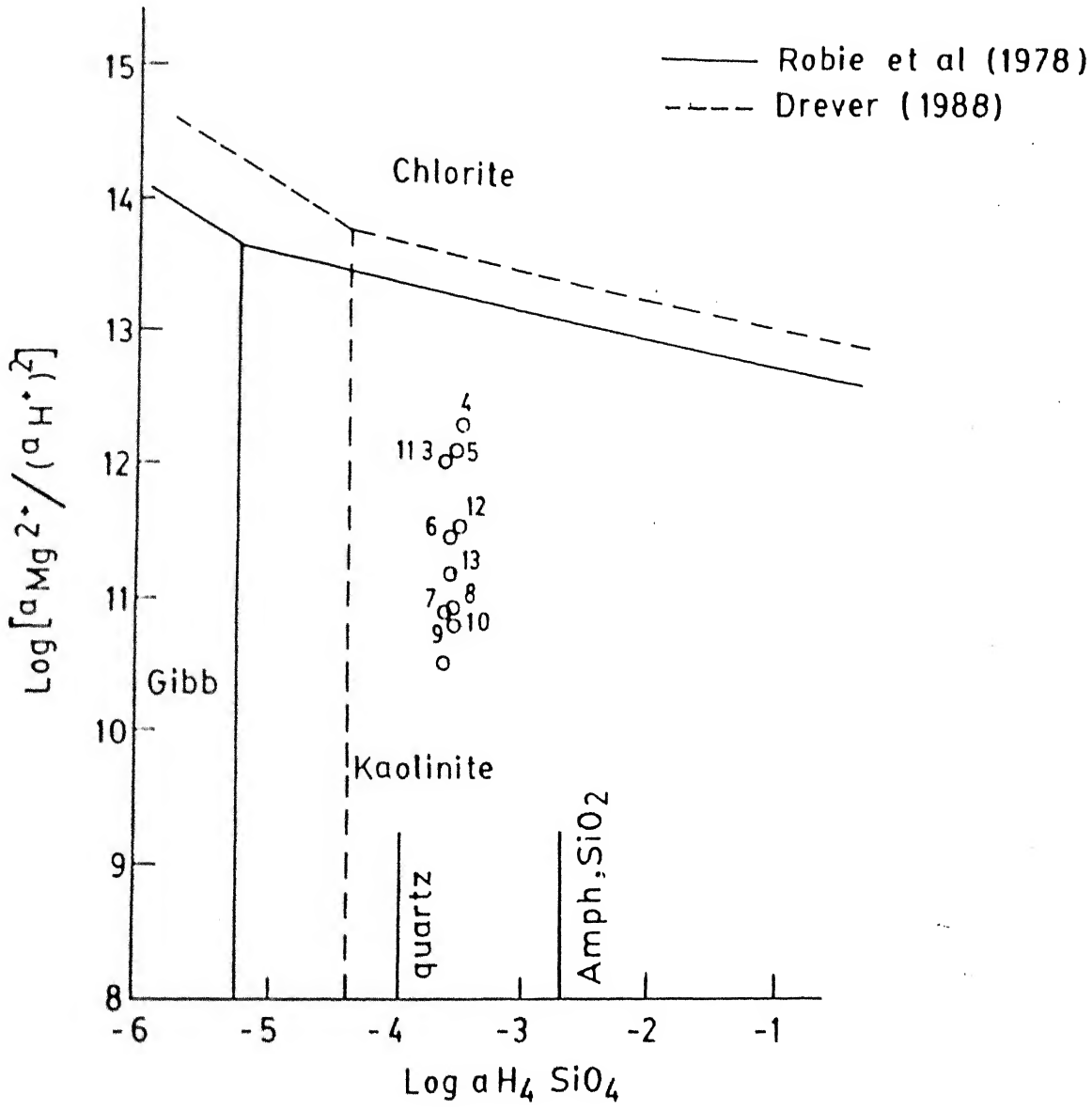

FIG 6.10 Stability diagram: $MgO - Al_2O_3 - SiO_2 - H_2O$ System

This line intersects the gibbsite-kaolinite boundary [log $a_{H_4SiO_4}$ = -5.24] at log [$a_{Mg^{2+}}/(a_{H^+})^2$] = 13.63.

11) Chlorite-Gibbsite boundary

$$Mg_5Al_2Si_3O_{10}(OH)_8 + 10H^+ = Al_2(OH)_6 + 5Mg^{2+} + 3H_4SiO_4$$

A line of slope -3:5 through the point of intersection of gibbsite-kaolinite and chlorite-kaolinite boundaries. The stability diagram (Fig. 6.12) also shows the relative position of chlorite field based on gibbsite-kaolinite boundary at log $a_{H_4SiO_4}$ = 4.4 (Drever, 1988).

It is clear from the stability diagrams that positions of the boundaries in the K, Na, Ca and Mg system are slightly different from the diagrams constructed by Drever (1988). It is to be recalled that Drever selected ΔG_f^o values to match the boundaries with natural water composition which were expected to be in equilibrium with the appropriate minerals. On the other hand, the boundaries in the stability diagrams are based on thermodynamic data mostly from Robie et al. (1978). Another reason for the difference between the two sets of diagrams is the ΔG_f^o value of H_4SiO_4 calculated in this work (-1307.74 kJ/mole) from 6 ppm SiO_2 for quartz solubility which is higher than the value -1316.6 kJ/mole used by Drever (1988) to construct his stability diagrams. However, a value of -1308.1 kJ/mole has been listed in the appendix of Drever (1988) after adjustment for

consistency with other values. This is almost equal to the value used in this thesis.

6.5.2 Silicate Mineral-Water Equilibria

Once the stability diagrams were constructed as discussed above, the river water chemistry was evaluated by calculating the relevant ion activities from concentrations in mole/litre, ionic strength and activity co-efficients. The sodium concentration was corrected for cyclic salt contribution by assuming that 0.39 ppm chloride in rainwater collected at Raipur, came as NaCl. Therefore, an equivalent amount of sodium (0.017 millimole/litre) was subtracted from the sodium value in river water. The appropriate calculations for plotting river water analyses on the stability diagrams have been summarized in Tables 6.14, 6.15, 6.16 and 6.17. The position of water compositions show the following features.

i) Kaolinite is a stable mineral in the river water environment with reference to potassium, sodium, calcium and magnesium systems. This is supported by the observation that this mineral is a common component of suspended sediments and bank deposits in the samples collected from the upper part of the basin during this investigation. Naidu et al. (1985) have reported that kaolinite is a constituent of the bed sediments in the downstream part of river. Similarly, Chakrapani and Subramanian (1990a) also found kaolinite in both bed and suspended sediments at various locations in the Mahanadi river basin.

Table 6.14 Water composition data used in the stability diagram for K_2O-Al_2O_3-SiO_2-H_2O system

Stn.	pH	K^+ m.mole/lit	$a_{K^+} \cdot 10^3$	$\log(a_{K^+}/a_{H^+})$	$\log a_{H_4SiO_4}$
1)	7.23	0.052	0.050	2.929	-3.633
2)	7.21	0.050	0.047	2.882	-3.623
3)	7.75	0.128	0.118	3.822	-3.629
4)	7.76	0.106	0.097	3.745	-3.496
5)	7.77	0.100	0.092	3.734	-3.564
6)	7.57	0.048	0.045	3.223	-3.625
7)	7.35	0.078	0.074	3.219	-3.609
8)	7.73	0.080	0.075	3.605	-3.559
9)	7.33	0.057	0.054	3.062	-3.542
10)	7.39	0.038	0.036	2.946	-3.577
11)	7.83	0.045	0.042	3.453	-3.613
12)	7.64	0.056	0.053	3.364	-3.519
13)	7.47	0.044	0.042	3.113	-3.618

Table 6.15 Water composition data used in the stability diagram for $Na_2O-Al_2O_3-SiO_2-H_2O$ system

Stn.	pH	Na^+ m.mole/lit	Cylic salt corrected*			log $a_{H_4SiO_4}$
			Na^+ m.mole/lit	$a_{Na^+}.10^3$	$\log(a_{Na^+}/a_{H^+})$	
1.	7.23	0.210	0.193	0.184	3.494	-3.633
2.	7.21	0.307	0.290	0.269	3.639	-3.623
3.	7.75	0.852	0.835	0.772	4.638	-3.629
4.	7.76	1.896	1.879	1.713	4.994	-3.496
5.	7.77	0.989	0.972	0.899	4.724	-3.564
6)	7.57	0.592	0.575	0.538	4.301	-3.625
7)	7.35	0.486	0.469	0.442	3.995	-3.609
8)	7.73	0.674	0.657	0.615	4.519	-3.559
9)	7.33	0.248	0.231	0.220	3.672	-3.542
10)	7.39	0.424	0.407	0.386	3.976	-3.577
11)	7.83	0.970	0.953	0.890	4.779	-3.613
12)	7.64	0.643	0.626	0.589	4.410	-3.519
13)	7.47	0.342	0.323	0.307	3.957	-3.618

* 0.39 ppm or 0.017 milli-mole/litre of chloride equivalent-Na^+ in rain water has been subtracted from the total sodium concentration in river water.

Table 6.16 Water composition data used in the stability diagram for $CaO-Al_2O_3-SiO_2-H_2O$ system

Stn.	pH	$(Ca^{2+})_{tot}$ m.mole/lit	$(a_{Ca^{2+}})_{tot}$ $\times 10^3$	$\log\left[\frac{a_{Ca^{2+}}}{(a_{H^+})^2}\right]_{tot}$	$\log\left[\frac{(a_{Ca^{2+}})_{si}}{(a_{H^+})^2}\right]$	$\log a_{H_4SiO_4}$
1)	7.23	0.317	0.262	10.878	10.293	-3.633
2)	7.21	0.458	0.370	10.988	10.403	-3.623
3)	7.75	0.776	0.567	12.254	11.669	-3.629
4)	7.76	0.989	0.683	12.354	11.769	-3.496
5)	7.77	0.771	0.564	12.291	11.706	-3.564
6)	7.57	0.665	0.512	11.849	11.164	-3.625
7)	7.35	0.441	0.349	11.243	10.658	-3.609
8)	7.73	0.587	0.450	12.113	11.528	-3.559
9)	7.33	0.287	0.235	11.031	10.446	-3.542
10)	7.39	0.341	0.276	11.220	10.634	-3.577
11)	7.83	0.660	0.501	12.360	11.775	-3.613
12)	7.64	0.516	0.404	11.886	11.301	-3.519
13)	7.47	0.504	0.399	11.541	10.956	-3.618

Table 6.17 Water composition data used in the stability diagram for $MgO-Al_2O_3-SiO_2-H_2O$ system

Stn.	pH	$(Mg^{2+})_{tot}$ m.mole/lit	$(a_{Mg^{2+}})_{tot}$ $\times 10^3$	$\log\left[\frac{a_{Mg^{2+}}}{(a_{H^+})^2}\right]_{tot}$	$\log a_{H_4SiO_4}$
1)	7.23	0.120	0.099	10.456	-3.633
2)	7.21	0.157	0.127	10.524	-3.623
3)	7.75	0.433	0.317	12.001	-3.629
4)	7.76	0.742	0.512	12.229	-3.496
5)	7.77	0.521	0.381	12.121	-3.564
6)	7.57	0.276	0.212	11.466	-3.625
7)	7.35	0.189	0.150	10.876	-3.609
8)	7.73	0.322	0.247	11.853	-3.559
9)	7.33	0.157	0.129	10.771	-3.542
10)	7.39	0.167	0.135	10.910	-3.577
11)	7.83	0.329	0.250	12.058	-3.613
12)	7.64	0.262	0.205	11.592	-3.519
13)	7.47	0.205	0.162	11.150	-3.618

ii) In the stability diagram for Ca-system (Fig. 6.9), the water compositions plot near the kaolinite-Ca montmorillonite boundary. This indicates that the kaolinite-Ca montmorillonite equilibrium controls river water composition. A correction for Ca concentration was introduced by considering the fraction derived from weathering of silicate minerals instead of the total Ca value. As discussed earlier

$$(Ca)_{si} = (Ca)_{tot} - (Ca)_{c}$$
$$= 1 - 0.74(Ca)_{tot}$$
$$= 0.26\ (Ca)_{tot}$$

The corrected values of $\left[a_{Ca^{2+}_{si}}/(a_{H^+})^2\right]$ have been listed in the penultimate column of Table 6.16. The shift of position of the stability fields is negligible and the earlier conclusion that the kaolinite-Ca montmorillonite equilibrium might control river water composition, remains valid. This idea appears to be feasible because suspended sediments and soil samples from Andhiyarkore (station 4) as well as soil samples from Simga (station 3) and Jondhra (station 5) showed a mixture of kaolinite and glycol expansive clay minerals during X-ray diffraction studies. However, it was not possible to confirm the exact composition of montmorillonite. Previous workers have reported montmorillonite in the suspended and bed loads of the Mahanadi river particularly in the lower reaches (Naidu et al., 1985; Chakrapani and Subramanian, 1990a). There is a strong possibility therefore, that a calcium rich montmorillonite forms by weathering of limestone and calcareous shale in the drainage basin.

6.6 Aluminium Speciation

The stability diagrams developed in the earlier section were based on the assumption that aluminium is immobile during rock weathering and does not appear in the solution phase. On the other hand, the range of Al concentration listed in Table 5.1 indicates that the maximum concentration reaches nearly 1 ppm. Therefore, it is important to verify if the stability of an aluminium bearing mineral has any control on dissolved Al at this concentration level. Since kaolinite is always present as an Al-silicate phase in suspended sediments and soils within the Mahanadi basin, its solubility in terms of dissolved Al species has been evaluated in this section.

It is well established that the major dissolved Al species in natural waters are Al^{3+}, $Al(OH)^{2+}$, $Al(OH)_2^+$, $Al(OH)_3^0$ and $Al(OH)_4^-$. The total dissolved aluminium in moles per litre which is the analytical value, can be expressed as

$$m_{Al_T} = m_{Al^{3+}} + m_{Al(OH)^{2+}} + m_{Al(OH)_2^+} + m_{Al(OH)_3^{o+}} m_{Al(OH)_4^-} \qquad (A)$$

The activities of these dissolved species are related to one another through the following equilibrium constants.

$$Al^{3+} + H_2O = Al(OH)^{2+} + H^+ \qquad (1)$$

$$K_1 = \frac{a_{Al(OH)^{2+}} \cdot a_{H^+}}{a_{Al^{3+}}}$$

$$= \frac{\gamma_2 \cdot m_{Al(OH)^{2+}} \cdot a_{H^+}}{\gamma_3 \cdot m_{Al^{3+}}}$$

Therefore,

$$m_{Al(OH)^{2+}} = \frac{K_1 \cdot \gamma_3 \cdot m_{Al^{3+}}}{\gamma_2 \cdot m_{Al^{3+}}}$$

Similarly,

$$Al^{3+} + 2H_2O = Al(OH)_2^+ + 2H^+ \qquad (2)$$

$$K_2 = \frac{a_{Al(OH)_2^+} \cdot (a_{H^+})^2}{a_{Al^{3+}}}$$

$$= \frac{\gamma_1 \cdot m_{Al(OH)_2^+} \cdot (a_{H^+})^2}{\gamma_3 \cdot m_{Al^{3+}}}$$

$$m_{Al(OH)_2^+} = \frac{K_2 \cdot \gamma_3 \cdot m_{Al^{3+}}}{\gamma_1 \cdot (a_{H^+})^2}$$

$$Al^{3+} + 3H_2O = Al(OH)_3^o + 3H^+ \qquad (3)$$

$$K_3 = \frac{a_{Al(OH)_3^o} \cdot (a_{H^+})^3}{a_{Al^{3+}}}$$

$$= \frac{\gamma_o \cdot m_{Al(OH)_3^o} \cdot (a_{H^+})^3}{\gamma_3 \cdot m_{Al^{3+}}}$$

$$m_{Al(OH)_3^o} = \frac{K_3 \cdot \gamma_3 \cdot m_{Al^{3+}}}{\gamma_o \cdot (a_{H^+})^3} \qquad (4)$$

$$Al^{3+} + 4H_2O = Al(OH)_4^- + 4H^+$$

$$K_4 = \frac{a_{Al(OH)_4^-} \cdot (a_{H^+})^4}{a_{Al^{3+}}}$$

$$= \frac{\gamma_4 \cdot m_{Al(OH)_4^-} \cdot (a_{H^+})^4}{\gamma_3 \cdot m_{Al^{3+}}}$$

$$m_{Al(OH)_4^-} = \frac{K_4 \cdot \gamma_3 \cdot m_{Al^{3+}}}{\gamma_4 \cdot (a_{H^+})^4}$$

Substituting these values in equation (4),

$$m_{Al_T} = m_{Al^{3+}} + \frac{K_1 \cdot \gamma_3 \cdot m_{Al^{3+}}}{\gamma_2 \cdot a_{H^+}} + \frac{K_2 \cdot \gamma_3 \cdot m_{Al^{3+}}}{\gamma_1 \cdot (a_{H^+})^2} + \frac{K_3 \cdot \gamma_3 \cdot m_{Al^{3+}}}{\gamma_o \cdot (a_{H^+})^3}$$

$$+ \frac{K_4 \cdot \gamma_3 \cdot m_{Al^{3+}}}{\gamma_4 \cdot (a_{H^+})^4}$$

$$= m_{Al^{3+}} \left[1 + \frac{K_1 \cdot \gamma_3}{\gamma_2 \cdot a_{H^+}} + \frac{K_2 \cdot \gamma_3}{\gamma_1 \cdot (a_{H^+})^2} + \frac{K_3 \cdot \gamma_3}{\gamma_o \cdot (a_{H^+})^3} + \frac{K_4 \cdot \gamma_3}{\gamma_4 \cdot (a_{H^+})^4} \right]$$

$$= a_{Al^{3+}} \left[\frac{1}{\gamma_3} + \frac{K_1}{\gamma_2 \cdot a_{H^+}} + \frac{K_2}{\gamma_1 \cdot (a_{H^+})^2} + \frac{K_3}{\gamma_o \cdot (a_{H^+})^3} + \frac{K_4}{\gamma_4 \cdot (a_{H^+})^4} \right]$$

Some simplifications can be introduced in the above equation. For example, i) the neutral species $Al(OH)_3^o$ can be neglected with respect to other charged species. This is mainly because $Al(OH)_3$ is precipitated as a solid phase under pH conditions where $Al(OH)_3^o$ is the dominant species in solution; ii) the activity coefficients of the univalent species $Al(OH)_2^+$ and $Al(OH)_4^-$ can be considered to be equal i.e. $\gamma_1 = \gamma_4$.

Therefore,

$$m_{Al_T} = a_{Al^{3+}} \left[\frac{1}{\gamma_3} + \frac{K_1}{\gamma_2 . a_{H^+}} + \frac{K_2}{\gamma_1 . (a_{H^+})^2} + \frac{K_4}{\gamma_1 . (a_{H^+})^4} \right]$$

$$= a_{Al^{3+}} / f$$

or $a_{Al^{3+}} = m_{Al_T} / f$

where 'f' represents the terms within bracket.

The values of K_1, K_2 and K_4 calculated from the free energy data listed in the Table 6.18 are $10^{-5.004}$, $10^{-9.788}$ and $10^{-23.166}$ respectively at 25°C. Using the activity co-efficient (γ) values from Table 5.6, the function 'f' can be evaluated for a given pH to set the relationship between the analytical aluminium concentration and activity of Al^{3+} ion as suggested by Neal (1988). At river water pH value, the dominant dissolved aluminium species is $Al(OH)_4^-$. Therefore, the value of 'f' becomes practically equal to $K_4 / \gamma_1 (a_{H^+})^4$.

Table 6.18 Free energy data (kJ/mole) for aluminium speciation calculation at 25°C and 1 atmosphere

			Reference
Gibbsite $[Al(OH)_3]$	:	-1154.89	Robie et al.(1978)
Kaolinite $[Al_2Si_2O_5(OH)_4]$	:	-3799.36	-do-
Poorly crystalline kaolinite $[Al_2Si_2O_5(OH)_4]$	:	-3766.18	Kittrick, 1966
H_4SiO_4	:	-1307.74	This report[a]
H_2O	:	- 237.14	Robie et al. (1978)
Al^{3+}	:	- 484.88	Wagman et al.(1968).
$Al(OH)^{2+}$	:	- 693.46	-do-
-do-			
$Al(OH)_2^+$	:	- 903.30	Reesman et al.(1969)
$Al(OH)_4^-$	:	-1301.23	-do-

[a] Calculated from 6 ppm SiO_2 for quartz solubility

The solubility of kaolinite can be expressed as

$$\frac{1}{2}\,Al_2Si_2O_5(OH)_4 + 3H^+ = Al^{3+} + H_4SiO_4 + \frac{1}{2}\,H_2O$$

The equilibrium constant

$$K_{kaol.} = \frac{a_{Al^{3+}} \cdot a_{H_4SiO_4}}{(a_{H^+})^3}$$

$$\log K_{kaol.} = \log a_{Al^{3+}} + \log a_{H_4SiO_4} + 3pH$$

$$= \log m_{Al_T} - \log f + \log a_{H_4SiO_4} + 3pH$$

$$\therefore \quad \log m_{Al_T} + \log a_{H_4SiO_4} = \log f - 3\,pH + \log K_{kaol.}$$

The value of $K_{kaol.}$ calculated from the free energy data listed in Table 6.18 can be expressed as $\log K_{kaol} = 2.017$ at $25^{o}C$. The above relationship results in a straight line with 1:1 slope when $[\log m_{Al_T} + \log a_{H_4SiO_4}]$ is plotted against (log f - 3pH) in Fig.6.11.

Using the free energy data of poorly crystalline kaolinite listed in Table 6.18, a parallel straight line representing its solubility has the equation

$$[\log m_{Al_T} + \log a_{H_4SiO_4}] = (\log f - 3pH) + 4.924$$

Table 6.19 Data for kaolinite stability diagram

Stn.	$-\log m_{Al_T}$	log f	$-\log a_{H_4SiO_4}$	pH	(log f-3pH)	$[\log m_{Al_T} + \log a_{H_4SiO_4}]$
1.	6.68	5.81	3.63	7.23	-15.88	-10.31
2.	6.70	5.73	3.62	7.21	-15.90	-10.32
3.	6.96	7.87	3.63	7.75	-15.38	-10.59
4.	6.92	7.92	3.50	7.76	-15.36	-10.42
5.	6.66	7.95	3.56	7.77	-15.36	-10.22
6.	6.85	7.14	3.63	7.57	-15.57	-10.48
7.	6.70	6.26	3.61	7.35	-15.79	-10.31
8.	6.60	7.77	3.56	7.73	-15.42	-10.16
9.	6.60	6.18	3.54	7.33	-15.81	-10.14
10.	6.77	6.42	3.58	7.39	-15.75	-10.35
11.	7.00	8.18	3.61	7.83	-15.31	-10.61
12.	6.49	7.42	3.52	7.64	-15.50	-10.01
13.	6.05	6.74	3.62	7.47	-15.67	- 9.67

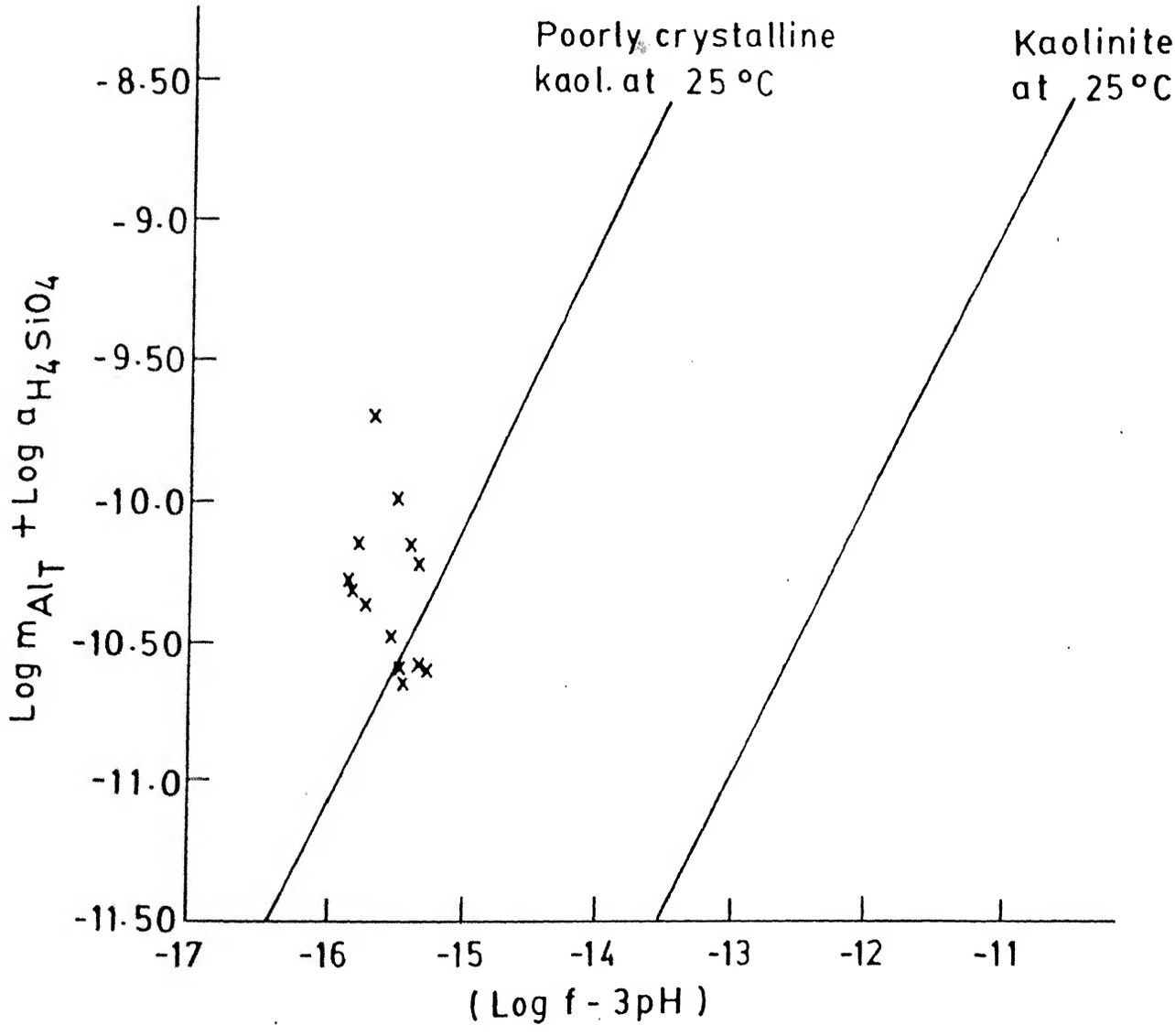

6.11 Diagram for kaolinite stability at 25°C in relation t
dissolved aluminium in water

The river water analyses have been utilized to calculate the relevant parameters of this plot (Table 6.19). As seen from the Fig 6.11, the composition of the Mahanadi river water plots along the solubility line for poorly crystalline kaolinite. It indicates that this phase may have some influence on the aluminium concentration in river water. In fact, Hem (1991), has suggested that at certain silica levels, poorly crystallized clay mineral species can precipitate from natural waters.

6.7 Heavy Metals in Sediments and Soils

Stream sediments and soils contain a host of heavy metals derived from the weathering of rocks and anthropogenic sources such as mine waste, industrial and domestic effluents. Although sediment analyses do not furnish quantitative information on the absolute degree of pollution, they can play a key role in ascertaining relative factors of enrichment which can trace the source of pollution of the aquatic environment (Forstner and Wittmann, 1981). A systematic study of heavy metals would, therefore, include determination of degree of enrichment with respect to some background concentration values. The present investigation concentrated on the analysis of less than 45 micron size fraction of soils and flood plain deposits to detect a general trend, if any. A total of seventeen samples were collected from different locations of upper part of the Mahanadi basin (Fig.6.12) and were analyzed for Pb, Zn, Cu and Mn by AAS. The method of sample preparation and procedure for analysis are

given in Chapter 2.

6.7.1 Degree of Enrichment in Limestone Terrain

Analytical data on Pb, Zn, Cu and Mn in both flood plain deposits and soils in the carbonate rock dominated terrain is presented in Table 6.20. The relative proportion of these elements are generally in the order of Pb < Zn < Cu < Mn. The same table also lists the average background heavy metal concentration in limestone from different sources for the sake of comparison. The enrichment, if any, of these metals due to weathering or anthropogenic sources can be best evaluated by comparing with background levels in local limestones. Geological Survey of India (1989) records a concentration of less than 10-40 ppm of zinc in limestones of this area while the sediments have a range of 39 to greater than 110 ppm with an average value of 57. Therefore, it seems that there has been an enrichment of zinc which can possibly be ascribed to urban effluents. Samples 1F and 8S with highest values are from Nawapara and Raipur towns respectively. On the other hand, lead in the sediments and soils (5-41 ppm), seems to be within the concentration range for limestone (10-100 ppm). Average copper level in soils and sediments is 100 ppm though occasional high values up to 185 were also obtained. But this does not seem unusual because Geological Survey of India reports a wide range of Cu concentration (<10-200 ppm) in the local limestone. With regard to manganese, the average value of 782 ppm in sediments and soils is less than that

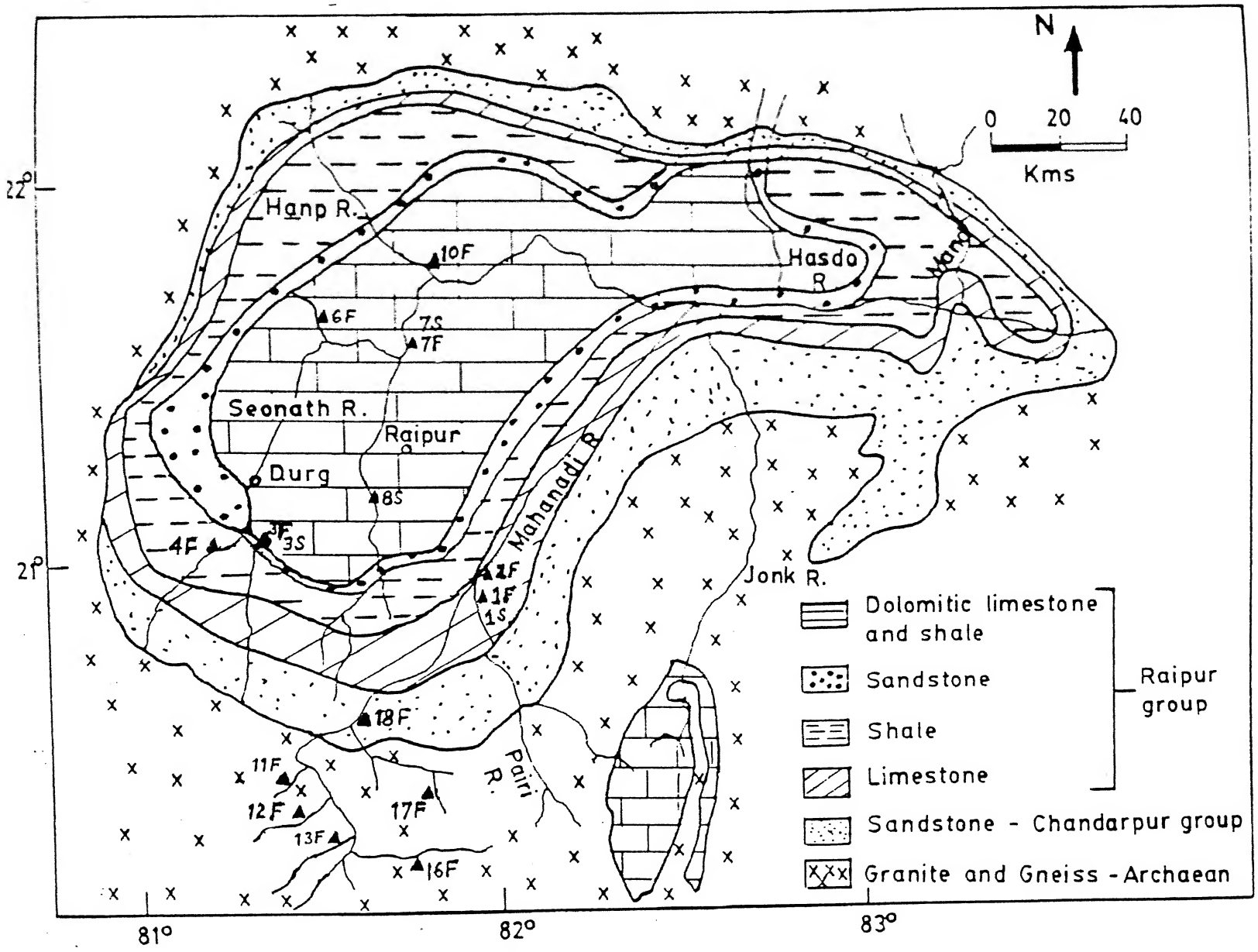

Fig. 6.12 Geologic map showing location of sediment and soil samples

in limestones quoted by Drever (1988) from the original data of Turekian and Wedepohl. This comparison indicates that there has been a relative depletion of Mn. Wedepohl (1978) suggested that Mn is more abundant in the carbonate than in the detrital fraction of the carbonate rocks. Therefore, weathering of local limestones may have caused the depletion of Mn in the residual soils.

6.7.2 Degree of Enrichment in Granitic Terrain

Another set of flood plain deposits were sampled in the granitic terrain near the source of the Mahanadi river. These samples were analyzed for Pb, Zn, Cu and Mn. Table 6.21 lists their concentration levels along with the background values in local granites and other reference granites from different sources. It is observed that average metal values of the sediments is in the order Pb < Cu < Mn < Zn. Lead concentrations are fairly constant for all the samples analyzed and is in the vicinity of the lowest value (20 ppm) reported for the local granite. Manganese concentration in the sediments shows considerable fluctuation (240-1810 ppm) while the background value of manganese in granites listed by Drever (1988) and Krauskopf (1979) ranges between 400-450 ppm. A high value of 1810 ppm of Mn at Gangrel (sample 18F) situated upstream of the Gangrel dam site may be due to precipitation of Mn in the reservoir sediments. Copper and zinc are enriched in the sediments. The reason for this enrichment is not clear from the limited data available at present. However, anthropogenic sources cannot be ruled out.

Table 6.21 Concentration(mg/kg) of heavy metals in rocks and flood plain deposits in the granitic terrain.

Sample (Flood plain deposit)	Pb	Zn	Cu	Mn	Relative proportion
11F	20	>1000	130	380	Pb < Cu < Mn < Zn
12F	31	60	125	870	Pb < Zn < Cu < Mn
13F	30	850	120	240	Pb < Cu < Mn < Zn
16F	29	>1000	125	260	-do-
17F	<5	>1000	140	320	-do-
18F	24	410	160	1810	Pb < Cu < Zn < Mn
Average	23.1	--	133.5	646.7	Pb < Cu < Mn < Zn
Granite@	20-75	10-75	10-75	--	
Granite#	17	50	20	450	
Granite$	20	40	10	400	

@ Local granite (Geological Survey of India, 1989)

Complied data listed by Drever(1988)

$ Krauskopf(1979)

6.7.3 Summary

The overall picture that emerges from the distribution and concentration of heavy metals in sediments and soils in the upper part of the Mahanadi river basin is as follows.

a) The relative concentration of heavy metals is Pb < Zn < Cu < Mn in carbonate terrain and Pb < Cu < Mn < Zn in granitic terrain.

b) In the granitic terrain, Pb and Mn values in the sediments and soils are similar to that in bed rock. They could have been derived by the weathering of rocks in the catchment area. Similarly, in the carbonate terrain, Pb and Cu levels in soil and sediment are comparable with bed rocks. On the other hand, Mn is perhaps depleted during weathering of the limestone.

c) Zinc is enriched in samples from both the terrains, more so in the granitic region. Urban effluents may be a factor in this pattern.

6.8 Factor Analysis

6.8.1 Introduction

As stated by Davis (1973), "factor analysis attempts to reveal a single underlying structure that is presumed to exist within a set of multivariate observations." This structure can be expressed in terms of variances and co-variances between the variables and the similarities between the observations. There

are several types or modes of factor analysis possible. R-mode factor analysis describes the relations among the variables in terms of the samples while Q-mode studies the correlations among the sampling sites. Separate interpretations are required for these two modes because the final results of such analyses produce a set of factors demonstrating the relations. But explanations to these relations are to be found from the knowledge of the geochemical environment.

Factor analysis is carried out in 3 steps :

i) Preparation of the correlation matrix which is produced by multiplying a data matrix or a normalized data matrix by its transpose.

ii) Extraction of initial factors so as to explore the possibility of data reduction. This is done by diagonalizing the correlation matrix and obtaining eigen values and principal components (eigen vectors). The factor-1 would then relate to the highest eigen value explaining the greatest percentage of variance in the data set, factor-2 would explain the greatest of the remaining variance and so on.

iii) Rotation of the initial factor matrix to a final solution which provides a set of simple and meaningful factors. Different rotations of orthogonal axes derived from principal component solution may result in different terminal solutions. In the

'varimax' rotation, orthogonal factor axes are located such that the variance of each factor is maximized. This results in equitable distribution of factor loading. In the 'oblique' rotation, the reference factor axes are not constrained to be orthogonal. Oblique solutions are appropriate where underlying causal factors are suspected to be correlated among themselves.

6.8.2 Factor Analysis of Chemical Data of the Mahanadi River Water

Water quality data at the 13 CWC stations along the Mahanadi river were subjected to factor analysis as discussed below. Chemical parameters chosen as variables for R-mode factor analysis were SiO_2, Na, K, Ca, Mg, HCO_3, Cl and SO_4. Monthly data for these variables at each sampling site were averaged out on annual basis. A set of five analyses for each station resulted from the five year data base. The raw data thus obtained were normalized by dividing the concentration of each chemical parameter by the highest among them (Table 6.22). Normalization was felt necessary because i) the basic data lacked normal distribution and ii) variables of higher magnitudes would have dominated over those of lower magnitude. Hitchon et al. (1971) and Stallard and Edmond (1983) preferred use of logarithmic transforms of data to raw data for factor analysis.

Factor analysis was carried out using SPSS (Statistical Package for Social Sciences) with an HP-9000/850 series supermini-computer at I.I.T, Kanpur. A minimum eigen value of 0.5

Table 6.22 Normalized data for factor analysis (n=65)

SiO_2	Na	K	Ca	Mg	HCO_3	Cl	SO_4
0.713	0.074	0.539	0.312	0.186	0.263	0.429	0.081
0.536	0.090	0.823	0.264	0.106	0.183	0.485	0.125
0.554	0.128	0.409	0.363	0.133	0.204	0.715	0.227
0.431	0.104	0.281	0.270	0.121	0.177	0.400	0.116
0.213	0.184	0.246	0.291	0.126	0.199	0.381	0.153
0.671	0.108	0.363	0.451	0.229	0.358	0.454	0.104
0.681	0.173	0.360	0.463	0.192	0.302	0.550	0.029
0.541	0.171	0.316	0.493	0.181	0.319	0.609	0.073
0.426	0.127	0.284	0.387	0.146	0.250	0.450	0.116
0.186	0.149	0.320	0.417	0.136	0.270	0.463	0.149
0.677	0.350	1.000	0.762	0.595	0.644	0.804	0.260
0.602	0.483	0.942	0.727	0.518	0.567	0.740	0.254
0.580	0.392	0.743	0.774	0.483	0.577	0.741	0.262
0.440	0.347	0.691	0.714	0.363	0.524	0.637	0.378
0.236	0.378	0.849	0.759	0.449	0.556	0.836	0.297
0.918	0.825	0.740	0.935	0.955	0.955	0.718	0.597
1.000	1.000	0.909	1.000	0.819	0.889	0.750	0.919
0.592	0.896	0.635	0.974	0.720	0.932	0.866	1.000
0.717	0.650	0.498	0.839	0.675	0.666	0.650	0.563
0.282	0.949	0.648	0.988	1.000	1.000	0.800	0.821
0.698	0.434	0.749	0.719	0.653	0.626	0.729	0.397
0.745	0.443	0.638	0.736	0.605	0.539	0.900	0.492
0.629	0.463	0.637	0.885	0.643	0.615	1.000	0.468
0.664	0.423	0.613	0.719	0.433	0.534	0.780	0.441
0.263	0.516	0.632	0.668	0.602	0.580	0.762	0.442
0.433	0.166	0.287	0.597	0.329	0.447	0.443	0.157
0.672	0.270	0.317	0.633	0.306	0.465	0.660	0.124
0.542	0.283	0.363	0.726	0.332	0.498	0.622	0.130
0.598	0.263	0.294	0.587	0.286	0.421	0.500	0.149
0.274	0.351	0.311	0.632	0.314	0.473	0.590	0.314
0.720	0.193	0.430	0.399	0.256	0.350	0.517	0.230
0.601	0.186	0.415	0.409	0.188	0.283	0.450	0.179
0.593	0.172	0.399	0.361	0.181	0.250	0.565	0.299
0.389	0.232	0.523	0.414	0.223	0.278	0.538	0.402
0.315	0.317	0.691	0.525	0.219	0.304	0.812	0.261
0.837	0.262	0.571	0.611	0.436	0.522	0.600	0.274
0.705	0.283	0.449	0.518	0.303	0.373	0.633	0.243
0.536	0.320	0.493	0.537	0.331	0.438	0.716	0.231
0.627	0.311	0.512	0.549	0.339	0.410	0.645	0.211
0.294	0.348	0.594	0.610	0.400	0.469	0.600	0.351
0.683	0.114	0.411	0.300	0.218	0.293	0.436	0.209
0.756	0.113	0.377	0.268	0.161	0.214	0.481	0.171
0.688	0.118	0.368	0.269	0.183	0.213	0.395	0.147
0.537	0.109	0.374	0.269	0.140	0.195	0.337	0.303
0.287	0.117	0.356	0.272	0.192	0.197	0.387	0.226
0.641	0.138	0.283	0.328	0.245	0.344	0.421	0.114
0.721	0.239	0.233	0.313	0.176	0.248	0.504	0.113
0.638	0.199	0.244	0.329	0.177	0.248	0.425	0.151
0.600	0.199	0.240	0.328	0.185	0.260	0.410	0.357
0.233	0.247	0.244	0.340	0.162	0.266	0.416	0.196
0.577	0.327	0.297	0.665	0.402	0.574	0.504	0.121
0.681	0.476	0.311	0.643	0.377	0.548	0.608	0.047
0.575	0.485	0.314	0.615	0.354	0.575	0.605	0.105
0.515	0.407	0.265	0.627	0.364	0.546	0.563	0.140
0.264	0.526	0.292	0.596	0.362	0.543	0.631	0.213
0.765	0.241	0.368	0.530	0.349	0.477	0.510	0.166
0.790	0.341	0.398	0.478	0.289	0.376	0.436	0.126
0.704	0.266	0.395	0.498	0.278	0.406	0.554	0.053
0.688	0.318	0.360	0.494	0.305	0.420	0.533	0.180
0.259	0.291	0.343	0.480	0.270	0.391	0.544	0.201
0.471	0.104	0.315	0.475	0.226	0.397	0.537	0.205
0.571	0.163	0.287	0.510	0.216	0.337	0.520	0.050
0.553	0.166	0.299	0.479	0.210	0.360	0.571	0.006
0.637	0.176	0.263	0.479	0.253	0.341	0.536	0.233
0.335	0.178	0.280	0.483	0.254	0.353	0.533	0.197

was assigned for extraction of factors. The size of the eigen value represents the variance of the original data that has been extracted on to each factor. Principal component analysis extracted 3 factors. Communality was found to be high except for Cl(0.85), and SO_4(0.71). The generally high communalities indicated that most of variance (90%) is explained by a set of 3 factors. Initial factor matrix thus obtained by principal component solution requires some form of rotation. Oblique rotation was preferred to others because the controlling processes in hydrogeochemistry are often correlated. Sampson (1968) illustrated the use of oblique solutions in the analysis of formation water data. Usunoff and Guzman' (1989) also favoured oblique rotation because geochemical processes often evolve through very dynamic and highly interrelated mechanisms. Therefore, upon oblimin rotation of the initial factor matrix with Kaiser normalization, the following factor matrix given in Table 6.23a was obtained.

6.8.3 Geochemical Interpretation

The factor analysis shows three trends or groupings among the variables. They are :

i) $Na-Ca-Mg-HCO_3$: Factor-1

ii) SiO_2 : Factor-2

iii) K-Cl : Factor-3

Table 6.23a Oblimin rotated factor matrix of chemical data (R-mode)

Variable	Factor			Communality
	1	2	3	
SiO_2	0.160	0.996	0.149	0.993
Na	0.968	0.120	0.629	0.945
K	0.651	0.178	0.946	0.900
Ca	0.938	0.133	0.768	0.901
Mg	0.967	0.221	0.745	0.949
HCO_3	0.971	0.191	0.679	0.946
Cl	0.744	0.042	0.909	0.852
SO_4	0.837	0.241	0.624	0.710
Eigen value (Principal component solution)	5.616	0.986	0.594	
Percentage variance explained	70.20	12.30	7.40	
Cumulative percentage of variance	70.20	82.50	89.99	

Table 6.23b Factor correlation matrix

	Factor-1	Factor-2	Factor-3
Factor-1	1.00		
Factor-2	0.13	1.00	
Factor-3	0.71	0.13	1.00

Factor-1 : More than 70% of variance among the ions is explained by this factor. The interrelationship between Ca, Mg and HCO_3 in water can be easily explained by carbonate weathering in the basin. On the other hand, association of Na with these ions may be related to the weathering of silicate impurities in limestone. As discussed earlier, the acid-leached residue of the dolomitic limestone contains albitic felspar. Therefore, factor-1 can be interpreted as essentially carbonate weathering factor.

Factor-2 : This factor explains more than 12% of total variance among the ions and is characterized by high factor score for silica. Therefore, this factor may be interpreted in terms of weathering of silicate rocks.

Factor-3 : This factor accounts for only 7% of total variance among the variables. Significant loadings were obtained for K and Cl followed by moderate loadings for other ions. Although a control of evaporite weathering is indicated, available geologic information is insufficient to confirm this possibility. This factor, however, is related to factor-1 (r = 0.71) as obtained from the factor correlation matrix (Table 6.23b).

Another R-mode factor analysis with the same variables was also performed. Initial factor matrix was subjected to 'varimax' rotation with Kaiser normalization. The varimax converged in four iterations. The rotated factor scores for 3 factors extracted (Table 6.24) showed no significant changes from

Table 6.24 Varimax rotated factor matrix (R-mode)

Variable	Factor		
	1	2	3
SiO_2	0.079	0.059	0.992
Na	0.933	0.267	0.057
K	0.353	0.872	0.121
Ca	0.823	0.469	0.067
Mg	0.866	0.417	0.155
HCO_3	0.907	0.329	0.127
Cl	0.502	0.775	-0.019
SO_4	0.769	0.342	-0.034
Percentage variance explained	70.20	12.30	7.40
Cumulative percentage of variance	70.20	82.50	89.90

the obliquely rotated factor scores. But factor-2 and factor-3 in the oblique transformations were interchanged i.e. factor-2 is now related to K-Cl while factor-3 is SiO_2 factor. The percentage of variance explained by K-Cl is 12 and that of SiO_2 is 7. This indicates that the basic composition of factors did not change. Therefore, the variance of chemical constituents in adequately explained by orthogonal and oblique factors but the latter was preferred for geochemical interpretations.

The primary control of factor-1 (carbonate weathering) on Mahanadi river water composition is clearly indicated by the statistical method adopted in this section. This agrees with the conclusion drawn from the ternary diagrams developed in the preceding section which were based on standard geochemical arguments.

CHAPTER-7

WEATHERING IN PILOT AREA

7.1 Introduction

The ultimate product of rock-water interaction discussed in the previous chapter is an assemblage of secondary minerals which appear in the soils and sediments. The formation of soil over limestone bed rock is particularly interesting. The conventional scheme of limestone weathering involves congruent dissolution of carbonate minerals. Theoretically, therefore, a pure limestone bed rock cannot support a residual soil profile. One would expect to see only solution features and a karst topography. On the other hand, most limestones contain enough silicate minerals to give rise to clay-rich soils which normally develop over silicate terrains. The study of these soil profiles requires large scale mapping of a small area where all information regarding limestone weathering including mineralogical and water chemical data can be readily obtained. For this purpose, the terrain around Baloda Bazar ($21^{o}39'$ N, $82^{o}10'$ E) was selected as a Pilot Area for recording the pattern of soil formation over a stromatolitic limestone bed rock.

7.2 Geology of the Area

The formations exposed in the area belong to Raipur series. From the geologic map (Fig. 7.1), it is seen that Tarenga shale, Chandi limestone and Gunderdehi shale are exposed in the pilot area. Stratigraphic superposition and primary minerals of these rocks have been discussed in Chapter 3.

Limestone rocks belonging to the Chandi formation cover a considerable portion of the pilot area. These stromatolitic limestones are indicative of a shallow marine condition of sedimentation (Murti, 1987). The weathering surface of limestone shows solution features like open cavities, solution caves, open joints, stylolites etc. Because of their deposition in a near shore environment, these limestones contain a relatively large proportion of silicate minerals in addition to common carbonate minerals. The weathering of this impure limestone should involve parallel congruent and incongruent reactions. An attempt has been made to interpret the mechanisms of the weathering of carbonate and silicate fractions and consequent soil formation.

7.3 Weathering of Carbonate Minerals

Calcite and dolomite are the major carbonate minerals present. In addition, ankerite was detected in some samples on the basis of the characteristic X-ray peak between 2.89 and 2.9 A.

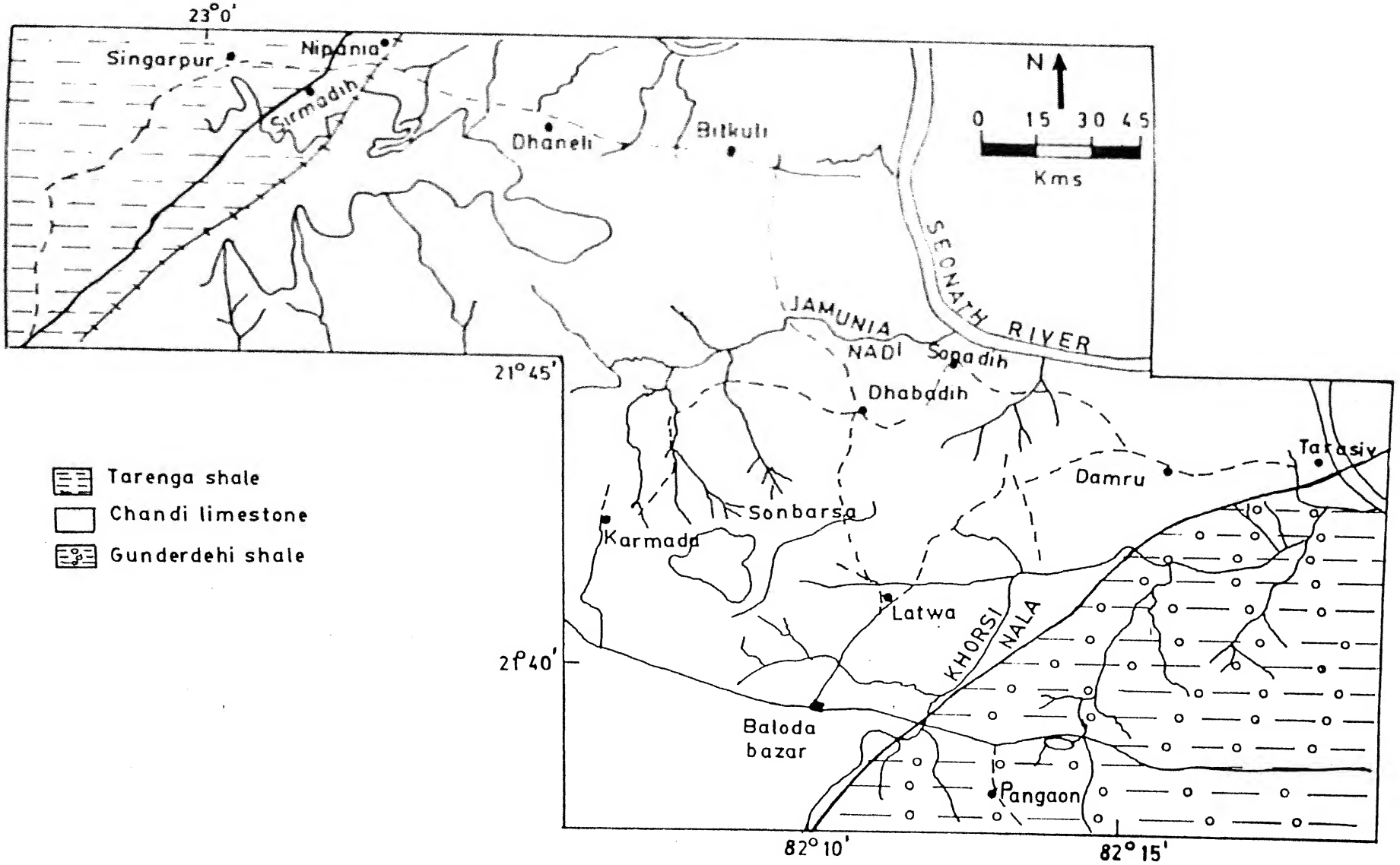

7.1 Geologic map of the pilot area

It was confirmed by the presence of an endothermic DTA peak below 800°C (Fig. 7.2). Weathering of these carbonate minerals takes place by a process of congruent dissolution in presence of CO_2-saturated water:

a) $CaCO_3 + CO_2 + H_2O = Ca^{2+} + 2HCO_3^-$

b) $CaMg(CO_3)_2 + 2CO_2 + 2H_2O = Ca^{2+} + Mg^{2+} + 4HCO_3^-$

As the mineral goes completely into solution, the limestone develops cavities, sink holes and cavernous zones depending on the scale of weathering. If CO_2 escapes from the solution saturated with calcite and dolomite, the above reactions are reversed and reprecipitation occurs. Cave deposits and carbonate concretions are well known examples of this situation.

A set of groundwater analyses from this area (Ramanna, 1976) was utilized to test saturation with calcite and dolomite. The calculations summarized in Table 7.1 show that the ionic activity product $a_{Ca^{2+}} \cdot a_{CO_3^{2-}}$ range from $10^{-8.82}$ to $10^{-7.46}$ and brackets the solubility product of calcite, $K_c = 10^{-8.40}$ at 25°C. Similarly, the value of $a_{Ca^{2+}} \cdot a_{Mg^{2+}} \cdot (a_{CO_3^{2-}})^2$ ranging from $10^{-17.76}$ to $10^{-15.23}$ brackets the solubility product of dolomite, $K_d = 10^{-17.0}$ at 25°C. Most of the ground water samples as well as Seonath river water are super-saturated with respect to calcite

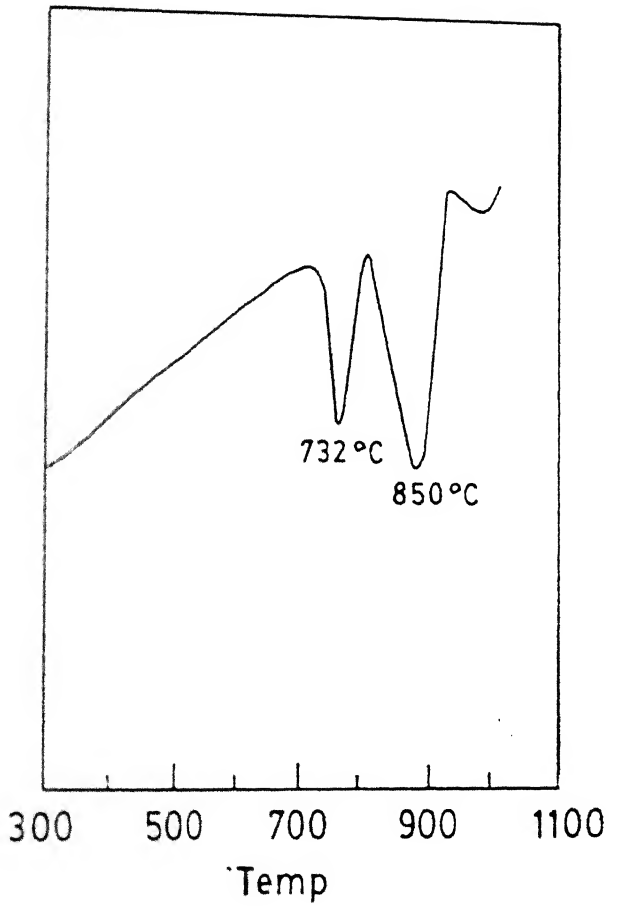

FIG. 7.2 DERIVATOGRAPH OF ANKERITIC LIMESTONE

Table 7.1 Calculated ion activity products in river and ground water of Chhattisgarh Basin. Original water analysis from Ramanna (1976).

Sample No. (location)	$\log(a_{Ca^{2+}} . a_{CO_3^{2-}})$	$\log[a_{Ca^{2+}} . a_{Mg^{2+}} . (a_{CO_3^{2-}})^2]$
1C - 1 (Bortara)	-7.88	-15.50
1C - 15 (Chamri)	-7.46	-15.26
2C - 6 (Dhobnidih)	-8.44	-17.02
2C - 9 (Kesli)	-8.82	-17.57
2C - 1 (Diggi)	-7.84	-15.38
2C - 3 (Bhatbera)	-8.53	-17.76
2C - 12 (Bitkuli)	-7.80	-15.57
2C - 15 (Senodha)	-7.72	-15.70
1C - 5 (Gogia)	-7.67	-15.23
Seonath River (Nandghat)	-7.67	-15.28

and dolomite. This may explain the widespread occurrence of carbonate concretions in this area.

7.4 Weathering of Silicate Minerals

Limestone bed rocks are observed to support two types of soil cover which match with the calcimorphic soils described by Loughnan (1969). One is a concretionary red soil (Terra Rossa). The other is a plastic, organic rich black soil (Rendzina). X-ray diffraction studies (Table 7.2) revealed that the assemblage kaolinite + illite + quartz is common to both soils. However, the red soil is characterized by concretions of goethite while a swelling clay (montmorillonite) and poorly crystalline chlorite were detected in some samples of the black soil. This soil mineralogy can be traced to the silicate minerals trapped during the deposition of the stromatolitic limestone. Examination in hand specimen and thin section along with X-ray pattern of HCl leached residue of this limestone (Fig. 7.3) showed the presence of quartz, alkali felspar, kaolinite, illite, chlorite and glauconite. Among these glauconite is probably a primary source of iron for the formation of goethite by weathering as discussed in the following sub-section. Additional iron can be derived in the soil zone by dissolution of ankerite.

$$(Ca, Mg, Fe)CO_3 + CO_2 + H_2O \longrightarrow Ca^{2+} + Mg^{2+} + Fe^{2+} + HCO_3^-$$

Table 7.2 Soil mineralogy in the pilot area from XRD

Red soil (Terra Rossa)		Black soil (Rendzina)	
Sample No.	Mineralogy	Sample No.	Mineralogy
S-5 (Damru)	Q + I + K + Go	S-4 (Tarasiv)	Q + I + K + Mo
S-6 (Sonbarsa)	Q + I + K + Go	S-8 (Karmada)	Q + I + K + Chl

Q-Quartz, I-Illite, K-Kaolinite, Go-Goethite, Mo-Montmorillonite, Chl-Chlorite

7.4.1 Identification and Weathering of Glauconite

Identification of glauconite in limestone was carried out through a series of steps. Examination in hand specimen and thin sections showed green coloured, rounded to elliptical pellets. Particles in thin section have optical properties similar to chlorite. However, the X-ray diffraction pattern of acid-leached residue (Fig.7.3) showed a sharp $10A^{0}$ peak which could be due to a mica-type mineral. Therefore, in order to confirm the presence of glauconite, such green coloured pellets were separated from the carbonate matrix for analysis under scanning electron microscope. SEM photographs showed laths of irregular crystals. Energy dispersive X-ray analysis (EDAX) of these grains (Table 7.3) established them to be potassium and iron rich silicate. The composition provided a fairly good match with the idealized glauconite given by Burst (1958).

The weathering of glauconite has been recorded by Loughnan (1969) and Courbe et al. (1981). In the soil environment, glauconite initially alters to a montmorillonite (nontronite) which in turn gives rise to an assemblage of kaolinite and goethite. Wolf (1967) suggested that spheroidal particles of goethite could be pseudomorphs after glauconite. It is obvious that these mineralogical changes are similar to standard silicate weathering reactions with the added parameter of

Table 7.3 Chemical composition of glauconite by SEM-EDAX

Element	Normalized wt. %		Ideal glauconite*
	G-1	G-2	
Na	0.00	0.00	1.84
Ca	9.60	8.34	
Mg	0.00	0.00	5.67
Al	11.93	15.40	13.90
Si	35.71	44.28	48.51
K	19.91	17.73	14.18
Fe	22.85	14.25	19.29
Total	100.00	100.00	100.00

G-1, G-2 are glauconite pellets in limestone.

*Element composition recalculated from the glauconite formula

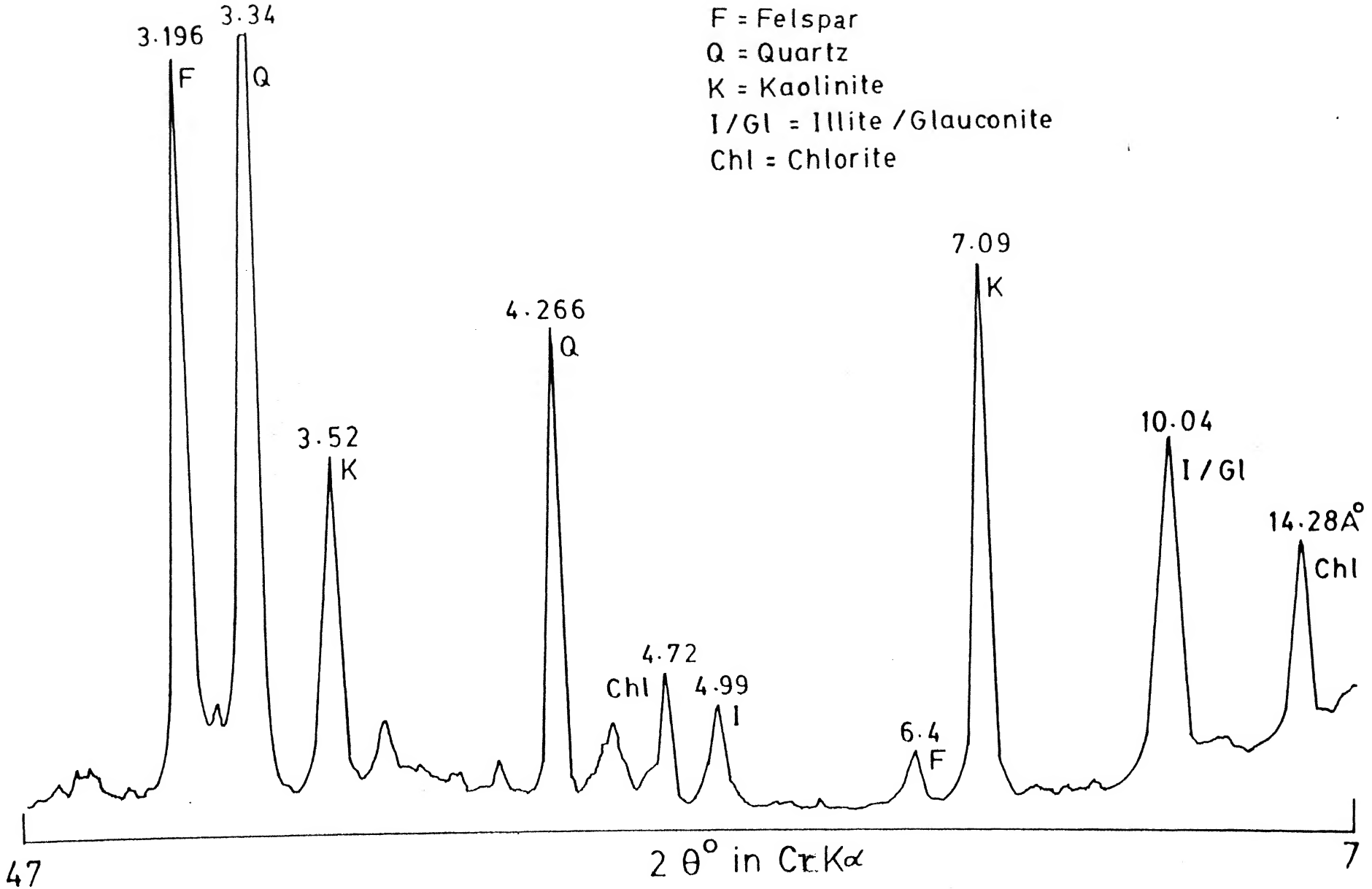

Fig. 7.3 Sketch of x-ray diffraction pattern of HCl treated limestone

oxidation of ferrous to ferric iron. The ferric iron is ultimately fixed in goethite.

From a crystallo-chemical point of view, glauconite is a ferrous-ferric equivalent of illite. An idealized formula adopted from Burst (1958) can be written as $K_{1.5}(Fe^{3+}_{3.16}Fe^{2+}_{0.84})X$ where X = $Al_{0.66}Si_{3.74}O_{20}(OH)_4$. Weathering in the presence of dissolved CO_2 is essentially a reaction with H^+ ions contributed by the weak acid H_2CO_3. Conversion of glauconite to an ideal nontronite, $K_{0.66}(Fe^{3+})_4X$ involves the following steps :

glauconite = $K_{0.66}Fe^{3+}_{3.16}$ X + 0.84 Fe^{2+} + 0.84 K^+

0.84 Fe^{2+} + 0.21 O_2 + 0.84 H^+ = 0.84 Fe^{3+} + 0.42 H_2O

$K_{0.66}Fe^{3+}_{3.16}$ X + 0.84 Fe^{3+} = nontronite

---

glauconite + 0.21 O_2 + 0.84 H^+ = nontronite + 0.84K^+ + 0.42 H_2O

Similarly, the weathering of nontronite to kaolinite plus goethite involves release of K^+ ion and dissolved silica, H_4SiO_4. The overall reactions for glauconite-nontronite, nontronite-kaolinite + goethite and glauconite-kaolinite +goethite equilibria have been provided in Table 7.4. The Gibbs energy values used to calculate equilibrium constants of these reactions have been listed in Table 7.5. From these data, a stability

Table 7.4 Equilibrium constants for stability of glauconite in the soil environment at 25°C, 1 atm.

Glauconite (gl), $K_{1.5}(Fe^{3+}_{3.16}Fe^{2+}_{0.84})Al_{0.66}Si_{7.34}O_{20}(OH)_4$

Nontronite (no), $K_{0.66}(Fe^{3+})_4Al_{0.66}Si_{7.34}O_{20}(OH)_4$

Kaolinite (ka), $Al_4Si_4O_{10}(OH)_8$

Goethite (go), FeOOH

gl-no boundary:

$$gl + 0.21\ O_2 + 0.84\ H^+ = no + 0.84\ K^+ + 0.42\ H_2O$$

$$\log(a_{K^+}/a_{H^+}) = 19.3 \text{ for } P_{O_2} = 0.21 \text{ atm in earth's atmosphere}$$

no-ka+go boundary:

$$6\ no + 4\ H^+ + 82\ H_2O = ka + 24\ go + 4\ K^+ + 40\ H_4SiO_4$$

$$\log(a_{K^+}/a_{H^+}) + 10 \log a_{H_4SiO_4} = -43.85$$

gl-ka+go boundary:

$$6\ gl + 1.26\ O_2 + 9.04\ H^+ + 79.48\ H_2O = ka + 24\ go + 9.04\ K^+ + 40\ H_4SiO_4$$

$$\log(a_{K^+}/a_{H^+}) + 4.42 \log a_{H_4SiO_4} = -8.64$$

Note - Relevant Gibbs energy data are listed in Table 3.

diagram (Fig. 7.4) in terms of the thermodynamic activity of K^+, H^+ and H_4SiO_4, has been constructed by the method of Garrels and Christ (1965). The idealized composition might introduce considerable uncertainty in the position of boundaries. However, from the position of the glauconite-nontronite-kaolinite triple point, it is reasonable to conclude that glauconite weathers to kaolinite plus goethite at relatively high pH, high K^+ ion activity and low silica activity.

7.5 Relative Mobility of Elements

The proposed weathering scheme for the carbonate and silicate fractions in lime stone is based on the removal of major elements in solution and fixation of Al in clay minerals and Fe in goethite. Comparison of chemical analysis of limestone bed rock near Baloda Bazar and of the local soil confirms the same trend. Table 7.6 shows the oxide analysis recalculated to element percentage. The soil to rock ratio is high for Al and Fe but much lower for Ca and Mg. These values indicate that the relative mobility of elements during weathering has been Ca > Mg > Na $\geq$ K > Si > Al >Fe.

Table 7.5 Standard state Gibbs energy of formation of minerals and related species for glauconite weathering reactions

Substance	$\Delta G^{\circ}f$ KJ/mole	Source
Glauconite	-9296.80	1
Nontronite	-9053.30	1
Kaolinite, $Al_4Si_4O_{10}(OH)_8$	-7598.72	2
Goethite	-488.55	2
O_2 gas	0.0	2
H^+	0.0	2
K^+	-282.49	2
H_2O	-237.13	2
H_4SiO_4	-1307.74	3

(1) Calculated by the oxide summation method (Tardy and Garrels, 1974).

(2) Converted to KJ/mole from Robie et al. (1978).

(3) Calculated from 6 ppm SiO_2 for quartz solubility and $\Delta G^{\circ}f$ of quartz = -856.29 KJ/mole (Robie et al., 1978).

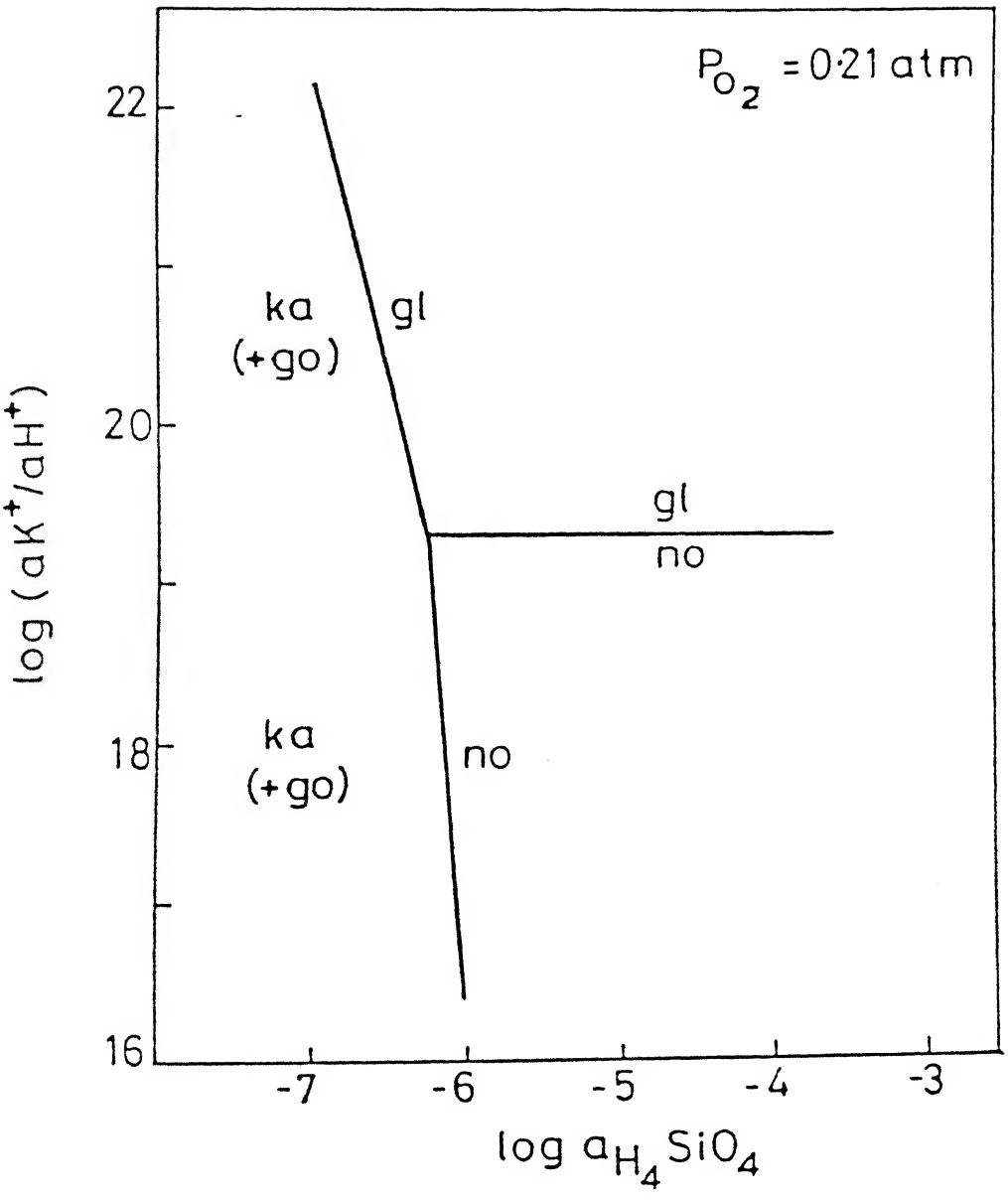

Figure 7.5 Stability fields of glauconite (gl), nontronite (no) and kaolinite (ka) with goethite (go) at 25°C.

Table 7.6 Calculation of relative mobility of elements during weathering of limestone in Bhatapara area

A. Chemical analysis (TISCO/Sonadih Project, unpublished report)

	Average limestone	Average soil
SiO_2	7.72	39.52
Al_2O_3	2.91	16.57
Fe_2O_3	0.98	27.20
CaO	46.89	1.78
MgO	2.40	0.72
Na_2O	0.14	0.35
K_2O	0.33	0.82
LOI	38.24	13.69
	99.61	100.65

B. Element concentration (Recalculated to 100 percent)

	Limestone	Soil	Soil/Limestone
Si	8.77	37.80	4.31
Al	3.73	17.86	4.79
Fe	1.66	38.90	23.43
Ca	81.40	2.60	0.03
Mg	3.51	0.89	0.25
Na	0.25	0.53	2.12
K	0.66	1.39	2.11

CHAPTER 8

CONCLUDING REMARKS

8.1 Summary

This thesis describes the geochemical aspects of rock weathering in the Mahanadi river basin. A discussion on weathering in major world river basins and possible controls on river water composition is followed by a review of Indian river basins. This leads to the objectives of the present work. A representative area of bed rock exposures in the upper reaches of the Mahanadi river has been selected for detailed observation. The effect of recent deposits and human activities is minimum in this area. Moreover, the exposures of silicate and carbonate rocks were expected to provide a contrasting picture of rock weathering.

Geomorphological analysis of a tributary in the source area indicates that the river is actively eroding granitic rocks. The hypsometric curve shows that 64% of the land mass has been eroded out. On the other hand, a study of satellite imagery and field observations reveals the presence of karst features in the adjoining limestone terrain of the Chhattisgarh basin.

Size analysis of suspended sediments of four upland tributaries show that 70% of the material is carried in the silt fraction. These sediments contain unweathered felspar and occasional calcite. These features point to a transport dominated (weathering limited) denudation regime in the upper part of the

river basin. Sediment load is strongly related to discharge because calculations show that nearly 99% of the suspended load is carried during the monsoon period. Total annual load of the Mahanadi river at the farthest downstream CWC sampling point near Tikarpara is 35.24 million tonnes out of which physical load constitutes 30.89 million tonnes and chemical load is 4.35 million tonnes. The overall ratio of physical to chemical erosion up to this part of the basin is estimated to be around 7:1.

Ca^{2+}, Mg^{2+}, Na^{+}, K^{+} are major cations and HCO_3^-, Cl^- and SO_4^{2-} are major anions in river water. Ca^{2+}, Mg^{2+} and HCO_3^- show lowest concentrations during the monsoon period. Dissolved silica and sulphate concentrations are directly related to discharge. The concentration of major ions at the confluence of tributaries matches fairly well with the predicted value obtained by area-weighting the concentration in individual tributaries. This suggests a substantial contribution from weathering of rocks in the catchment area.

Dissolved CO_2 in river and ground water acts as the principal weathering agent. Apparent partial pressure of CO_2 in the river water is more than the atmospheric CO_2 pressure. The acquisition and proportion of three major ions Ca, Mg and HCO_3 in river water have been evaluated in terms of weathering of carbonate and silicate minerals in the rocks. Using the global average for fractionation of Ca and Mg (Holland, 1978), the total HCO_3 in river water can be divided between parts derived by carbonate and silicate weathering. It is found that the ratio of

carbonate derived HCO_3 to silicate derived HCO_3, approaches a value of 2.0 for the limestone terrain while it is more than 1.0 in other parts of the basin. This implies a relatively greater influence of carbonate weathering over silicate weathering even in the downstream part of the river basin. This conclusion is confirmed by a balance between $(Ca+Mg)_{total}$ and $(HCO_3)_{total}$ as well as a cluster of river water analyses near the HCO_3 vertex in a ternary plot of HCO_3, SiO_2 and SO_4 on an equivalent basis. Further support comes from an R-mode factor analysis of major ions in water in which Na-Ca-Mg-HCO_3 factor alone explains 70% of the total variance among the ions.

Carbonate and silicate mineral equilibria have also been evaluated in terms of thermodynamic data. The ion activity products for calcite and dolomite fall in the range of $10^{-8.184}$ to $10^{-9.748}$ and $10^{-16.494}$ to $10^{-19.918}$ respectively, indicating a general undersaturation with respect to these carbonate minerals in river water. This explains the aggressive weathering of dolomitic limestone in the river basin. Water analyses from different sampling siations plot within the kaolinite field in the standard stability diagrams for K, Na and Mg systems. On the other hand, the analyses plot near the kaolinite-Ca montmorillonite boundary in the stability diagram for Ca-system. This suggests that kaolinite and Ca-montmorillonite can co-exist in the river water environment. This theoretical observation is supported by the presence of kaolinite and a glycol expansive 14A^{o} clay mineral in suspended sediments and soils. The dissolved Al concentration

also indicates the stability of poorly crystalline kaolinite phase in the river water environment.

Analysis of selected heavy metals in soils and sediments show a general distribution pattern of Pb < Cu < Mn < Zn in the granitic terrain. Zinc specifically, seems to be enriched in soils and sediments from both the terrains indicating a possible anthropogenic source.

A detailed mineralogical study of dolomitic limestone interbedded with shales and the pattern of soil formation in a pilot area within the Chhattisgarh Basin indicate two parallel weathering schemes. A congruent weathering of calcite and dolomite results in typical solution features and incongruent weathering of glauconite gives rise to a red lateritic soil cover over the limestone bed rock. The order of relative mobility during weathering of elements is Ca > Mg > Na ≥ K > Si > Al > Fe.

8.2 Suggestions for Further Work

1) As discussed above, the thesis project focussed on the weathering of bed rocks exposed in the upper part of the Mahanadi basin. There were indications that heavy metals like Zn in soils and sediments may have an anthropogenic source. This aspect can be further elaborated. A correlation with mining areas and high Fe, Mn, Cu, Zn and Pb concentration has been suggested by Chakrapani and Subramanian (1990). The Hasdo, Mand and Ib valleys may be

suitable pilot areas to decipher the role of coal mining and chemical industries in contributing trace metals to river water and sediment.

2) The discharge and sediment transport by the Mahanadi is controlled by one of the largest earth dams in the country located at Hirakud. A comparison between upstream and downstream segments through controlled sampling should bring out interesting patterns.

3) There have been reports on the possible impact of polluted river water on the construction materials of the Hirakud dam. This aspect is worth future investigation.

4) The influence of alkaline soils and saline groundwater on river chemistry can be studied particularly in the alluvial deposits near the river mouth (Sarin et al., 1989).

5) The role of rock-water interaction has been interpreted in terms of thermodynamic equilibria in this thesis. It would be important to go into the kinetic aspects of these reactions. An attempt may be made to estimate rates from weathering rind, as outlined by Whitehouse et al. (1986).

6) For a complete mass balance study, the influence of bio-mass on uptake of weathering related chemical constituents must be documented. A study in small watersheds similar to the works of Cleaves et al. (1970) and Velbel (1986) may be taken up within the Mahanadi basin.

7) Both stable and radioactive isotopes have been successfully utilized in river geochemistry in recent times. A

distribution pattern of ^{18}O and ^{2}H may supplement the weathering models established in this thesis. Sedimentation rates may be determined by the ^{226}Ra - ^{210}Pb method on cores recovered from river banks (Subramanian et al., 1985).

REFERENCES

1) Berner A. and Berner R.A.(1987) *The Global Water Cycle: Geochemistry and Environment.* Prentice Hall, Englewood Cliffs, New Jersey, 397p.

2) Blatt H. and Middleton G. (1972) *Origin of Sedimentary Rocks.* John Wiley and Sons, New York, 295p.

3) Brownlow A.H. (1979) *Geochemistry.* Prentice Hall, Englewood Cliffs, New Jersey, 448p.

4) Burst J.E. (1958) Mineral heterogeneity in glauconite pellets. *Am. Miner.*, **43**, 481-497.

5) Carson M.A. and Kirby M.J. (1972) *Hillslope, Form and Process.* Cambridge University Press, New York.

6) Gerling T.E., Pederson B.L. and Von Damm, K.L. (1989) Sodium-calcium ion exchange in the weathering of shales : Implications for global weathering budgets. *Geology*, **17**, 552-554.

7) Chakrapani G.J. and Subramanian V. (1990a) Preliminary studies on the geochemistry of the Mahanadi river basin, India. *Chem. Geol.*, **81**, 241-253.

8) Chakrapani G.J. and Subramanian V. (1990b) Factors controlling sediment discharge in the Mahanadi basin, India. *J. Hydrol.*, **117**, 169-185.

9) Cleaves E.T., Godfrey A.E. and Bricker O.P. (1970). Geochemical balance of a small watershed and its geomorphic implications. *Geol Soc. Am. Bull.*, **81**, 3015-3052.

10) Courbe C., Velde B. and Meunier A. (1981) Weathering of glauconites : Reversal of glauconitization process in a soil profile in western France. *Clay Minerals*, **16**, 231-243.

11) Das N., Das M. and Mishra V.P. (1989) Geology of Bemetra-Kodwa-Bera area, Durg district, Madhya Pradesh. *Rec. Geol. Surv. Ind.* **122**, Pt 6, 16-17.

12) Das N., Das M.G. and Arora Y.K. (1990) Microfacies assemblage of gypsum from Chhattisgarh Basin - A Sabkha model of evaporite formation. *Geol. Surv. Ind.*, Spl. Publ. No. **28**, 639-647.

13) Davis J.C. (1986) *Statistics and Data Analysis in Geology*, 2nd ed., John Wiley and Sons, New York, 646p.

14) Davis S.N. (1964) Silica in streams and ground water. *Am. J. Sci.*, 262, 870-875.

15) Drever J.I. (1988) *The Geochemistry of Natural Waters*, 2nd ed., Prentice Hall, Englewood Cliffs, New Jersey, 437p.

16) Dutt N.V.B.S. (1962) Chemical composition of certain limestone formations of M.P. and A.P. *Indian Minerals*, 16, 367-379.

17) Dutt N.V.B.S. (1964) A suggested succession of the Purana Formations of the southern part of Chhattisgarh, M.P. *Rec. Geol. Surv. Ind.*, 93, 143-148.

18) Förstner U. and Wittmann, G.T.W. (1981) *Metal Pollution in the Aquatic Environment*, 2nd revised ed., Springer-Verlag, New York, 486p.

19) Garrels R.M. and Christ C.L. (1965) *Solutions, Minerals and Equilibria*. Harper and Row, New York, 450p.

20) Garrels R.M. and Mackenzie F.T. (1971) *Evolution of Sedimentary Rocks*. W.W. Norton, New York, 397p.

21) Geological Survey of India (1989) *Rec. Geol. Surv. Ind.*, 122, Pt 6, 16-17.

22) Gibbs R.J. (1970) Mechanisms controlling world water chemistry. *Science*, 170, 1088-1090.

23) Helgeson H.C. (1969) Thermodynamics of Hydrothermal systems at elevated temperatures and pressure. *Am. J. Sci.*, 267, 729-804.

24) Helgeson H.C., Delany J.M., Nesbitt H.W. and Bird D.K. (1978) Summary and critique of the thermodynamic properties of rock-forming minerals. *Am. J. Sci.*, 278, 1-229.

25) Hem J.D. (1991) *Study and interpretation of the chemical characteristics of natural water*. Scientific Publishers, Jodhpur, 264p.

26) Hess P.C. (1966) Phase equilibria of some minerals in the K_2O-Na_2O-Al_2O_3-SiO_2-H_2O system at 25°C and 1 atmosphere. *Am. J. Sci.*, 264, 289-309.

27) Hitchon B., Billings G.K. and Klovan, J.E. (1971) Geochemistry and origin of formation waters in the western Canada sedimentary basin : III. Factors

controlling chemical composition. *Geochim. Cosmochim. Acta*, **35**, 567-598.

28) Holland H.D. (1978) *The Chemistry of The Atmosphere and Oceans*. John Wiley, New York, 351p.

29) Kale V.S. (1991) Constraints on the evolution of Purana Basins of Peninsular India. *J. Geol. Soc. Ind.*, **38**, 231-252.

30) Karanthanasis A.D. (1989) Soil solution : A sensitive index of mineral stability in pedogenic environments. In *Weathering : its products and deposits* (eds. K.S.Balasubramaniam et al.) Vol. 1, Process, pp 157-195. Theophrastus Publ., Athens.

31) Khan M.W.Y. and Mukherjee A. (1990) Petrography and depositional environments of Chandarpur sandstones around Lohara, Durg distt., M.P. India. *J. Earth Sciences*, **17** 44-50.

32) Kittrick J.A. (1966) Free energy of formation of kaolinite from solubility measurements *Am. Miner.*, **51**, 1457-1466.

33) Krauskopf K.B. (1979) *Introduction to Geochemistry* 2nd ed., McGraw Hill Book Co., Singapore, 617 p.

34) Laxmi Narayan, T. and Kuity, D.P. (1988) Study of granitization around Kanker, Bastar, M.P. *Pub. Cent. Adv. Stud. Geol.*, Punjab Univ, Chandigarh, 3, 29-32.

35) Meade R.H. (1969) Errors in using modern stream load data to estimate natural rates of denudatioh. *Geol. Soc. Am. Bull.*, **80**, 1265-1274.

36) Meybeck M. (1987) Global chemical weathering of surficial rocks estimated from river dissolved loads. *Am. J. Sci.*, **287**, 401-428.

37) Milliman J.D. and Meade R.H. (1983) World-wide delivery of river sediment to the oceans. *J. Geol.*, **91**, 1-21.

38) Mukherjee A. and Khan M.W.Y. (1989) Petrography and Facies analysis of Charmuria limestones (Raipur group) around Lohara, Durg district, M.P. *J. Ravi Shankar Univ.*, **2**, 47-55.

39) Mukherjee A. (1990) Phosphogenesis in Pre-cambrian rocks of Durg district, M.P. *Unpubl. Ph.D. dissertation*, Ravi Shankar Univ., Raipur, 246p.

40) Murti K.S. (1987) Stratigraphy and sedimentation in Chhattisgarh Basin. *Proc. Purana Basins of Peninsular India, Memoir 6, Geol. Soc. Ind.*, 239-260.

41) Naidu A.S., Mowatt T.C., Somayajulu B.L.K. and Rao K.S.(1985) Chracteristics of clay minerals in the bed loads of major rivers in India. *Scope/UNEP*, Hamburg, 559-569.

42) Neal C. (1988) Aluminium solubility relationships in acid waters - A practial example for radical reappraisal. *J. Hyrol.*, **104**, 141-159.

43) Norton D. (1974) Chemical mass transfer in the Rio Tanama system, west-central Pueto Rico. *Geochim. Cosmochim. Acta*, 38, 267-277.

44) Nriagu J.O.(1975) Thermochemical approximations for clay minerals. *Am. Miner.*, 60, 834-839.

45) Pascoe E.H. (1965) *A Manual of Geology of India and Burma*, 3rd ed., V-1, Controller of Publications, Government of India, Delhi 485p.

46) Ramana K. (1976) Chemical analysis of water from parts of Raipur, Durg and Bilaspur districts, M.P. *CGWB unpubl. progress report for 1975-76.*

47) Ray S.B., Mohanti M. and Somayajulu B.L.K. (1984) Suspended matter, major cations and dissolved silicon in the estuarine waters of the Mahanadi river, India. *J. Hydrol.*, **69**, 183-196.

48) Raymahashay B.C.(1968) A geochemical study of rock alteration by hot springs in the Paint Pot Hill area, Yellowstone Park. *Geochim. Cosmochim. Acta.*, , , 32, 499-522.

49) Raymahashay B.C. (1973) Characteristics of stream erosion in the Himalayan region of India. *Proc. Symp. on Hydrogeochemistry and Biogeohemistry*, Vol-1, Clark and Co., Washington, D.C., 82-89.

50) Rayamahashay B.C. (1986) Geochemistry of bicarbonate in river water J. *Geol. Soc. Ind.*, **27**, 114-118.

51) Reesman A.L., Picket, E.E. and Keller W.D. (1969) Aluminium ions in aqueous solutions. *Am. J. Sci.*, 267, 99-113.

52) Robie R.A., Hemingway B.S. and Fisher J.R. (1978) Thermodynamic properties of minerals and related substances at 298.15°K and 1 bar (10^5 pascals) pressure and at higher temperatures. *USGS Bull.*, **1432**, 456 p.

53) Sampson R.J. (1968) R-mode factor analysis program in Fortan II for the IBM 1620 computer. In *Computer Programs for Multivariate Analysis in Geology*, 13-38. Computer Contribution 20, State Geol. Surv., Univ. of Kansas, Lawrence, Kansas.

54) Sarin M.M., Krishnaswami S., Dilli K., Somayajulu B.L.K. and Moore W.S.(1989) Major ion chemistry of the Ganga-Brahmaputra river system : Weathering proesses and fluxes to the Bay of Bengal. *Geochim. Cosmochim. Acta*, **53**, 997-1009.

55) Sarin M.M., Krishnaswami S., Somayajulu B.L.K. and Moore W.S. (1990) Chemistry of uranium, thorium and radioactive isotopes in the Ganges-Brahmaputra river system : Weathering processes and fluxes to the Bay of Bengal. *Geochim. Cosmochim. Acta*, **54**, 1387-1396.

56) Schnitzer W.A. (1975) Mineral resources as a basis for India's economy. *Natural Resources and Development*, Vol-1, 145-168.

57) Stallard R.F. and Edmond J.M. (1983) Geochemistry of the Amazon,2 : The influence of geology and weathering environment on the dissolved load. *J. Geophys. Res.*, **88**, 9671-9688.

58) Strahler A.N.(1952) Hypsometric analysis of erosional topography. *Geol. Soc. Am. Bull.*, **63**, 1117-1141.

59) Stumm W. and Morgan J.J. (1981) *Aquatic chemistry : An introduction emphasizing chemical equilibria in natural waters* 2nd ed., John Wiley, New York, 780p.

60) Subramanian V. (1979) Chemical and suspended sediment characteristicsof rivers in India. *J. Hydrol.*, **44**, 37-55.

61) Subramanian V., Sitasawad R. and Joshi L.U. (1985) Rate of sedimentation in the Yamuna river around Delhi using ^{226}Ra - ^{210}Pb method. *J. Radio. Nucl. Chem.*, **90**, 271-276.

62) Subramanian V. (1987) Environmental geochemistry of Indian river basins - a review. *J. Geol. Soc. India.*, **29**, 205-220.

63) Subramanian V., Biksham G. and Ramesh R. (1987a) Environmental geology of peninsular river basins of India. *J.Geol. Soc. Ind.*, **30**, 393-401.

64) Subramanian, Sitasawad R., Abbas N. and Jha P.K. (1987b) Environmental geology of the Ganga river basin. *J. Geol. Soc. Ind.*, 30, 335-355.

65) Tandon S.K. and Gupta K.R. (1990) Goals for Earth Sciences activities in the nineties. *Geol. Soc. Ind.*, Memoir 18, 1-24.

66) Tardy Y. and Garrels R.M. (1974) A method for estimating Gibbs energy of formation of layer silicates. *Geochim. Cosmochim. Acta*, 38, 1101-1116.

67) Usunoff E.J. and Guzman-Guzman A (1989) Multivariate analysis in hydrochemistry : An example of the use of factor and correspondence analysis. *Ground Water*, 27, 27-34.

68) Velbel M.A. (1986) The mathematical basis for determining rates of geochemical and geomorphic processes in small forested watersheds by mass balance. In *Rates of Chemical Weathering of Rocks and Minerals* (eds. S.M. Colman and D.P. Dethier), pp439-451. Academic Press.

69) Wagman D.D., Evans W.H., Parker V.B., Halow I., Bailey S.M. and Schumm R.H. (1968) Selected values of chemical thermodynamic properties. *U.S. Natl. Bureau of Standards Tech. Note*, Vol-27(3), 264p.

70) Wahlstrom E.E. (1955) *Petrographic Mineralogy*, 5th ed., John Wiley and sons, New York, 408p.

71) Wedepohl K.H. (1978) *Handbook of Geochemistry*, Mn-Vol II/5, Springer Verlag.

72) Whitehouse I.E., McSaveney M.J., Kneupfer P.L.K. and Chin T.J.H. (1986) Growth of Weathering rinds on Torlesse sandstone, Southern Alps, New Zealand. In *Rates of Chemical Weathering of Rocks and Minerals* (eds. S.M. Colman and D.P. Dethier) pp 419-435. Academic Press.

73) Wolf R.G. (1967) X-ray and chemical study of weathering of glauconite. *Am. Miner.*, 52, 1129-1138.

74) Woods T.L. and Garrels R.M. (1987) Eds. *Thermodynamic Values at low temperature for natural inorganic materials : An uncritical summary*, Oxford, 242p.

(Appendix I)

(A C T I C A L)

(***************)

```
{ THIS PROGRAM IS WRITTEN IN TURBO PASCAL. IT ESTIMATES MOLE/LITRE, IONIC  }
{ STRENGTH, IONIC ACTIVITY COEFFICIENT, ION ACTIVITIES FROM THE GIVEN PPM  }
{ CONCENTRATIONS OF IONS  IN  WATER.  IT  FURTHER CALCULATES ION ACTIVITY  }
{ PRODUCTS FOR CALCITE, DOLOMITE AND GYPSUM.                               }

program panigrahy(input,output);
const
        max_exp = 100;
        max_com = 20;
        A       = 0.5085;
type
        name          = string[4];
        analysis_arr  = array[1..max_exp,1..max_com] of real;
        comp_arr      = array[1..max_com] of real;
        name_arr      = array[1..max_com] of name;
var
        pH : array[1..max_exp] of real ;
        act_val, ppm : analysis_arr;
        valency, fW    : comp_arr;
        ion_name       : name_arr;
        i,j,tot_ana,
        tot_comp       : integer;
        Ionic_str,Ionic_coeff,log_coeff,m      : real;
```

```
        G,H : text;

procedure print_matrix_value ( matrix : analysis_arr);
var
        i,j : integer;
begin
        for i := 1 to tot_ana do
            begin
                 write(i,'   ');
                 for j := 1 to tot_comp do
                     write(matrix[i,j]:5:5,'  ');
                     writeln;
            end;
end;

procedure read_ion_information (max_val : integer; Var ion_name : name_arr;Var val,fwgt : comp_arr);
var
        i : integer;
begin
        for i := 1 to max_val do
           begin
                readln(G,ion_name[i],val[i],fwgt[i]);
           end;
end;

procedure read_ppm (max_val1, max_val2 : integer; var ppm : analysis_arr);
```

```
var
        i, j : integer;
begin
        for i := 1 to max_val1 do
           begin
               writeln('Enter values for Analysis No : ',i);
               write('Please give the pH value      : ');
               readln(pH[i]);
               for j := 1 to max_val2 do
                  begin
                    write('Enter ion concentration in ppm ',ion_name[j],' : ');
                    readln(ppm[i,j]);
                  end;
                writeln;writeln;
            end;
end;

function mole_per_lit (fun_ppm,fun_fw : real) : real;

begin
   mole_per_lit := ( fun_ppm/ fun_fw ) * 1E-3;
end;

function  calculate_ionic_strength (ana_no : integer) : real;
var
        i     : integer;
        value : real;
```

```
begin
        value := 0;
        for i := 1 to tot_comp do
        value := value + mole_per_lit(ppm[ana_no,i],fw[i]) * valency[i] * valency[i];
        calculate_ionic_strength := 0.5 * value;
end;

procedure co3_act(bicarb_act,pHi : real; var co3 : real);
begin
        co3:=(bicarb_act*exp((-10.33)*ln(10))/(exp(-pHi*ln(10))));
end;

Procedure calculate_ion_activity (var act_val : analysis_arr);
var
        i,j : integer;
        iap_cal,iap_dol,iap_gyp,co3 : real ;
begin
        for i := 1 to tot_ana do
            begin

               writeln(H,'Analysis No. : ',i);
               writeln(H,'ion       ppm        mole/lit      ionic-str   ionic act. coeff   activity');
               writeln(H,'-------------------------------------------------------------------------------
                for j := 1 to tot_comp do
                    begin

                       Ionic_str := calculate_ionic_strength(i);
```

```
        log_coeff := -1 * A * valency[j] * valency[j] *
        (sqrt(Ionic_str)/(1+sqrt(Ionic_str)) - 0.2 *(Ionic_str));
         m := mole_per_lit(ppm[i,j],fw[j]);
         Ionic_coeff := EXP(log_coeff * ln(10));
         act_val[i,j] := m * Ionic_coeff;
         write(H,ion_name[j],'    ');
         write(H,ppm[i,j]:7:3,'    ');
         write(H,m,'      ');
         write(H,Ionic_str:5:4,'        ');
         write(H,Ionic_coeff:4:3,'          ');
         write(H,act_val[i,j]);
         writeln(H);
    end;
writeln(H,'-------------------------------------------------------------------------------');
    writeln(H);
    writeln(H,' I.A.Ps are :- ');
    writeln(H,'--------------------------');
    write(H,'Calcite');
    co3_act(act_val[i,5],pH[i],co3);
    iap_cal := co3*act_val[i,3];
    writeln(H,'    ',iap_cal);
    writeln(H);
    write(H,'Dolomite');
    iap_dol := act_val[i,3]*act_val[i,4]*co3*co3;
    writeln(H,'    ',iap_dol);
    writeln(H);
    write(H,'Gypsum');
```

```
                    iap_gyp := act_val[i,3]*act_val[i,7];
                    writeln(H,'      ',iap_gyp);
                    writeln(H,'---------------------------');
                    writeln(H);
                end;
end;


begin
        assign(G,'ion.data');
        reset(H,'output');
        write('Enter maximum number of analysis  : ');
        readln(tot_ana);
        writeln;
        write('Enter maximum number of ions in each analysis : ');
        readln(tot_comp);
        writeln;
        writeln('Now, read the input values for ions.');
        read_ion_information (tot_comp,ion_name,valency,fw);
        writeln('Now, read the values of ppm for each analysis.');
        read_ppm(tot_ana,tot_comp,ppm);
        calculate_ion_activity(act_val);
        close(G);
        close(H);
end.
```

{Table 1}

{ ION DATA }

{ ******** }

Na	1	22.99
K	1	39.1
Ca	2	40.08
Mg	2	24.31
HCO_3	1	61.018
Cl	1	35.45
SO_4	2	96.06
Fe	3	55.85
Al	3	26.98
NH_4	1	18.01
NO_3	1	62.01
PO_4	3	94.97
SiO_2	0	92.00

APPENDIX II

(Summarized from Holland, 1978)

(1) Contribution of Sedimentary Rocks to TDS in river water

Out of total land surface of the earth, igneous and metamorphic rocks = 24.3% and sedimentary rocks = 75.7%

Also, TDS from sedimentary terrains

= 2 x TDS from igneous and metamorphic terrains.

If X is the contribution from igneous and metamorphic rocks, then weighted fractions for sedimentary and igneous + metamorphic rocks are 75.7 x 2X and 24.3 x X respectively.

Therefore, the ratio

$$\frac{\text{sedimentary}}{\text{igneous + metamorphic}} = \frac{75.7 \times 2X}{24.3 \times X} = 6.23$$

For TDS,

sedimentary + (igneous + metamorphic) = 100

or, 7.23 (igneous + metamorphic) = 100

or, (igneous + metamorphic) = $\frac{100}{7.23}$ = 13.83 ≅ 14%

Therefore,

the contribution of sedimentary rocks = 100-14 = 86%

(2) Ca and Mg in Sedimentary Rocks

Define $X_{Ca} = \frac{\text{Ca in carbonate minerals}}{Ca_{tot}}$

where all concentrations are in moles/kg of rock. Correcting for sulphate minerals, $CaO_{corr} = CaO - SO_3$

$$X_{Ca}^{max} = \frac{CO_2}{CaO_{corr}} \quad \text{when} \quad CO_2 < CaO$$

$$= 1.0 \quad \text{when} \quad CO_2 > CaO$$

$$X_{Ca}^{min} = \frac{CO_2}{CaO_{corr} + MgO}$$

when $$X_{Ca} = X_{Mg} = \frac{CaO_{carb} + MgO_{carb}}{CaO_{tot} + MgO_{tot}}$$

Available data from Russian and American sources (Holland, 1978; Tables 4-12) show that for platform sediments,

$$\left.\begin{aligned} X_{Ca}^{max} &= 1.0,\ 1.0 \\ X_{Ca}^{min} &= 0.81,\ 0.87 \end{aligned}\right\} \quad \text{avg } x_{Ca} = 0.92 \pm 0.08$$

for geosynclinal sediments,

$$\left.\begin{aligned} X_{Ca}^{max} &= 0.62,\ 0.81 \\ X_{Ca}^{min} &= 0.85,\ 1.0 \end{aligned}\right\} \quad \text{avg } X_{Ca} = 0.80 \pm 0.10$$

Existing data also indicate that the proportions of mass of platform and geosynclinal sediments are 27% and 73% respectively. Therefore, weighting the Ca and Mg fractions accordingly,

$$\begin{aligned} \bar{X}_{Ca} &= (0.92 \pm 0.08) \times 0.27 + (0.82 \pm 0.10) \times 0.75 \\ &= 0.85 \pm 0.08 \end{aligned}$$

Similarly, for Mg define

$$X_{Mg}^{max} = X_{Ca}^{min}$$

$$X_{Mg}^{min} = \frac{CaO - CaO_{corr}}{MgO}$$

For platform sediments,

$$\left.\begin{aligned} X_{Mg}^{max} &= 0.81,\ 0.87 \\ X_{Mg}^{min} &= 0.35,\ 0.53 \end{aligned}\right\} \quad \text{avg } X_{Mg} = 0.64 \pm 0.20$$

For geosynclinal sediments,

$$\left.\begin{array}{l} X_{Mg}^{max} = 0.62,\ 0.81 \\ X_{Mg}^{min} = 0.00,\ 0.36 \end{array}\right] \quad \text{avg } X_{Mg} = 0.45 \pm 0.20$$

$$\therefore \bar{X}_{Mg} = (0.64 \pm 0.20) \times 0.27 + (0.45 \pm 0.20) \times 0.73$$

$$= 0.50 \pm 0.20$$

Note : 1) TDS = Total Dissolved Solids, corr = corrected, max = maximum, min = minimum, avg = average, carb = carbonate, tot = total.

2) Compared to Ca, more Mg is tied up with silicates and uncertainty of Mg value is greater than Ca.